CONTINUOUS GRANULATION AND DRYING

Building a comprehensive process understanding based on Quality by Design principles

DISSERTATION

ZUR ERLANGUNG DES DOKTORGRADES (DR. RER. NAT.)

DER MATHEMATISCH-NATURWISSENSCHAFTLICHEN FAKULTÄT

DER RHEINISCHEN FRIEDRICH-WILHELMS-UNIVERSITÄT BONN

vorgelegt von

Judith Menth

aus Ulm

Bonn

Mai 2021

Angefertigt mit Genehmigung der Mathematisch-Naturwissenschaftlichen Fakultät der Rheinischen Friedrich-Wilhelms-Universität Bonn

Prüfungskommission:
Prof. Dr. Karl G. Wagner (Erstgutachter)
Prof. Dr. Alf Lamprecht (Zweitgutachter)
Prof. Dr. Diana Imhof (Fachnahes Mitglied)
Prof. Dr. Andreas Schieber (Fachfremdes Mitglied)

Tag der Promotion: 21. September 2021
Erscheinungsjahr: 2022

Auszüge aus der Arbeit wurden an folgender Stelle vorab veröffentlicht:

Menth J., Maus M., Wagner K. G.:
Establishing Twin screw wet granulation (TSG) as a continuous process step
Poster presentation
11th Worldmeeting on Pharmaceutics, Biopharmaceutics and Pharmaceutical Technology 2018, Granada, Spain

Menth J., Maus M., Wagner K. G.:
Evaluation of scale up of TSG combined with continuous drying
Poster presentation
1st APV Continuous Manufacturing Conference 2019, Antwerpen, Belgium

Menth, J., Maus, M., Wagner, K.G.:
Continuous twin screw granulation and fluid bed drying: A mechanistic scaling approach focusing optimal tablet properties.
International journal of pharmaceutics 2020, Volume 586, 119509
https://doi.org/10.1016/j.ijpharm.2020.119509

Menth, J., Maus, M., Wagner, K.G.:
Assessment of abrasion induced visual defects in twin screw wet granulation using wall friction measurements
submitted to AAPS PharmSciTech on 16th April, 2021

Für meine Eltern

Danksagung

Diese Arbeit entstand im Zeitraum von Februar 2017 bis August 2020 in Kooperation zwischen dem Institut für Pharmazeutische Technologie und Biopharmazie der Rheinischen Friedrich-Wilhelms-Universität Bonn und der Pharmazeutischen Entwicklung der Boehringer Ingelheim Pharma GmbH & Co.KG in Biberach. Ich danke Herrn Dr. Michael Braun, der mir die Promotion in dieser Konstellation mit der pharmazeutischen Industrie ermöglicht hat.

Mein außerordentlicher Dank gilt meinem Doktorvater Herrn Prof. Dr. Karl G. Wagner für das anwendungsbezogene, aktuelle Forschungsthema, die wissenschaftliche Begleitung und Unterstützung während aller Phasen dieser Arbeit und das immer wieder Aufzeigen neuer Perspektiven.
Herrn Prof. Dr. Alf Lamprecht danke ich für die Übernahme des Zweitgutachtens. Frau Prof Dr. Diana Imhof sowie Herrn Prof. Dr. Andreas Schieber sei für Ihre Bereitschaft der Prüfungskommission beizuwohnen gedankt.

Ein sehr herzliches Dankeschön geht an meinen BI-internen Mentor während der Promotionszeit, Herrn Dr. Martin Maus. Vielen Dank Dir für die engagierte Betreuung und Unterstützung während der ganzen Zeit, die unzähligen, wertvollen Diskussionen zu Conti & Co und Dein immer offenes Ohr für meine Anliegen. Du hast maßgeblich dazu beigetragen, mir die Freude an der Entwicklungsarbeit in der pharmazeutischen Industrie zu vermitteln.
Darüber hinaus möchte ich mich auch ganz herzlich bei meinen beiden direkten Kollegen aus dem ehemaligen Labor „LSDPD 3“, Herrn Hans Fink und Frau Angela Wendt, bedanken. Durch Euch habe ich sehr viel über das praktische Arbeiten in der Prozessentwicklung gelernt. Danke auch für die vielen gemeinsamen Stunden an der Conti-Anlage, die Zusammenarbeit hat mir immer sehr viel Freude bereitet.
In dieses Dankeschön möchte ich auch alle anderen Kollegen aus dem Prozessentwicklungslabor sowie den angrenzenden Laboren einschließen, die immer offen für meine Anliegen und Fragen waren und mich unterstützt haben. Dieses angenehme Arbeitsumfeld und -klima hat auf jeden Fall zum erfolgreichen Abschluss dieser Arbeit beigetragen.

Von ganzem Herzen möchte ich mich auch bei meiner Familie bedanken. Ich danke Dir, Michael, von Herzen für die Unterstützung und Begleitung während der letzten Jahre, v.a. für Deine Liebe, Geduld, Motivation und Zuversicht. Ein besonderer Dank gilt auch meinen Eltern. Ihr habt mich auf meinem bisherigen Lebensweg immer unterstützt, begleitet und darin bestärkt, meinen Weg zu gehen. Du, Papa, hast in mir darüber hinaus die grundlegende Begeisterung für die Pharmazie geweckt. Euch beiden ist deshalb diese Arbeit gewidmet.

TABLE OF CONTENTS

ACRONYMS AND ABBREVIATIONS

AEROSIL	highly-dispersed silicon dioxide
APAP	acetaminophen/paracetamol
API	active pharmaceutical ingredient
BD	*bulk density [g/mL]*
cMA	critical material attribute
COPV	copovidone
CP	*compression pressure [MPa]*
cPP	critical process parameter
cQA	critical quality attribute
CROS	crospovidone
D	*diameter [m] or [mm]*
DCP	*drying capacity parameter [(m³*°C)/g]*
DL	drug load
DoE	design of experiment
DRS	*dryer rotation speed [rph]*
DT	*drying time [min]*
F	*crushing strength [N]*
F1	formulation 1
F2	formulation 2
FFC	*flowability function*
FL	*fill level [%]*
FR	*Froude number [-]*

HPMC	hypromellose
HR	*Hausner ratio [-]*
IAFR	*inlet air flow rate [m³/h]*
IAT	*inlet air temperature [°C]*
ICH	International conference on harmonisation
IPC	in process control
IPT	*inlet product temperature [°C]*
L/D	length-to-diameter ratio
LFR	*liquid feed rate [kg/h]*
LoD	*loss on drying [%]*
LIW	loss in weight
LSR	*liquid-to-solid-ratio [-]*
MA	material attribute
MAN	mannitol
MC	*mass per chamber [kg]*
MCC	microcrystalline cellulose
MGST	magnesium stearate
ML	*moisture level [%]*
NCE	new chemical entity
PAT	process analytical technology
PEEK	poly-ether-ether-ketone
PFN	*powder feed number [-]*
PFR	*powder feed rate [kg/h]*

PM	premixture
PP	process parameter
PSD	particle size distribution
QA	quality attribute
QbD	Quality by design
RPH	*rounds per hour*
RPM	*rounds per minute*
RPS	*rounds per second*
RTRT	real-time release testing
SF	*solid fraction [-]*
SME	*specific mechanical energy [kWh/t]*
ST1500	pre-gelatinized starch
STA	starch
STundried	starch undried
T	*temperature [°C]*
t	*thickness [mm]*
TD	*tapped density [g/mL]*
TiN	titanium nitride
TS	*tensile strength [N/mm²]*
TSG	twin screw granulation / twin screw granulator
W	*height of tablet band [mm]*
WFA φ	*wall friction angle [°]*
σ_1	*consolidation stress [Pa]*

σ_c	*unconfined yield strength [Pa]*
σ_w	*normal stress [Pa]*
τ_w	*shear stress [Pa]*
$\varphi_{apparent}$	*apparent density [g/cm³]*
φ_{true}	*true density [g/cm³]*
ω	*angle velocity [rad/s]*

1. GENERAL INTRODUCTION

Continuous manufacturing has been in the focus of interest within the pharmaceutical field for several years now.

Talking about continuous manufacturing, it is important to have a clear differentiation between continuous manufacturing and traditional batch processing. A good comparison and definition of batch and continuous processing were given by Lee et al. (2015) [57] (see Figure 1).

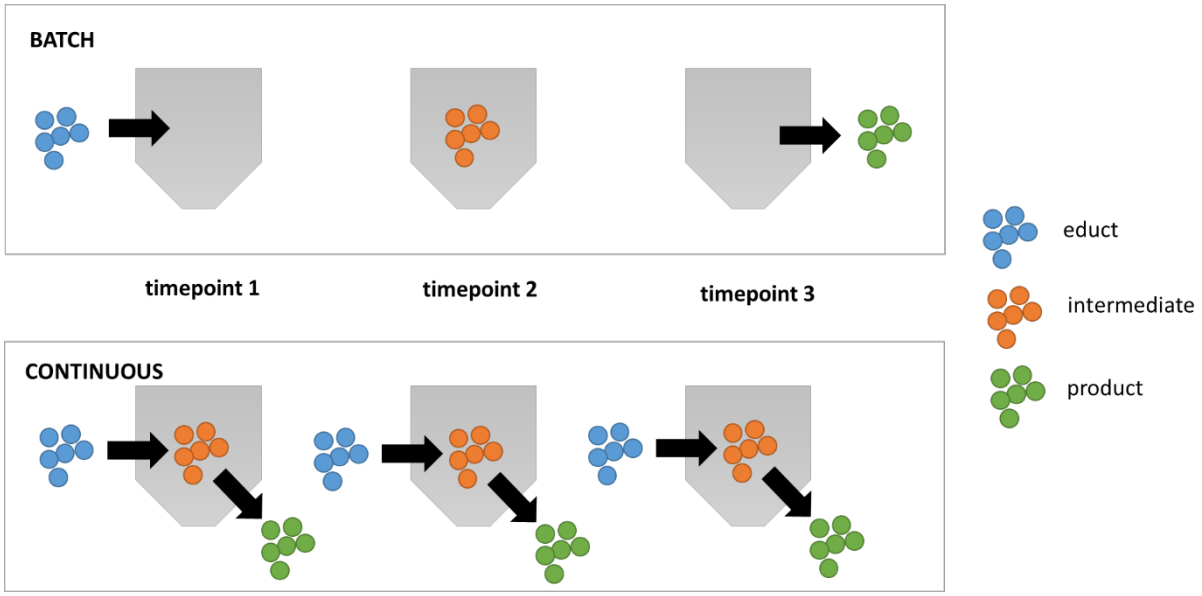

Figure 1 Comparison of batch processing and continuous processing (adapted from Lee et al. (2015) [57])

For a batch process the educts are charged into the equipment (timepoint 1), afterwards processed for a certain period (timepoint 2, intermediate state) and finally the product can be discharged (timepoint 3). In contrast to that, running a process in a continuous mode means educts being charged into the equipment, intermediates being processed, and product being discharged from the system simultaneously over the entire process period (except start-up and shutdown phase).

Main drivers for the interest to move from traditional batch to continuous manufacturing are the advantages offered by continuous manufacturing mentioned by several authors [1, 57, 58, 87, 115]:

- easy scale-up (scaling by time and throughput possible)
- small equipment footprint
- shorter equipment downtime
- less human resources necessary as higher automation level possible
- simplification
- higher product quality

To achieve higher product quality compared to batch processing, several quality aspects must be considered in the context of enhanced process understanding. That process understanding includes, e.g., knowledge about material traceability and residence time distributions [57, 77], the application of a risk management concept [91] and the implementation of process analytical technology (PAT) [57] which may offer the possibility for real time release testing (RTRT) [57, 65].

Despite of the mentioned examples, one of the most essential factors for a proper process understanding is the principle of the Quality-by-design (QbD) approach as presented in the ICH guidelines [42, 43, 44]. Yu et al. (2014) [127] described the QbD approach as a principle that “emphasizes product and process design, understanding and control”. Therefore, a target product quality has to be defined, a manufacturing process has to be designed, critical quality attributes (cQAs) and critical process parameter (cPPs) have to be defined and the manufacturing process has to be controlled (according to Yu et al. (2008) [126]). Tools which can be used for QbD have been also described by Yu et al. (2014) [127]. He mentioned prior knowledge, a risk assessment, mechanistic models, DoEs, data analysis and PAT to be beneficial to reach the targets of QbD. Furthermore, the six sigma principle was also presented by Yu et al. (2017) [128] as an option to “eliminate drug shortages and recalls” and result in “less risk to the customer”.

2. AIM AND OBJECTIVE

The aim of this thesis was to build sound process understanding and risk assessment based on the described QbD principles for a new continuous granulation and drying line comprising the four continuous process units dosing (1), twin screw wet granulation (2), fluid bed drying (3) and transportation of the material by a pneumatic conveying system (4) (see sketch in Figure 3).
In the first part of the thesis (chapters 4, 5 & 6), the building of process understanding regarding the three process units of the continuous line (continuous dosing, twin screw wet granulation and fluid bed drying) by investigation of the relationships between critical process parameters (cPPs), critical material attributes (cMAs) and the critical final drug product quality attributes (cQAs) is presented. Chapter 4 deals with the process unit continuous dosing and investigates the impact of powder properties of starting materials (excipients) on volumetric dosing behaviour using a twin screw feeder. Chapter 5 focuses on twin screw wet granulation unit and how different process parameters influence granule material properties as well as tableting behaviour. In contrast to that, in chapter 6 the focus is set on the continuous fluid bed drying unit evaluating the impact of different process parameter settings on granule as well as tablet material attributes.
In the second part of the thesis (chapter 7), the process knowledge gained in the first part is applied to establish a scale up approach. Background for that scaling approach was to transit from small lab scale equipment over pilot scale equipment to production scale equipment with the aim to result in consistent high product quality over all three scales.
The third part of the thesis (chapter 8) deals with the evaluation of long-term operation of the continuous line. Aspects of continuous gravimetric dosing and twin screw wet granulation are taken into account, with a focus on the robustness of the process.
In the last part of the presented work (chapter 9), a special process risk for twin screw wet granulation process – abrasion and friction – is investigated by a supportive characterization method that enables the understanding of that process risk.
All evaluations were done based on quality considerations and the QbD approach that drive the principle of building the quality of the final drug product into the system from the beginning and during the whole manufacturing process. Therefore, that thesis should serve as a base for a successful development of a NCE using the new continuous granulation and drying technique and resulting in a final drug product of high quality.

3. MODEL

All investigation within this thesis deal in general with a tablet manufacturing process including a continuous granulation and a continuous drying step (see Figure 2). A powder preblend is prepared out of the API and the excipients applying a batch-wise sieving and blending step. Afterwards, the powder preblend is further processed via a continuous granulation and drying step resulting in dry granules. A batchwise processing of dry granules follows resulting in a final blend after a sieving step and a blending step where the extragranular phase (additional disintegrant and lubricant) is added. In a last step, the tableting process takes place.

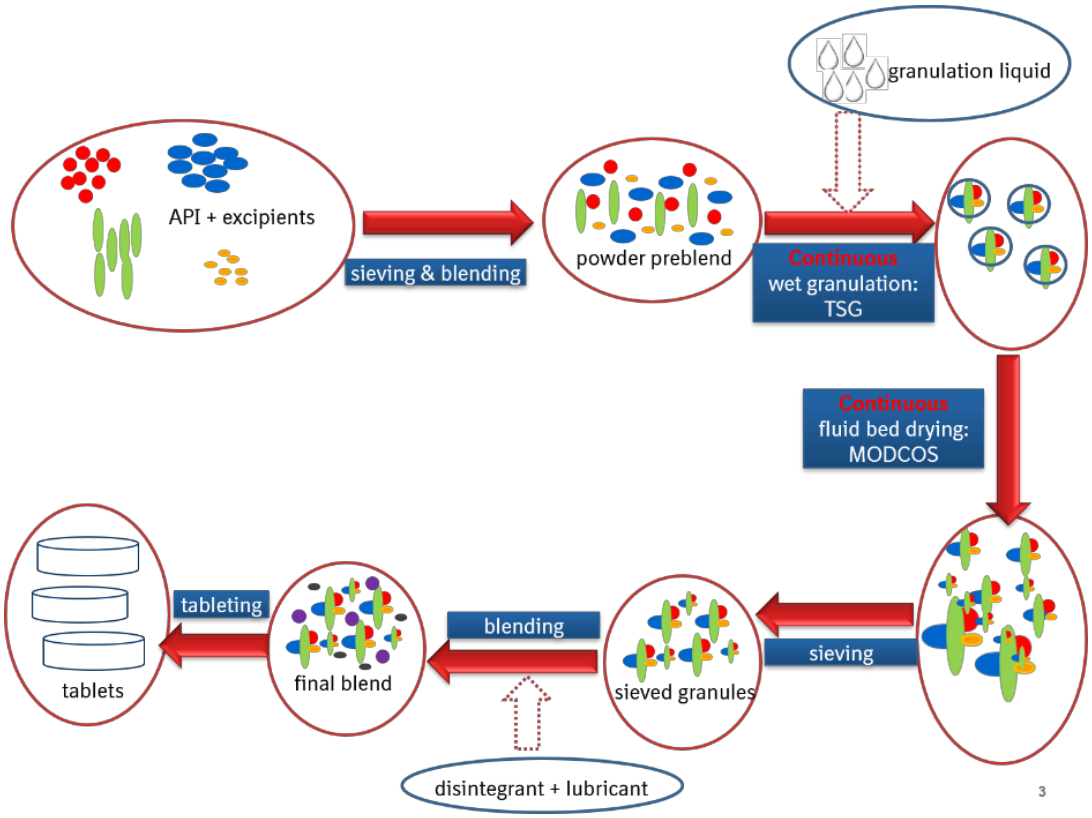

Figure 2 Flowchart of tablet manufacturing including a continuous granulation and drying step

As the focus of this thesis is set on the continuous process steps (granulation and drying), a more detailed description of the process units for these continuous process steps is given in Figure 3.

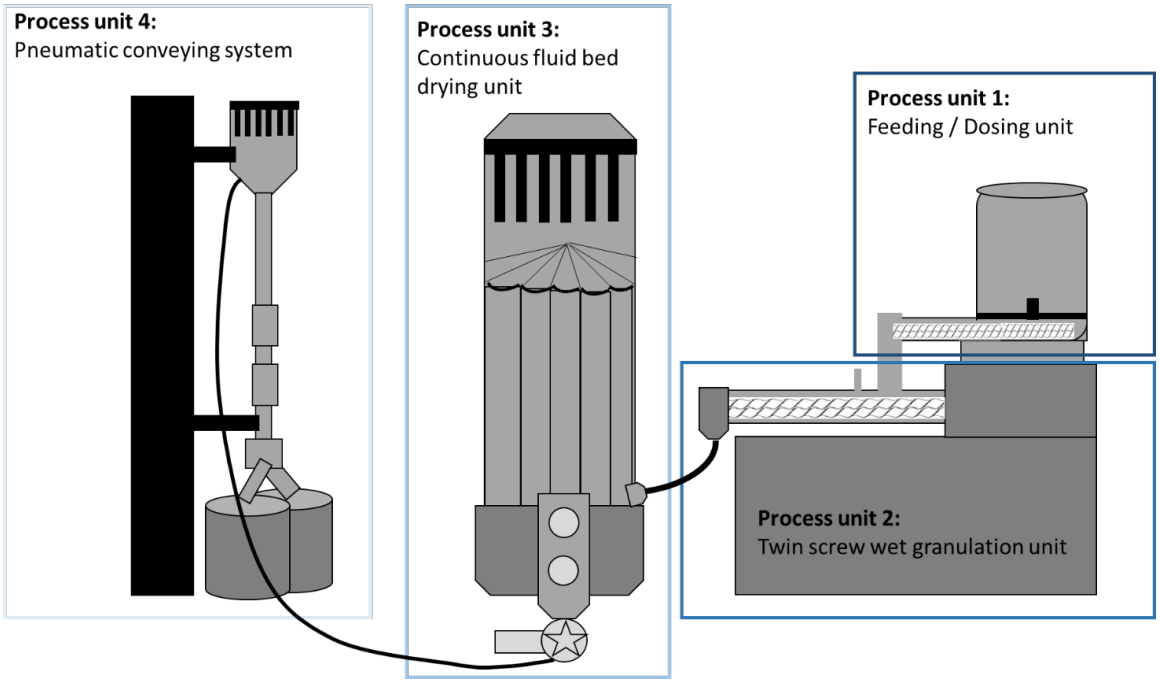

Figure 3 Overview on general experimental setup of the continuous granulation & drying line (source of the screw pictures: [109])

For the continuous granulation step the both process units feeding / dosing (process unit 1) and twin screw wet granulation (process unit 2) are essential. Continuous dosing is performed within this thesis using twin screw feeders. The twin screw feeder continuously doses the powder material into the twin screw granulator. More theoretical details of twin screw feeding can be found in chapter 4.1. Inside the twin screw wet granulator (process unit 2) particle agglomeration takes place by intermixing / shearing of powder material and granulation liquid (more theoretical aspects see chapter 5.1).

The important process units for the continuous drying step are of course the continuous fluid bed drying unit (process unit 3) and additional the pneumatic conveying system (process unit 4). More explanation on the continuous fluid bed drying system used within this thesis can be found in chapter 6.1. The pneumatic conveying system facilitates a smooth transportation of dry granules out of the dryer into the collecting container and is therefore – especially at larger scale equipment – beneficial.

The following table (Table 1) gives an overview on the included process units and the corresponding manufacturing chapter per results & discussion chapter (chapters 4 – 9).

Table 1 Overview on used process units, equipment, and corresponding manufacturing chapter per results & discussion chapter

Results & Discussion chapter	**Process unit 1:** Feeding / Dosing	**Process unit 2:** Twin screw wet granulation	**Process unit 3:** Continuous fluid bed drying unit	**Process unit 4:** Pneumatic conveying system	Equipment	Corresponding manufacturing chapter
chapter 4	x	-	-	-	volumetric dosing system ZD 12 FB	11.1.4.1
chapter 5	x	x	x	x	M-line	11.1.4.3.3 11.1.4.3.4
chapter 6	x	x	x	x	M-line	11.1.4.3.3 11.1.4.3.4
chapter 7	x	x	x	x	XS-line S-line M-line	11.1.4.3.1 11.1.4.3.2 11.1.4.3.3 11.1.4.3.4
chapter 8	x	x	x	x	M-line	11.1.4.3.3 11.1.4.3.4
chapter 9	x	x	-	-	volumetric dosing system ZD 12 FB twin screw granulator ZE 16	11.1.4.2

4. POWDER CHARACTERISATION OF STARTING MATERIALS USING VOLUMETRIC DOSING

As dosing is always the first process step within a continuous manufacturing process chain, it is essential to gain knowledge about this specific process step to avoid issues in the subsequent process steps. The set feed rate of the dosing step persists along the entire process chain. Therefore, an accurate feed rate over time is essential.

The aim of this chapter is to link material attributes of raw material (excipients) and mixtures of these excipients to their dosing behaviour. Therefore different excipients and binary mixtures (see Table 21) were characterised according to their material attributes (particle size distribution via sieve analysis, bulk and tap density, and flowability value FFC determined by a ring shear tester; see chapter 4.2) in a first step. In a next step, experiments were performed using a volumetric feeding mode (experimental setup see 11.1.4.1) instead of a gravimetric feeding mode for that investigation. Using a volumetric operation mode material attributes directly affect the powder feed rate, whereas using a gravimetric operation mode changes in material attributes of powder can be masked by the gravimetric controller. Linking the material attributes with the observed volumetric dosing behaviour enabled to figure out the importance of the material attributes regarding an accurate dosing feed rate over time (= good dosing behaviour).

4.1 THEORETICAL ASPECTS

The most common feeders, being used for dosing processes within continuous pharmaceutical manufacturing, are the loss-in-weight feeders (LIW) [5, 9, 24, 25, 26, 27, 39, 40, 47, 60, 67, 117, 119, 124, 125]. The general setup of such a loss-in-weight-feeder with its three main components is depicted in Figure 4. The three main components are [5, 24, 25]:

1. volumetric feeder
2. load cell
3. gravimetric controller

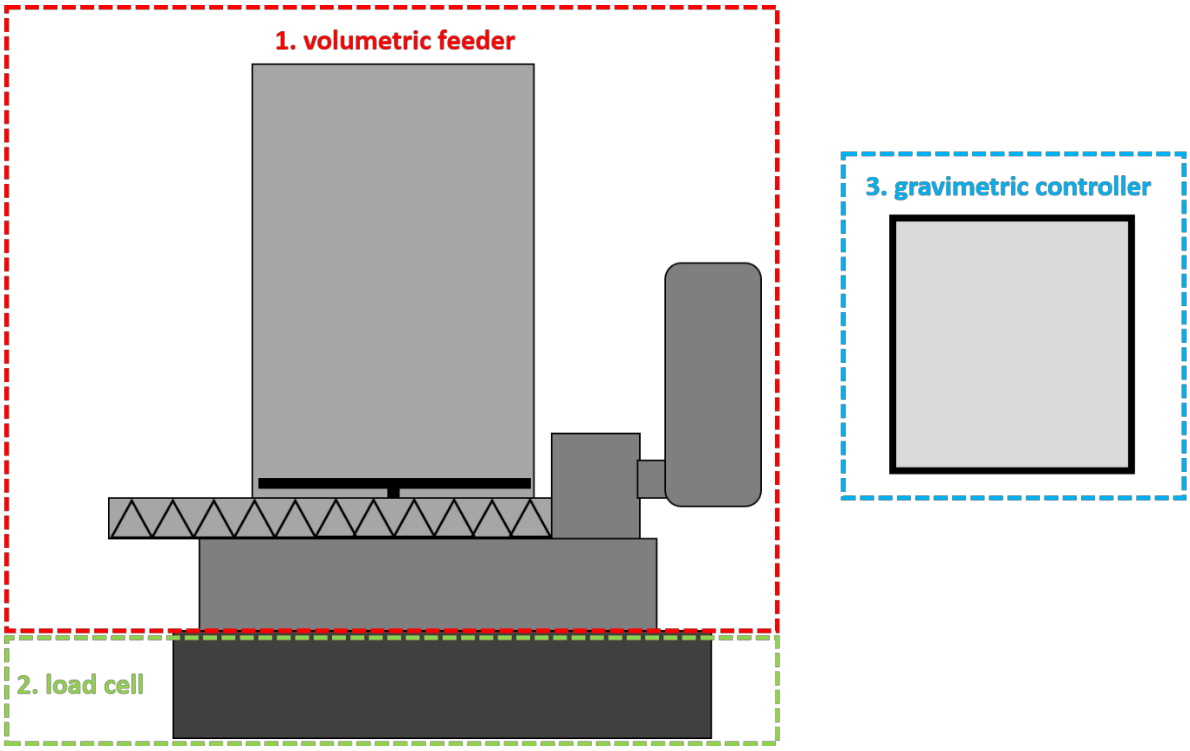

Figure 4 Overview on the three main components of a loss-in-weight feeder [5, 24, 25]

The loss-in-weight feeder can be operated in an either volumetric or a gravimetric mode [5, 24, 25, 27, 40]. In a volumetric operation mode, the screws of the feeder transporting the powder are running at a constant screw speed resulting in a certain powder feed rate. Changes in powder feed rate may occur in this operation mode, as inconsistencies in the powder bulk directly affect the powder feed rate [39]. Furthermore, a decrease of the powder feed rate at decreasing fill level inside the hopper was observed by several researchers [26, 40]. Therefore, the volumetric feeding mode is not as reliable and accurate as the gravimetric feeding mode. For the gravimetric operation mode, the dosed mass per time unit is simultaneously measured by a balance (load cell) the feeder is sitting on. Based on this measurement a gravimetric controller controls the screw speed of the feeder in order to keep powder feed-rate as constant as possible and to avoid deviations. For the gravimetric mode, a calibration is mandatory [39] in order to have an accurate powder feed rate already from start of the dosing process step on.

Loss-in-weight-feeders offer a broad variance of accessories in terms of screw and hopper design (see Figure 5) [9, 24, 40, 60, 124, 125] to optimize powder feed-rate and the emptying behaviour of the hopper for various powders.

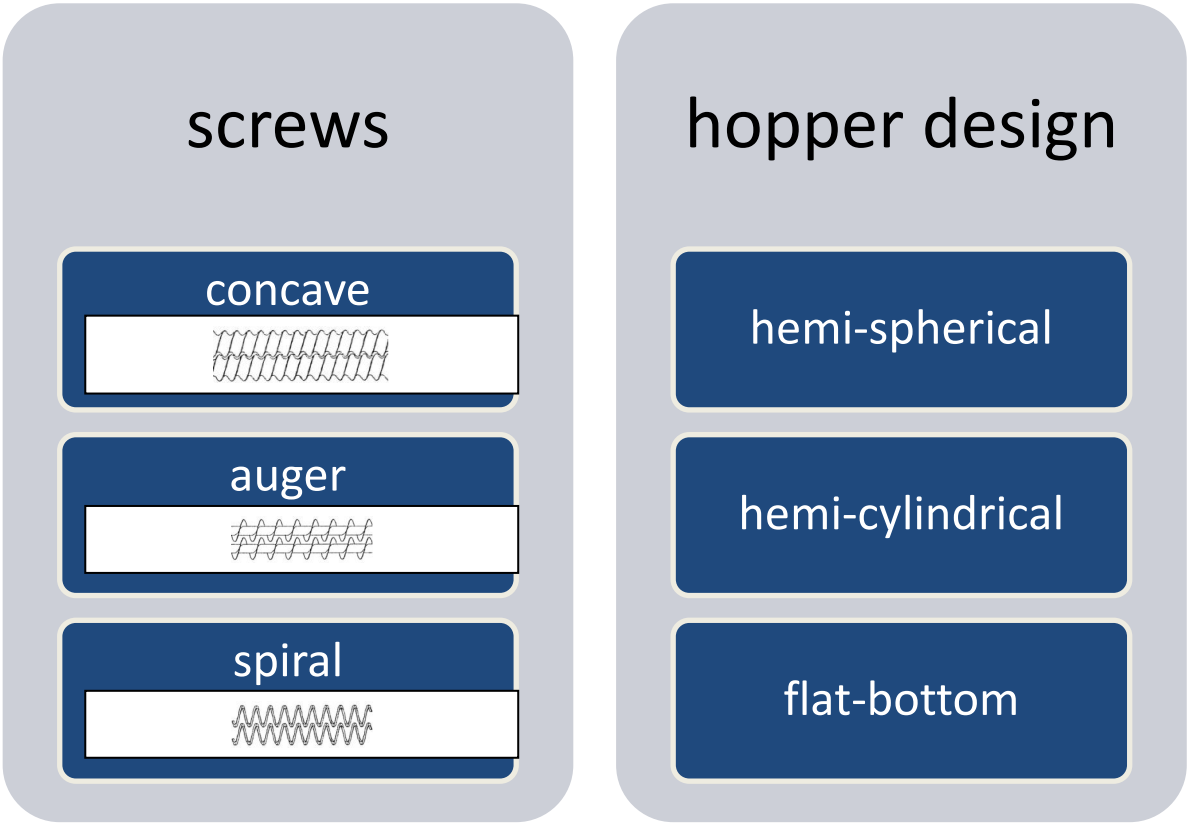

Figure 5 Accessories for loss-in-weight feeders: screws and hopper design (source of the screw pictures: [110])

An additional point that must be considered is the refill regime. Engisch et al. [26] evaluated the importance of hopper fill level FL [%] for refilling. Additionally, they found more frequent and short refilling times to be beneficial in terms of accurate powder feed-rate.

Feedability – the possibility to accurately feed a certain powder feed rate over time - is also been affected by different material properties of powder bulk like flowability behaviour and the bulk and tap density [25, 27, 60, 117, 124, 125]. Knowing these relationships between material attributes and feedability, helps to avoid possible challenges like adhesion of powder to the screws or bridging of powder inside the hopper [24, 25] and to optimize dosing process at the same time.

As dosing is always the first step within continuous processes knowledge about residence time distributions [47, 119] and the impact on resulting process intermediates like granules [47, 67] is essential, too.

4.2 INVESTIGATION OF MATERIAL ATTRIBUTES OF RAW MATERIALS AND BINARY MIXTURES

As described above, all excipients and binary mixtures thereof were characterized for their bulk and tap density (see 11.2.2.2), as well as for their flowability by determination of the FFC value with a ring shear tester (see 11.2.2.5). The results of that characterisation are given in Table 2 (n=3; average is given). Bulk and tap densities of the investigated powder bulks were in a broad range between 0.34 g/mL (MCC) and 1.03 g/mL (CA) for bulk density and between 0.46 g/mL (MCC) and 1.50 g/mL (CA) for tap density.

As all FFC values reached a value < 4, excipients and mixtures were in the range of a cohesive (2 < FFC < 4) or even very cohesive (1 < FFC < 2) flow behaviour [103].

Table 2 Characterization of raw materials and preblends (binary mixtures) according to density (bulk and tap density; n=3), flowability (FFC; n=3) and particle size distribution (D10, D50, 90; only raw materials; sieve analysis; n=1)

raw material / preblend	avg bulk density [g/mL] (n=3)	avg tap density [g/mL] (n=3)	avg FFC [-] (n=3)	D10 [µm]	D50 [µm]	D90 [µm]
MCC	0.34	0.46	2.9	9	45	88
MAN	0.52	0.76	1.8	9	47	108
LAC	0.53	0.82	1.9	10	51	106
STundried	0.54	0.71	1.3	7	33	59
ST1500	0.63	0.84	3.7	12	58	138
CA	1.03	1.50	1.7	7	35	63
LAC:MCC = 2:1	0.47	0.71	2.3	-	-	-
MAN:MCC = 2:1	0.46	0.64	2.5	-	-	-
MAN:STundried = 1:1	0.53	0.72	1.7	-	-	-
CA:MCC = 2:1	0.71	1.07	2.6	-	-	-
LAC:MCC = 1:2	0.40	0.55	2.9	-	-	-
MAN:MCC = 1:2	0.38	0.53	3.0	-	-	-
MAN:STundried = 9:1	0.54	0.78	2.0	-	-	-

The raw materials (excipients) were additionally characterized for their particle size distribution (PSD) by sieve analysis (see 11.2.2.4, n=1). D50 [µm] was in a range between 33 µm (STundried) and 58 µm (ST1500). So, all excipients were quite fine regarding the PSD and no big differences between the excipients became visible.

Comparing the different material attributes, it came up that the densities (bulk and tap density) were the main driver for differences between the excipients and binary mixtures as FFC values and PSD parameters were quite similar for all excipients and binary mixtures.

4.3 RELATIONSHIP BETWEEN MATERIAL ATTRIBUTES AND VOLUMETRIC DOSING BEHAVIOUR

Volumetric dosing experiments for all excipients and mixtures were performed like described in chapter 11.1.4.1. Figure 6 shows the dependence of dosed mass per revolution on the filling level of the hopper – exemplary for the three excipients lactose, mannitol and microcrystalline cellulose. Fill level of the hopper was calculated according to equation (1).

$$fill\ level_{hopper}[\%] = \frac{mass_{actual_{hopper}}[kg]}{mass_{maximum_{hopper}}[kg]} * 100 \quad (1)$$

For the experiments presented in this chapter a 100 % fill level was defined to be at 80 % nominal fill level of the hopper. The maximum mass which the hopper is capable to be filled with was calculated based on the measured bulk density of the certain excipient or mixture and the 80 % volume of the hopper.

For the experiments presented in chapter 8.1 a 100 % fill level was defined to be at a 100 % nominal fill level of the hopper. Therefore, the maximum mass of the hopper was determined empirically by testing the maximum mass of powder preblend the hopper was capable to be filled with.

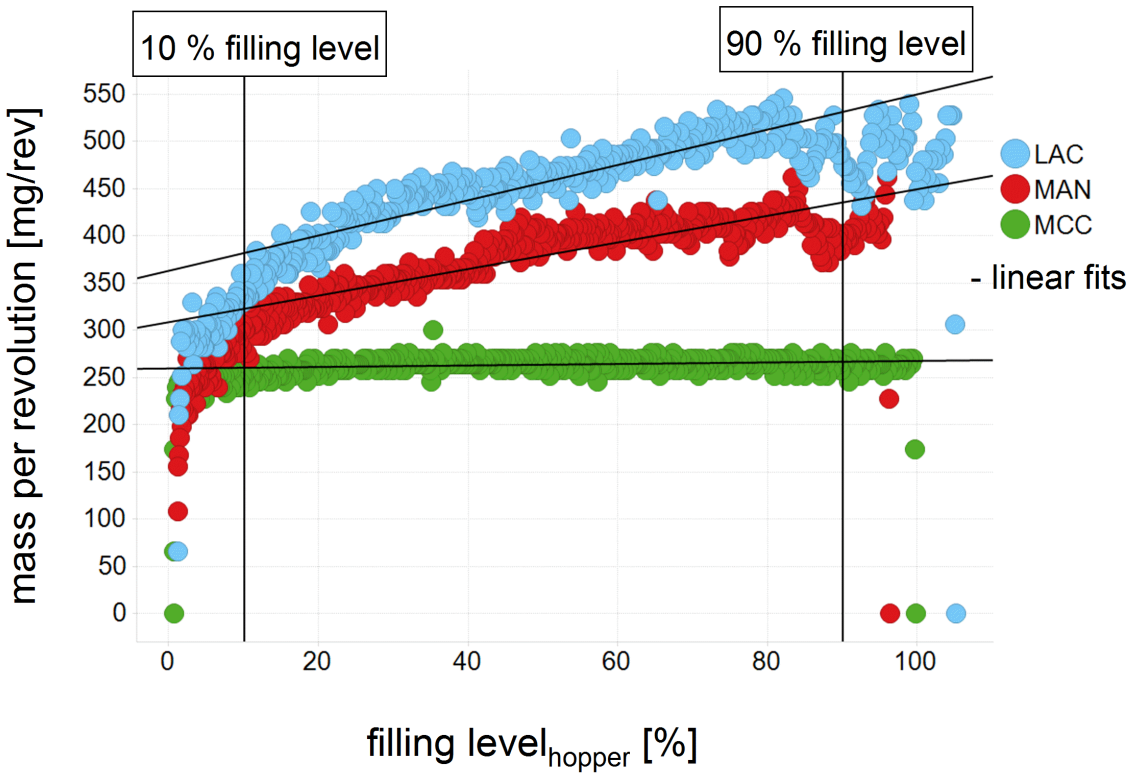

Figure 6 Dependence of dosed mass per revolution on filling level of the hopper; different colours: excipients; screw speed of volumetric feeder = 50 rpm; linear fits according to equation (2) between 90 % and 10 % of hopper filling level

The dosed mass per revolution decreased with decreasing fill level of the hopper which is in accordance with several other researchers [26, 40].

Furthermore, the dosed mass per revolution was different for each excipient and mixture. The dosed mass per revolution for a volumetric feeding mode depends on two parameters – the free volume inside the screws (equipment factor = const) and the density of the dosed material (material attribute = different per excipient and mixture). A linear correlation could be observed plotting mass per revolution at a hopper fill level of 90 % measured at a feeder screw speed = 200 rpm against the bulk density of each excipient and mixture (see Figure 7). This correlation was also found by Li et al. [60] and Van Snick et al. [117].

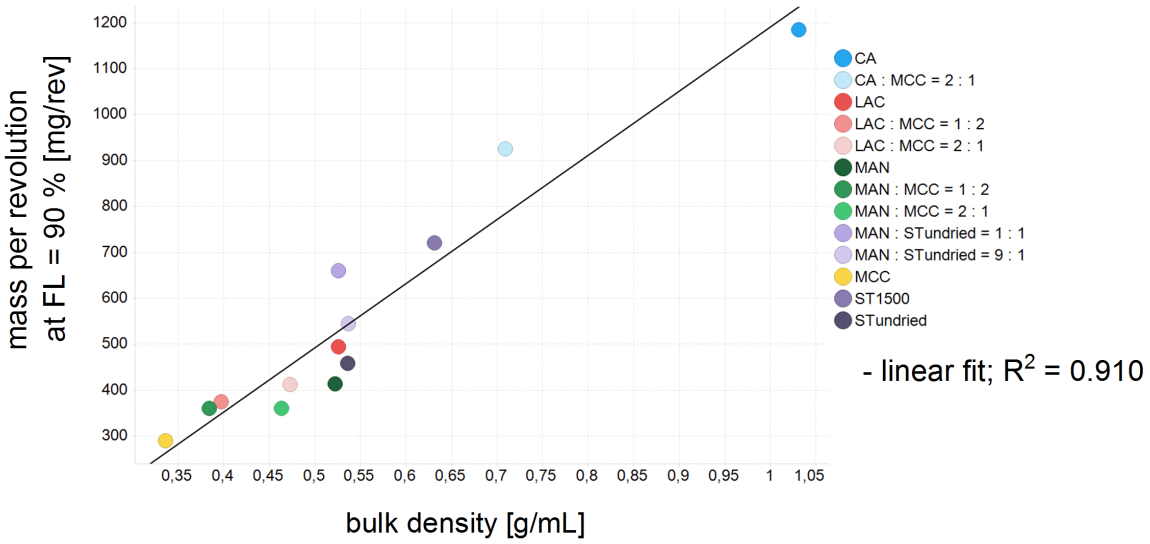

Figure 7 Linear correlation between bulk density [g/mL] and dosed mass per revolution [mg/rev] at a feeder screw speed = 200 rpm for all raw materials and binary mixtures

In a next step, linear fits for each excipient and mixture were calculated for the relationship between dosed mass per revolution measured at a certain screw speed (50 rpm, 125 rpm and 200 rpm) and the fill level of the hopper (see Figure 6 exemplarily) in a range between 10 % fill level and 90 % fill level according to equation (2). The upper limit of 90 % filling level was chosen to exclude effects regarding the dosed mass per revolution during the start-up phase of each dosing experiment (between 100 % and 90 % hopper filling level) from the linear fit. The lower limit of 10 % filling level was taken to avoid confounding of the linear fits by effects during the shutdown phase (e.g., emptying of the screws, strong decrease of dosed mass per revolution in a filling level range between 0 % and 10 %).

$$mass\ per\ revolution\ \left[\frac{mg}{rev}\right] = a * \left[\frac{mg}{rev * \%\ FL}\right] * FL\ [\%] + b\ \left[\frac{mg}{rev}\right] \quad (2)$$

The average slope *a* of equation (2) for the three different applied screw speeds was defined as dosing parameter *a.* Plotting *a* against the quotient of the two material attributes bulk density and flowability value FFC a linear correlation could be found (see Figure 8).

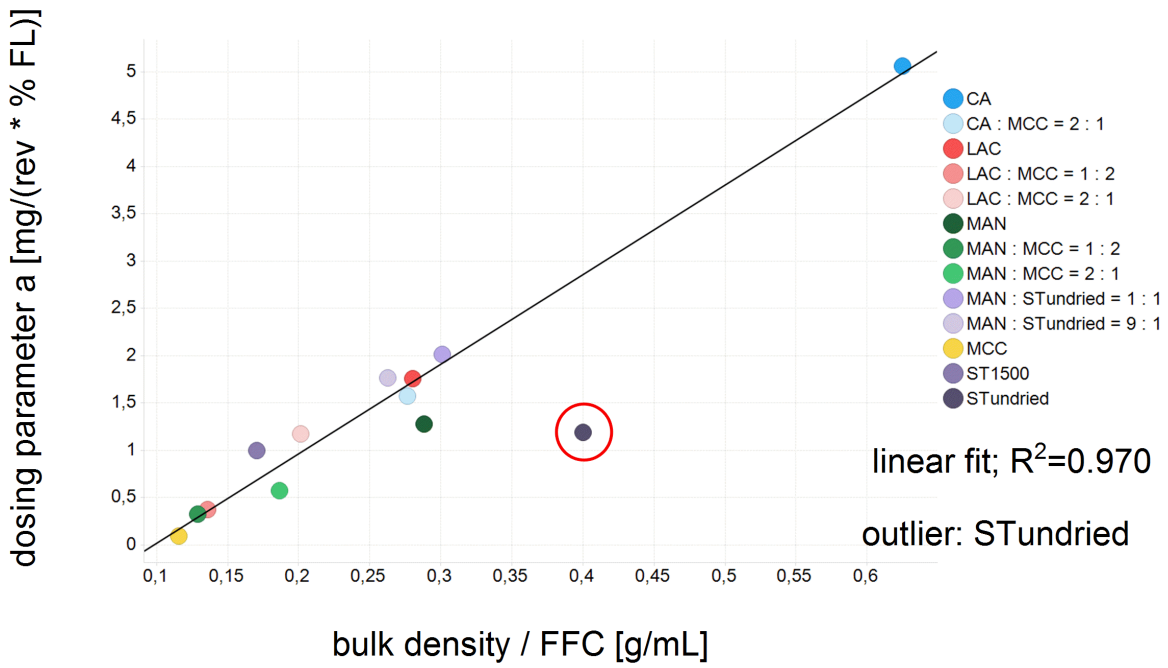

Figure 8 Correlation between dosing parameter *a* and the quotient *bulk density / FFC* of single excipients and binary mixtures

These correlations (see Figure 7 and Figure 8) show that good volumetric dosing behaviour (= constant dosed mass per revolution during emptying of the hopper) is mainly affected by bulk density and flowability of the powder bulk. A low dosing parameter a < 1.2 indicating a good volumetric dosing behaviour was obtained at bulk densities BD < 0.5 g/mL and flowability values FFC ≥ 2. As an outlier from that stated specification limits (BD, FFC and parameter a) Starch 1500 (ST1500) could be found. ST1500 resulted in a dosing parameter a = 1.0 indicating a good volumetric dosing behaviour, too, but did not hit the just given specification limits of bulk density (BD (ST1500) = 0.63 g/mL; FFC (ST1500) = 3.7). As the FFC value of 3.7 was the highest value (best flowability) compared to all other excipients and binary mixtures, that example showed that a higher bulk density BD > 0.5 g/mL could be compensated by a superior flow behaviour in that case. So, both parameters are important to estimate the dosing behaviour. Undried starch was identified as a total outlier of the correlation between dosing parameter *a* and the quotient of bulk density / FFC. Following the correlation found in-between the two parameters (*a* and quotient bulk density / FFC), Starch undried should have resulted in a higher dosing parameter *a* based on its quotient out of bulk density and FFC value than it actually did.

Reason for that could be the pronounced elastic behaviour of Starch undried. This behaviour could be also pointed out having a look at the correlation between Hausner ratio and flowability value FFC. For all other excipients and binary mixtures (without Starch undried) it was found that a higher FFC value led to a lower Hausner ratio. A low Hausner ratio as well as a high FFC value indicate a good flowing behaviour in general. For Starch undried that behaviour was different. Starch undried resulted in the lowest FFC value (FFC = 1.34) and the lowest Hausner ratio (HR = 1.33) of all excipients and binary mixtures at the same time. Hausner ratio is more driven by the densification of the powder whereas FFC value results out of a measurement of shearing powder and the cohesiveness of the powder facing / resisting that shear stress. Starch undried shows less densification under pressure (low Hausner ratio) but nevertheless a high cohesiveness (low FFC value) whereas all other excipients show a low Hausner ratio and a high FFC value (or vice versa) simultaneously. Therefore, FFC value is not the best indicator for volumetric dosing behaviour in case of the Starch undried as it does not consider the "special" densification behaviour of that material.

4.4 SUMMARY & QBD LEARNING

To sum up the evaluation of powder characterisation via volumetric dosing, several important relationships between material attributes of investigated excipients and mixtures and their volumetric dosing behaviour could be found:

1. Dosed mass per revolution decreases with decreasing fill level of the hopper (linear correlation between 10 % filling level and 90 % filling level).
2. Dosed mass per revolution at a certain fill level of the hopper depends on bulk density.
3. A good dosing behaviour (= accurate dosed mass per revolution during emptying of the hopper) is indicated by a low dosing parameter a < 1.2. A low dosing parameter a can be linked to the powder material attributes bulk density BD < 0.5 g/mL and flowability value FFC ≥ 2 (cohesive flowing behaviour at least or better). Starch (1500 and undried) are outliers to that general relationship. The explanations for that are given above (see chapter 4.3).

The evaluation of continuous dosing using a feeder in a volumetric feeding mode enabled to understand the relationship between material attributes and resulting dosing behaviour. Knowing these relationships is essential for a proper material selection for continuous manufacturing as continuous dosing is always the first step in a continuous process. As mentioned in the theoretical section using a gravimetric feeder (loss-in-weight feeder) the material attributes can be masked by the gravimetric controller facilitating to keep a constant feed rate over time. Evaluation of volumetric dosing behaviour can therefore be stated to be some kind of “worst case scenario” where one would assume that dosing behaviour of a certain excipient or binary mixture would even improve when switching from volumetric to gravimetric feeding mode.
More investigation on a refill regime for continuous dosing using a gravimetric feeding mode is described in chapter 8.1.

5. TWIN SCREW WET GRANULATION: IMPACT OF PROCESS PARAMETERS ON MATERIAL ATTRIBUTES

The subsequent process step after dosing is the twin screw wet granulation step. Several process parameters have to be defined for twin screw wet granulation process (liquid feed rate, powder feed rate, screw speed, barrel temperature) resulting in specific response parameters (moisture level, barrel filling level, particle size of granules, granule temperature) (see Figure 10). Experiments presented in this chapter were performed according to the description in chapters 11.1.4.3, 11.1.4.3.3 and 11.1.4.3.4.

Aim of this chapter is to evaluate the impact of process parameters and their response parameters for twin screw wet granulation process on the material attributes for resulting granules as well as tablets.

In a first step, two different formulations were compared with regard to their twin screw wet granulation performance at different process parameter settings (see 5.2). To assess granulation performance, several material attribute limits were predefined. Good granulation performance was to be stated at:

- particle fine fraction < 20 % (particle fraction p3 < 63 µm; measured with dynamic image analysis (Camsizer))
- flowability value FFC > 4 at least indicating an easy flow behaviour (FFC value determined with Schulze ring shear tester)
- residual water content < 2.5 % (measured via Loss-on-drying method using a halogen dryer)

In a second step, the impact of different methods of binder addition during the twin screw wet granulation process were evaluated for one of the formulations (see Figure 23).

5.1 THEORETICAL ASPECTS

Wet granulation as a pharmaceutical process technique offers several advantages compared to a process technology without granulation step like e.g. direct compression. Direct compression can be challenging if the API and/or the formulation show poor flowability, sticking, segregation, compaction or bioavailability issues [11]. Applying a (wet) granulation technique can mask and improve such challenging attributes of the API, therefore it is reasonable to include granulation as an additional process step in that cases. A continuous wet granulation

technique is the twin screw wet granulation. Comparing this continuous wet granulation technique to traditional batch wet granulation techniques as high shear granulation or fluid bed granulation, twin screw wet granulation offers the advantage of no material intensive scale-up than observed for batch wet granulation processes [11].

Out of that reason, one additional driver for the transition from batch to continuous manufacturing is the replacement of batch high shear wet granulation (= batchwise operating "equivalent" to TSG process) by twin screw wet granulation. Therefore, several researchers compared batchwise high shear granulation with the new continuous twin screw wet granulation technique [48, 56, 70, 74] and found twin screw wet granulation performance to be equal or even better compared to batchwise high shear wet granulation.

Having a deeper look at twin screw wet granulation process, several important process parameters and their derived parameters exist. An overview is given in Figure 10.

Important design aspects of the twin screw granulator are the barrel temperature, the L/D ratio and the screw configuration.

The L/D ratio is the ratio between the length L of the barrel and the diameter D of the screw and enables comparison between different twin screw granulator scales, respectively.

Regarding screw configuration there are different screw elements available:

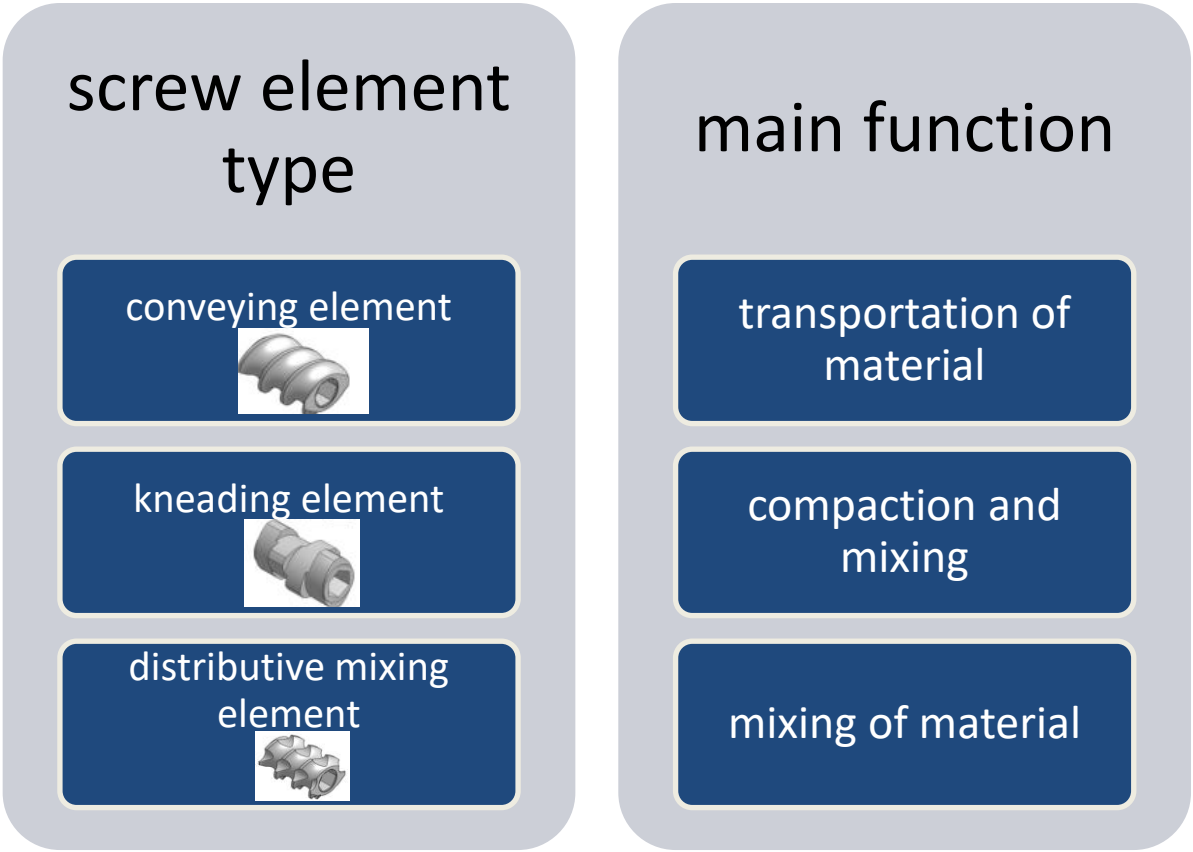

Figure 9 Overview on different screw elements available for TSG process (according to Seem et al. (2015) [104]) (source of the screw pictures: [111])

As the different screw elements have different functions, it is quite logical that using different screw configurations meaning different combinations of the available screw elements, has also impact on the resulting material attributes of the granules. These influences of screw configuration on granules attributes were investigated by several researchers [19, 51, 55, 59, 62, 98, 99, 108, 116, 120]. In general, they figured out to result in more dense and larger granules when kneading elements were part of the screw configuration.

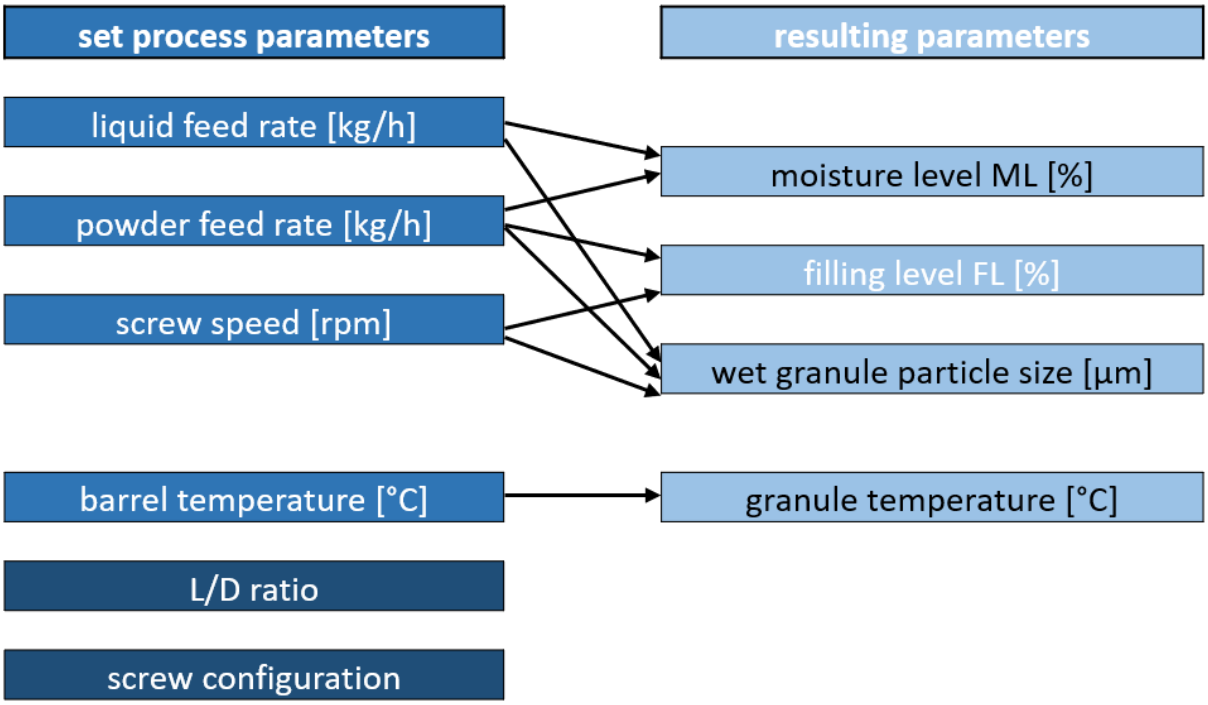

Figure 10 Set process parameters for continuous twin screw wet granulation process and their response parameters; black written response parameter: granule material attribute; white written response parameter: process condition

With regard to process parameters the two parameters defining the granulation moisture level (see equation (3)) are the liquid feed rate and the powder feed rate.

$$\mathrm{ML}\ [\%] = \frac{\mathrm{LFR}\ [\mathrm{kg/h}]}{\mathrm{PFR}\ [\mathrm{kg/h}] + \mathrm{LFR}\ [\mathrm{kg/h}]} * 100 \qquad (3)$$

The barrel filling level FL for a granulator equipped with conveying element screws (see equation (4)) is driven by the powder feed rate, the density of the powder preblend (bulk density), the screw speed of the granulator and the geometry of the granulator.

$$\mathrm{FL}\ [\%] = \frac{\frac{\mathrm{PFR}\ [\mathrm{kg/s}]}{\mathrm{density}_{\mathrm{powder}}\ [\frac{\mathrm{kg}}{\mathrm{m}^3}]}}{\frac{\mathrm{free\ volume}_{\mathrm{barrel}}[\mathrm{m}^3] * \mathrm{screw\ speed}\ [\mathrm{rps}]}{\mathrm{number\ of\ turns}}} * 100 \qquad (4)$$

The geometry of the granulator is represented in the formula by the free volume inside the barrel and the number of turns along the screw length. One turn is defined as a whole screw

joint. The length for such a whole screw joint along the screw is also called the pitch of the screw element. Therefore, for a screw consisting only of conveying elements with a pitch of 1 D, the L/D ratio is equivalent to the number of turns.

5.2 FORMULATION DEPENDENT TWIN SCREW WET GRANULATION PERFORMANCE

The two formulations F1 and F2 including Acetaminophen as model API in a DL of 5 % (compositions see Table 22 for F1 and Table 23) were compared according to their twin screw wet granulation behaviour using the M-line scale equipment (24mm TSG + MODCOS drying system; see chapter 11.1.4.3.3). For that purpose, the three process parameters/response parameters powder feed rate [kg/h], granulation moisture level ML [%] and barrel fill level FL [%] (equations see 5.1) were systematically varied. Overview on the experimental setup can be found in Table 3. A more detailed overview on all important process parameters including the drying parameters can be found in Table 32 in the appendix.

Table 3 Overview on experiments conducted for the evaluation of the granulation unit (24mm TSG [M-line scale]) for formulation 1 (F1) and formulation 2 (F2); blue = low level, green = middle level, red = high level

exp. no	PFR*$_1$ [kg/h] (F1 / F2)	ML*$_2$ [%] (F1 / F2)	barrel FL*$_3$ [%] (F1 / F2)	screw speed*$_4$ [rpm] (F1 / F2)	comment
1	15 / 10	15 / 10	19.8	225 / 150	processable
2	15 / 10	15 / 10	14.9	300 / 200	processable
3	15 / 10	23 / 20	19.8	225 / 150	processable
4	15 / 10	23 / 20	14.9	300 / 200	processable
5	20	19 / 15	17.3	343	processable
6	25 / 30	15 / 10	19.8	375 / 450	processable
7	25 / 30	15 / 10	14.9	500 / 600	processable
8	25 / 30	23 / 20	19.8	375 / 450	processable
9	25 / 30	23 / 20	14.9	500 / 600	not processable for F2

*$_1$ process parameter

*$_2$ response parameter

*$_3$ response parameter

*$_4$ process parameter

Differences in the experimental setup between formulation 1 (F1) and formulation 2 (F2) occurred with regard to the level for PFR and granulation ML. It was already evaluated by Schmidt et al. (2016) [99] that different formulations require different liquid-to-solid ratios which are directly linked to granulation ML (see equation (10)). As formulation 1 included cellulose in a significant amount, a higher granulation ML was necessary to obtain a proper agglomeration of particles. Cellulose is being stated to have a "sponge" effect [10, 29], i.e. water can be sucked into the cellulose reducing the available amount of granulation liquid.
Therefore, granulation ML was higher for F1 than for F2 (F1: ML1 = 15 %, ML2 = 23 %; F2: ML1 = 10 %, ML2 = 20 %). Because of the adaption of ML per formulation, PFR had to be adapted consequently. Aim of the experiments was a resulting moisture level enabling subsequent processing into tablets. The limiting step to reach this aim is the drying process as drying capacity of a continuous drying system is always limited to a certain PFR, which is formulation-dependent. Therefore, the range of PFR was limited to smaller PFRs for formulation 1 (F1: PFR1 = 15 kg/h, PFR2 = 25 kg/h; F2: PFR1 = 10 kg/h, PFR2 = 30 kg/h), as the granulation ML was higher.
The levels for barrel FL were the same for F1 and F2 and varied at a specific PFR by variation of screw speed. Barrel FLs were calculated for both formulations with an approximated powder bulk/tap density of 500 kg/m³.
Furthermore, for F2 the experiment no. 9 was not processable because the twin screw granulator was getting noisy at that process parameter setting (PFR = 30 kg/h, ML = 20 %, FL = 14.9 %, screw speed = 600 rpm). Reason for that was a disproportion of PFR and applied screw speed at that specified setting. A high screw speed in combination with a low barrel fill level is likely to result in a disbalance of screws as the screws of the used equipment (24mm TSG) are only fixed at one position.

5.2.1 Granule properties

Granules of all performed experiments were analysed according to their particle size distribution. The density distribution function (q3) plotted against the particle size and coloured by granulation ML is depicted in Figure 11 (F1) and Figure 12 (F2).

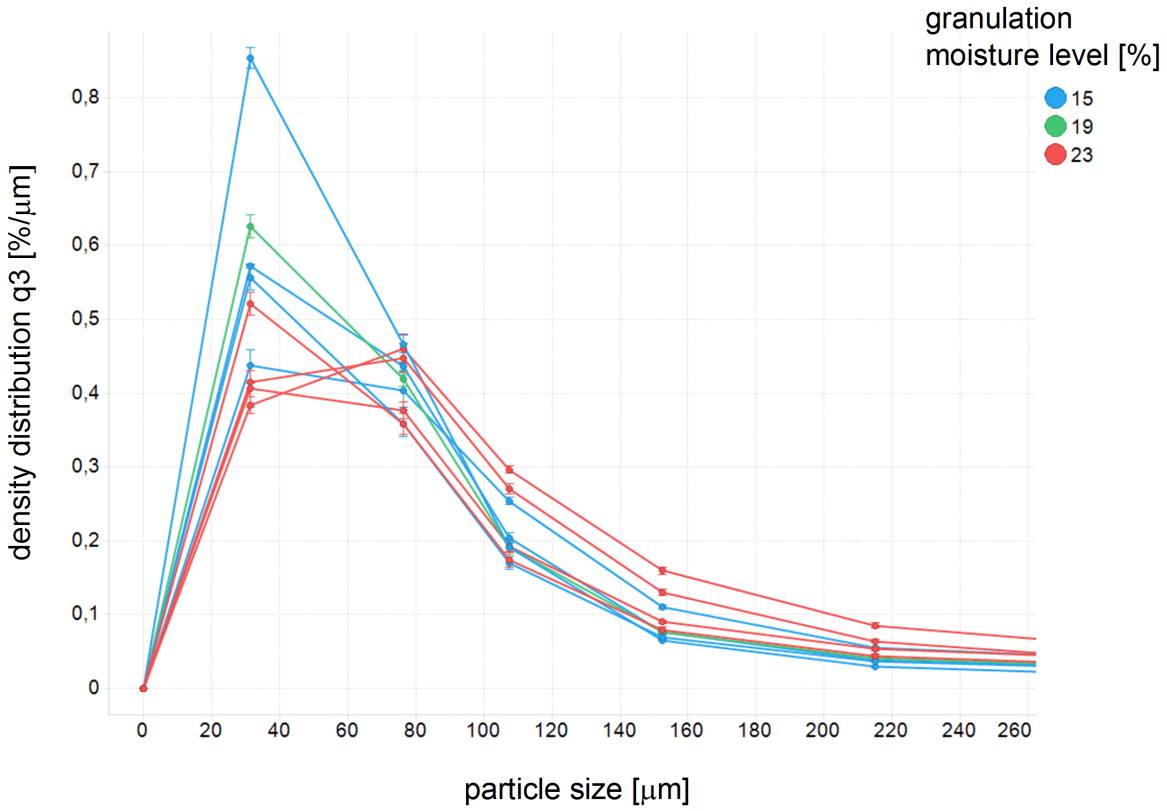

Figure 11 Density distribution q3 [%/µm] plotted against particle size [µm] from dynamic image analysis (Camsizer) for formulation 1 (F1), different colours: granulation ML [%]; n=3; error bars: +/- 1 SD

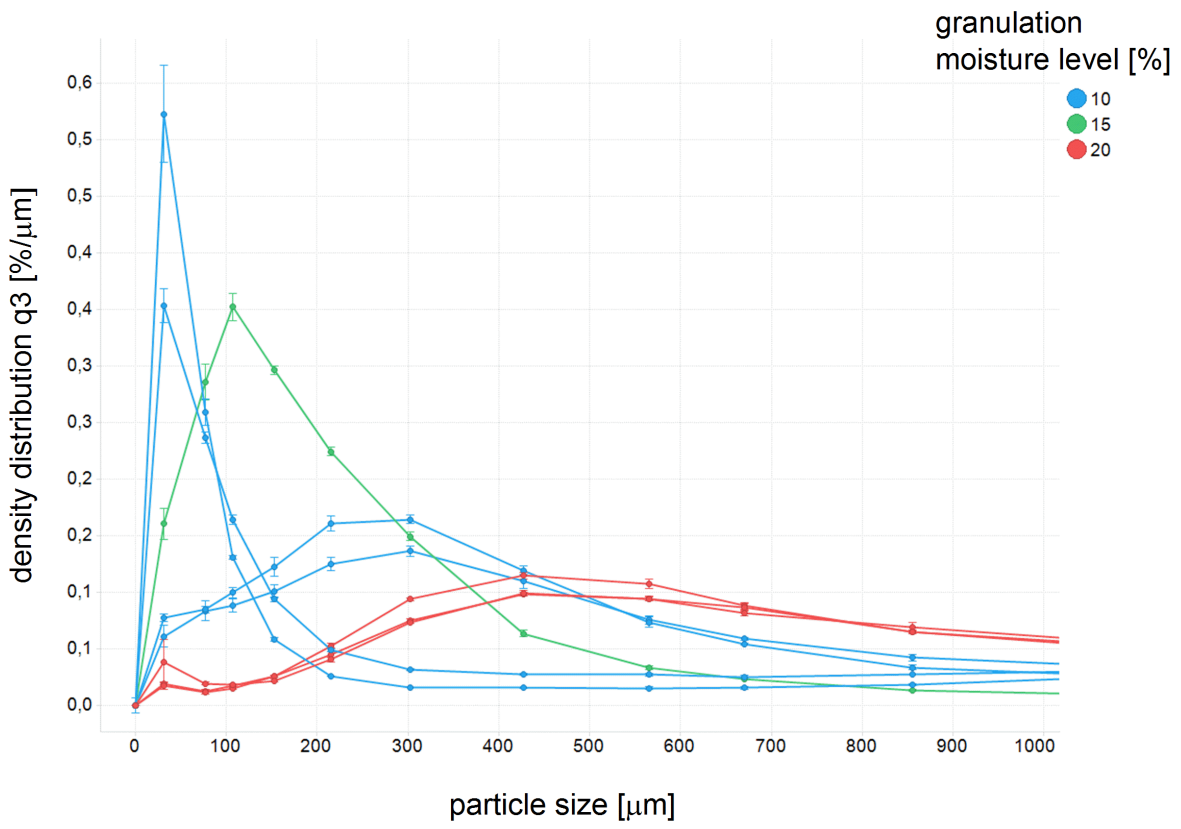

Figure 12 Density distribution q3 [%/µm] plotted against particle size [µm] from dynamic image analysis (Camsizer) for formulation 2 (F2), different colours: granulation ML; n=3; error bars: +/- 1 SD

For F1 no big differences between the density distribution curves became visible despite of one curve granulated at granulation ML = 15 % and resulting in smaller particle size (see Figure 11).

F2 showed more differences between the curves granulated at different granulation MLs (see Figure 12). The experiments at highest granulation ML = 20 % resulted in the largest particles. For the experiments granulated at ML = 10 % particles were smaller but also differences in-between the experiments occurred.

Sorting the particle density functions according to all three process parameters (granulation ML, PFR and barrel FL), more conclusions were possible (see Figure 13 for F1 and Figure 15 for F2). Furthermore, particle fine fraction (< 63 µm) and particle coarse fraction (> 1000 µm) sorted by all three process parameters is depicted in Figure 14 (F1) and Figure 16 (F2).

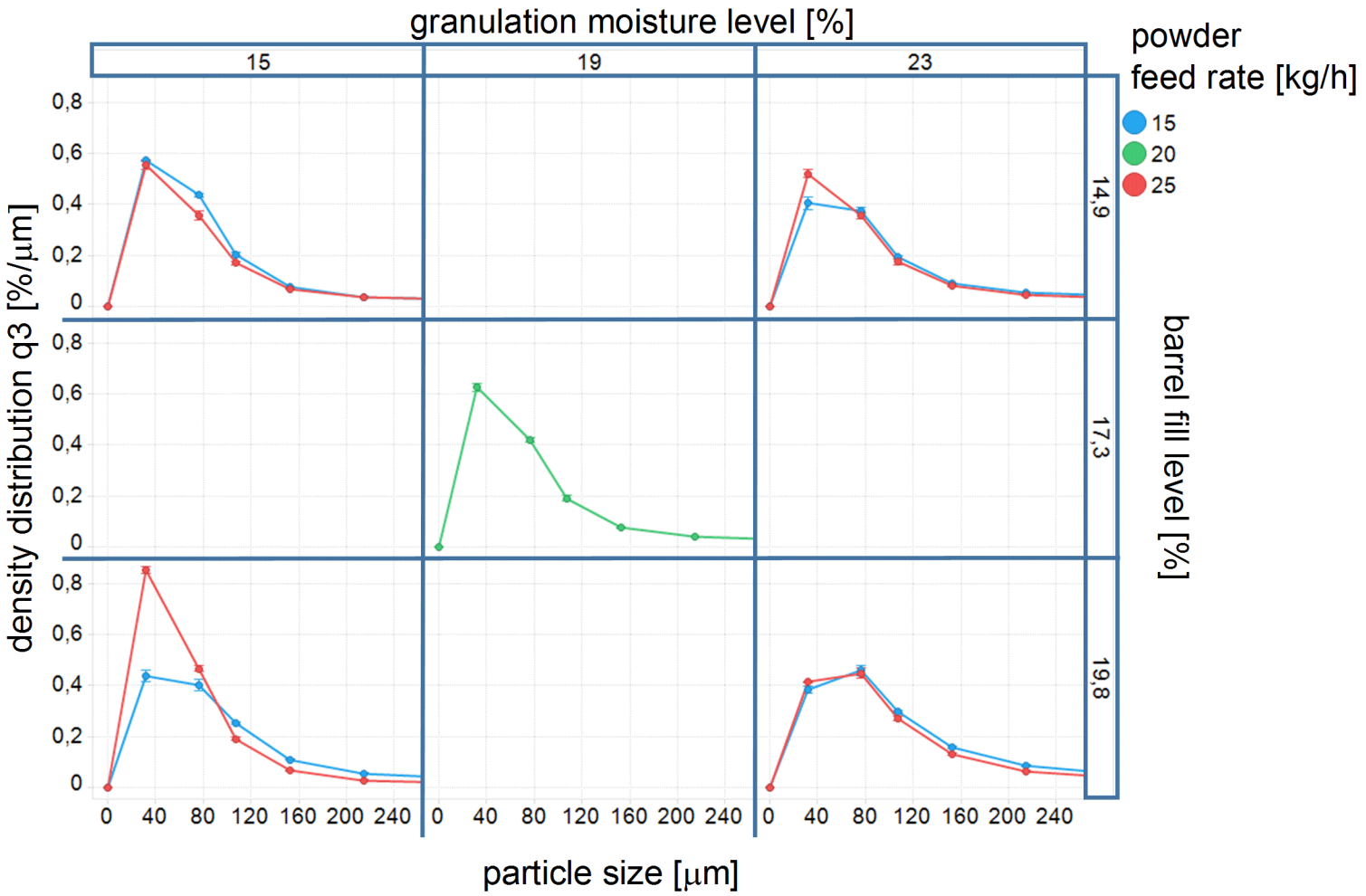

Figure 13 Density distribution q3 [%/µm] plotted against particle size [µm] for formulation 1 (F1); columns: different granulation ML [%]; rows: different barrel FL [%]; different colours: PFR [kg/h]; n=3; error bars: +/- 1 SD

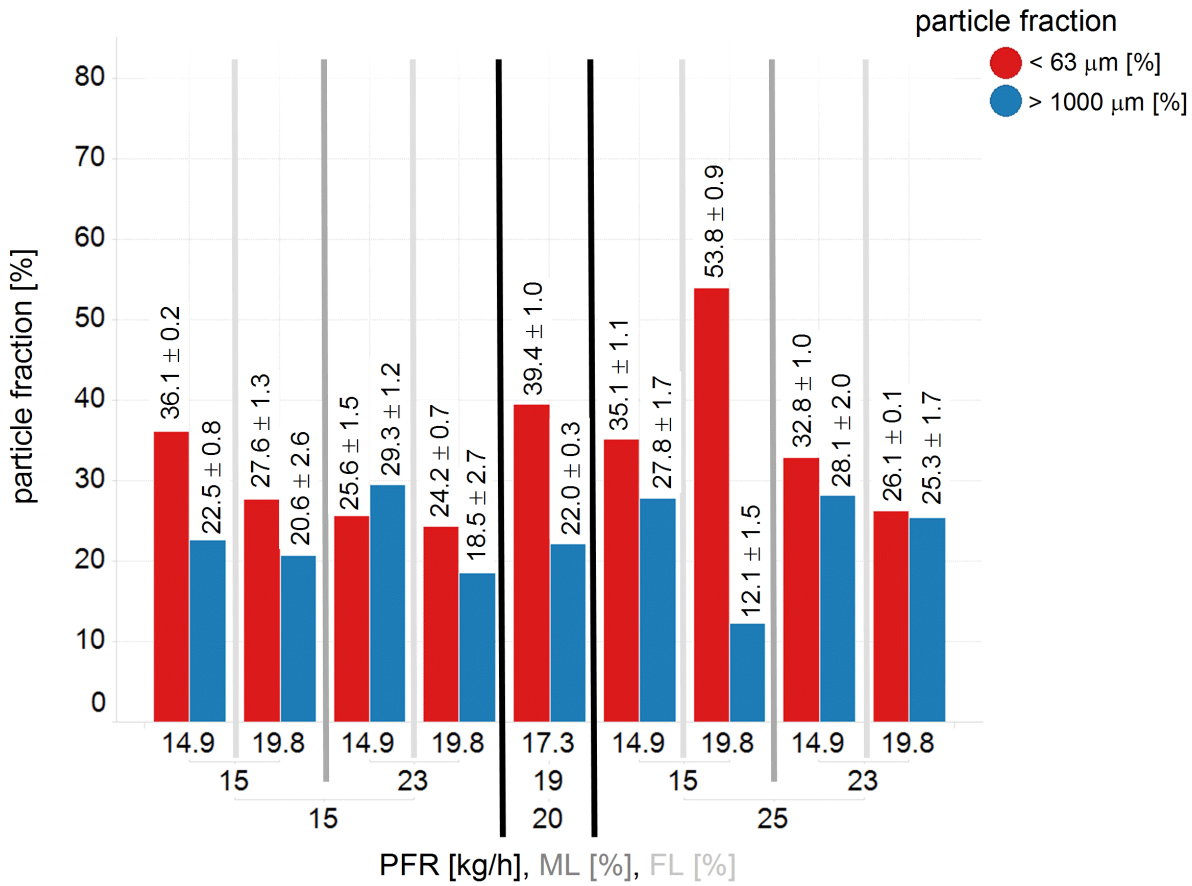

Figure 14 Particle fine fraction (< 63 µm; red bars) and particle coarse fraction (> 1000 µm, blue bars), sorted by PFR, granulation ML and barrel FL, for F1; n=3

Ranges for particle fine fraction were between 24.2 % and 53.8 % for F1 and between 1.1 % and 32.9 % for F2. So, using F1 the predefined target to result in a particle fine fraction < 20 % could not be reached. Coarse particle fraction ranged between 12.1 % and 29.3 % for F1 and between 2.8 % and 38.2 % for F2.

The impact of the three process parameters on particle size (fine fraction, coarse fraction, density function) for both formulations is discussed in the following.

Impact of **powder feed rate PFR [kg/h]**:

Adaption of PFR was linked to an adaption of screw speed at the same time to result in a specific equal barrel FL at a certain granulation ML (see Table 3). Therefore, increasing PFR went along with an increase in screw speed resulting in a higher shear energy and a lower residence time.

Particle fine fraction increased with increasing PFR for both formulations. The range of particle fine fraction for F1 for PFR1 = 15 kg/h was between 24.2 % and 36.1 % and for PFR2 = 25 kg/h between 26.1 % and 53.8 %. For formulation 2 the effect of increasing particle fine fraction at increasing PFR was especially pronounced at granulation ML = 10 % (see Figure 15 and Figure 16). At that low ML both, particle fine fraction and coarse fraction, were increasing with increasing PFR resulting in a more bimodal particle size distribution. Granules produced at ML = 20 % for F2 were that stable that increasing PFR, which results also in a lower residence time of granules inside the TSG, did not have any effect on particle size.

Impact of **granulation moisture level ML [%]**:

Comparing experiments performed at a specific PFR and barrel FL at high and low granulation ML, a decrease of particle fine fraction at increasing granulation ML could be detected for both formulations. For F2 that decrease was more pronounced at a high PFR = 30 kg/h, whereas at a low PFR = 10 kg/h particle fine fraction was also quite low (< 5 %) for the experiments performed at the low granulation ML = 10 %. Particle coarse fraction was increasing with increasing granulation ML for the experiments using F2, which were produced at the low PFR = 10 kg/h. For F1 no effect of granulation ML on particle coarse fraction could be found. So overall for both formulations, it can be stated that granulation ML has an impact on agglomeration behaviour of particles leading to a decrease of ungranulated particle fraction (= particle fine fraction) and formulation-dependent to an increase of coarse particle fraction, too.

Impact of **barrel filling level FL [%]**:

Different barrel FLs for the experiments were obtained by adapting screw speed at a specific PFR (see Table 3). So as a result, experiments at a low barrel FL were performed at a higher granulator screw speed, a higher shear energy and a lower residence time inside the granulator compared to the ones performed at a high barrel FL.

For both formulations particle fine fraction was decreasing with increasing barrel FL, comparing the experiments conducted at a specific PFR and granulation ML. One outlier for F1 occurred at the following process parameter settings (PFR = 25 kg/h, ML = 15 %, FL = 19.8 %).That means that using a higher densification of particles inside the barrel and

having a longer residence time inside the granulator at the same time, lead to a better agglomeration of particles and therefore to a decrease of ungranulated particle fraction.

Regarding the coarse particle fraction impact of barrel FL was different for the both formulations. Experiments with F1 lead to a decrease of coarse particle fraction at high barrel fill level whereas F2 showed an increase of coarse particle fraction at a high barrel fill level for the experiments conducted at a low PFR = 10 kg/h. The experiments performed at a high PFR = 30 kg/h showed no clear impact of barrel FL on coarse particle fraction. As barrel FL is directly linked to the screw speed of the granulator this evaluation showed that the formulation containing cellulose (F1) showed a more homogeneous agglomeration of particles (low particle fine fraction and coarse particle fraction) at conditions, where the residence time is longer, the shear energy is lower and the densification is higher inside the granulator (= high barrel fill level). For formulation 2 containing starch this effect was shown to be the other way around with regard to coarse particle fraction. So coarse fraction could be decreased at conditions of higher shear energy, shorter residence time and lower densification (= low barrel fill level).

As formulation 2 showed overall the better agglomeration and granulation behaviour compared to formulation 1, it was not surprising that for F2 a shorter residence time and a lower densification where sufficient to reach an adequate agglomeration of particles.

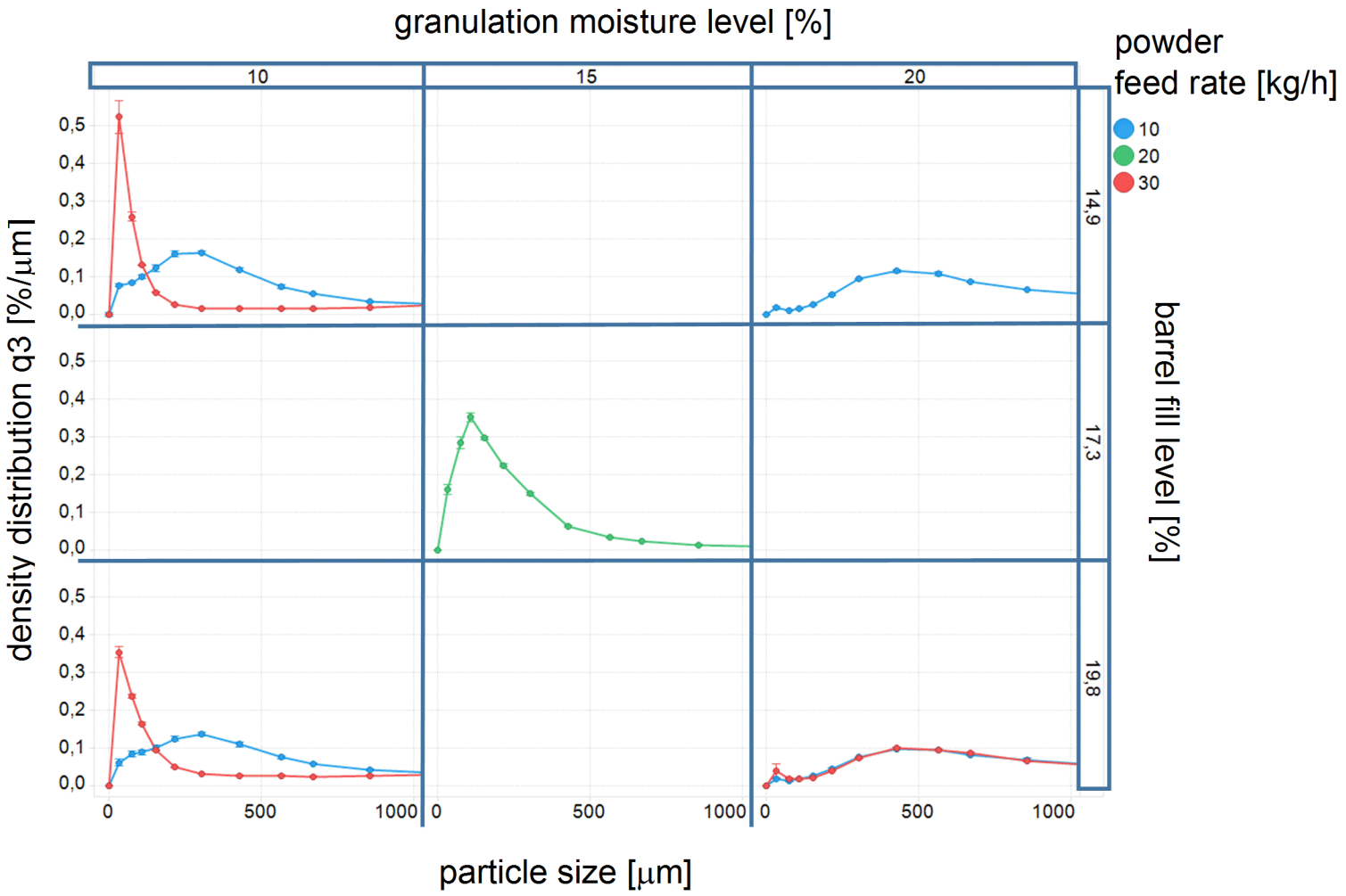

Figure 15 Density distribution q3 [%/µm] plotted against particle size [µm] for formulation 2 (F2); columns: different granulation ML [%]; rows: different barrel FL [%]; different colours: PFR [kg/h]; n=3; error bars: +/- 1 SD

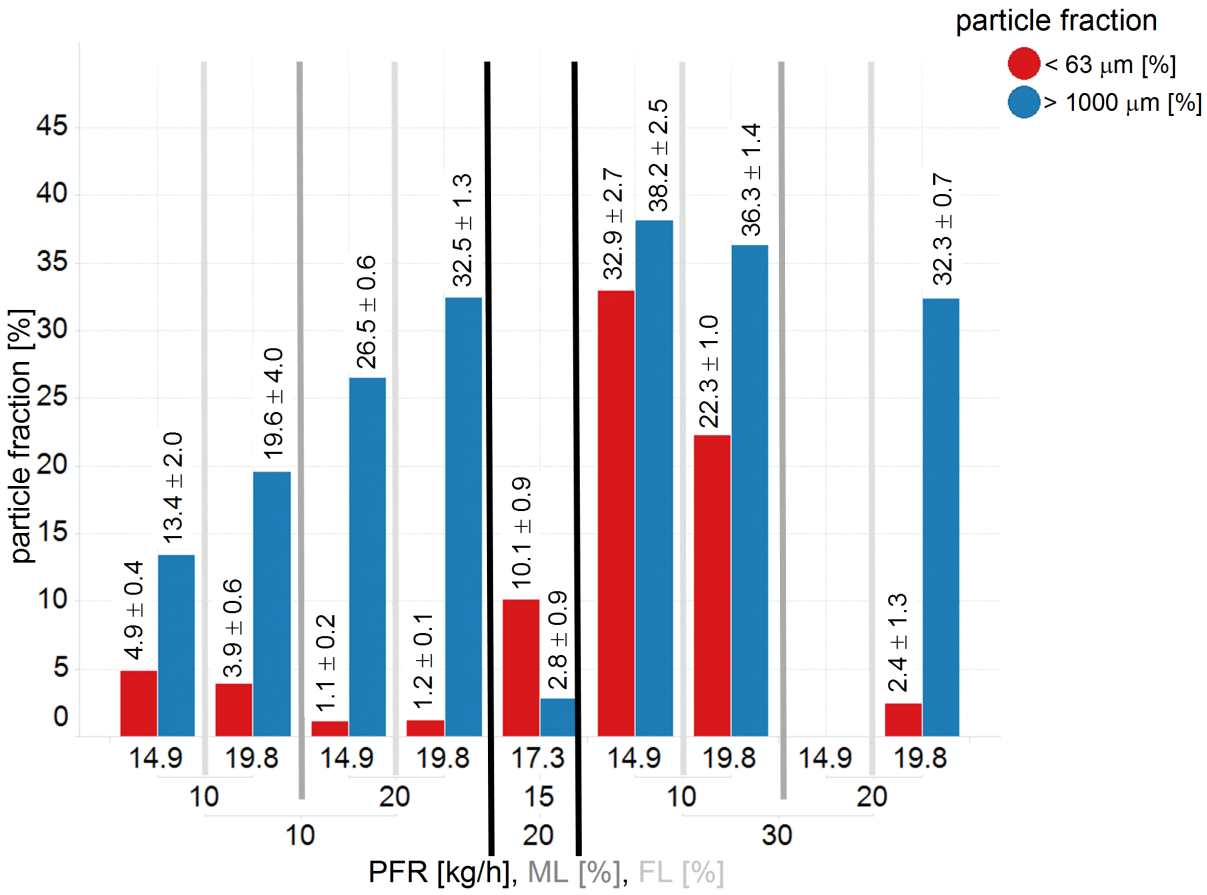

Figure 16 Particle fine fraction (< 63 µm; red bars) and particle coarse fraction (> 1000 µm, blue bars), sorted by PFR, granulation ML and barrel FL, for F2; n=3

The impact of PFR, granulation ML and barrel FL on flowability value FFC [-] and residual water content of the dried granules (LoD) is depicted in Figure 17 for F1 and Figure 18 for F2. The reference FFC value of the ungranulated physical mixture (PM) is also given in both figures.

For F1 all FFC values were in a range between 4 and 10 indicating an easy flowability independent of process parameter settings. Looking at F2 more differences with regard to flowability occurred. All experiments resulted in a FFC value > 10 indicating a free flowing behaviour despite of the ones produced at high PFR and low granulation ML. These two experiments resulted in an either good flowability value (FFC = 5.0 at high barrel FL) or even cohesive flowability behaviour (FFC = 2.7 at low barrel FL).

With regard to LoD values of dried granules all experiments of both formulations resulted in a LoD < 2 % despite of one outlier for each formulation. These outliers could be identified to be the ones produced at high PFR and high granulation ML.

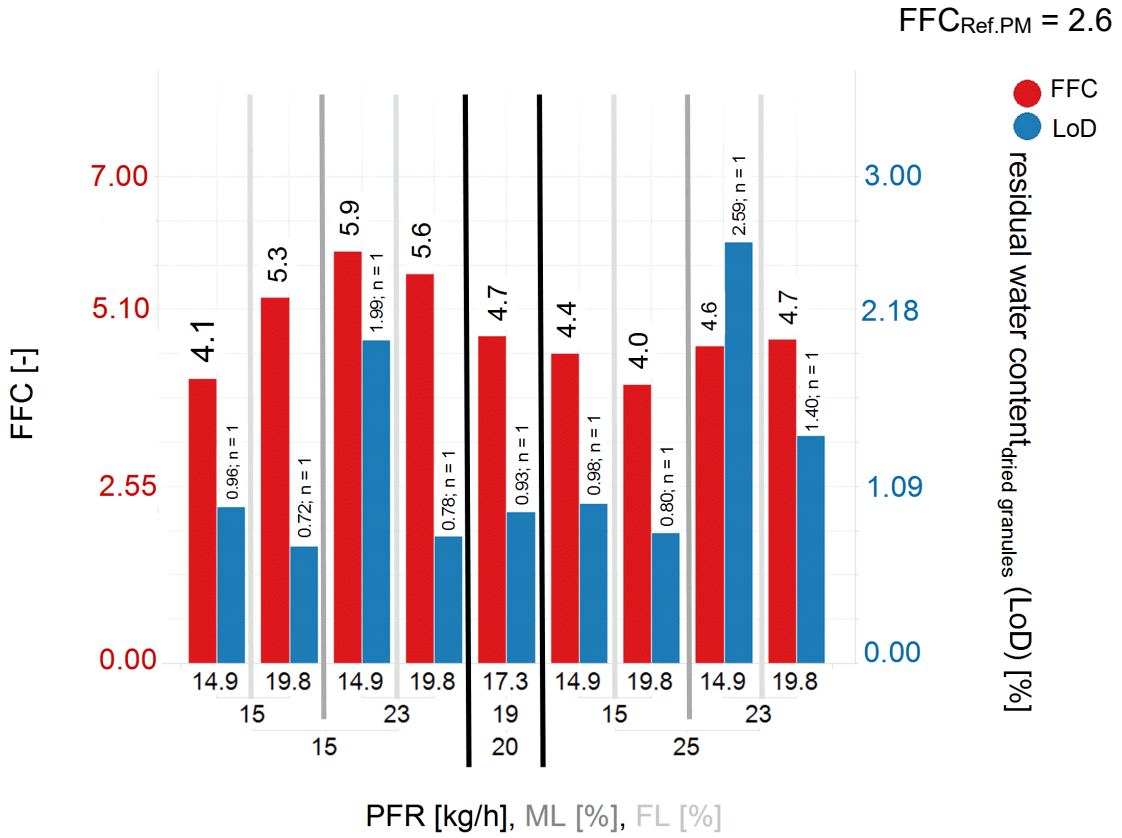

Figure 17 Flowability value FFC ([-]; red bars) and residual water content of dried granules ([%]; blue bars), sorted by PFR, granulation ML and barrel FL, for F1;

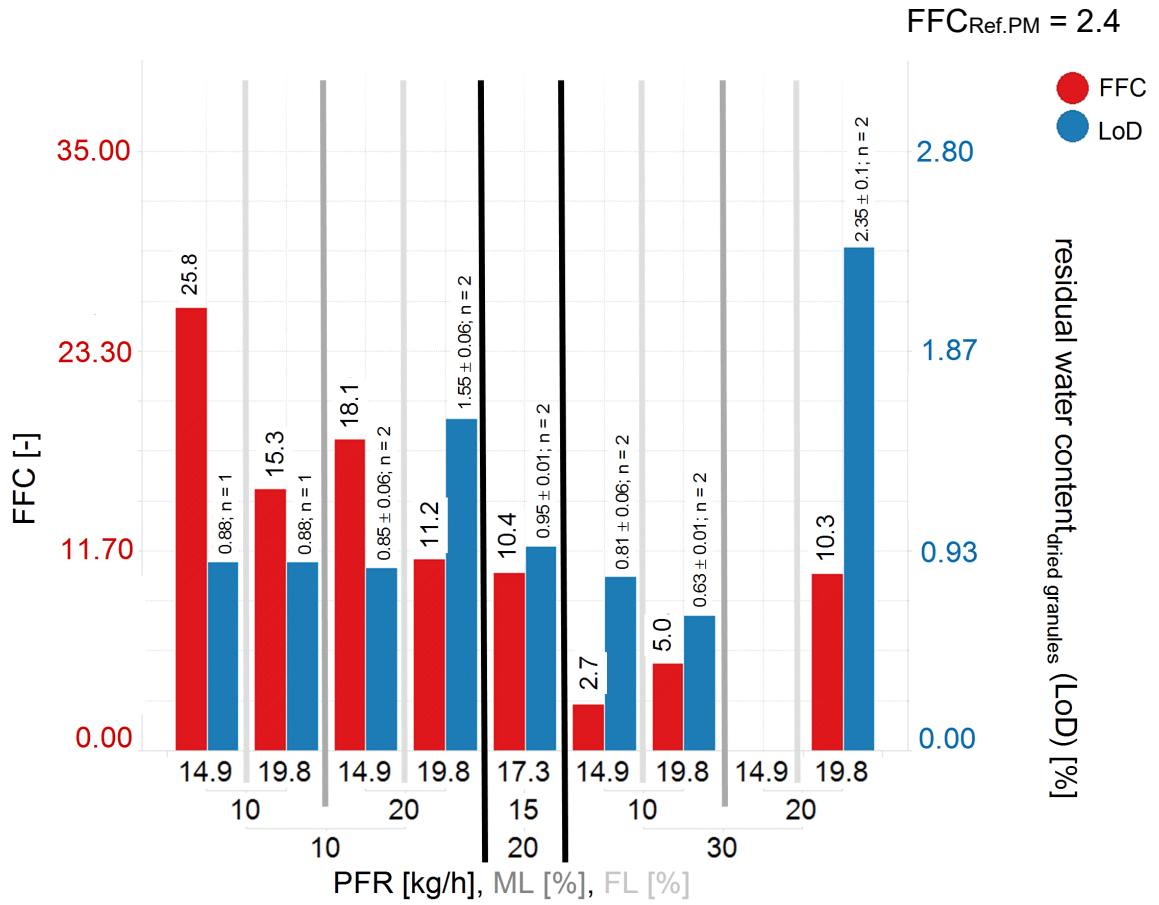

Figure 18 Flowability value FFC ([-]; red bars) and residual water content of dried granules ([%]; blue bars), sorted by PFR, granulation ML and barrel FL, for F2;

5.2.2 Tablet properties

All granules for both formulations and all different process parameter settings were compressed to tablets according to the description in chapter 11.1.6. Tablets were analysed with regard to their dimensions, mass and crushing strength which enabled to calculate tensile strength TS [N/mm²] and solid fraction SF [-]. Tensile strength TS and solid fraction SF were plotted against compression pressure CP [MPa] and sorted by the three different varied process parameters PFR, granulation ML and barrel FL in Figure 19 and Figure 20 for formulation 1 (F1) and in Figure 21 and Figure 22 for formulation 2 (F2). Tabletability is defined as the possibility to form a tablet with a certain tensile strength TS at a certain compression pressure CP (TS vs. CP), whereas compressibility is defined as the ability to form a tablet with a certain densification (solid fraction SF) at a certain compression pressure CP (SF vs. CP) [112].

The minimum and maximum TS [N/mm²] and SF [-] values for both formulations at lowest and highest applied compression pressure CP [MPa] and compared to ungranulated physical mixture (PM) at lowest CP = 94 MPa are given in Table 4.

Table 4 Minimum and maximum TS [N/mm²] and SF [-] values for both formulations at lowest and highest applied compression pressure CP [MPa]; comparison to ungranulated physical mixture (PM) at lowest CP = 94 MPa

	CP = 94 MPa						**CP = 468 MPa**					
	F1			**F2**			**F1**			**F2**		
	Min	Max	Ref. (PM)	Min	Max	Ref. (PM)	Min	Max	Ref. (PM)	Min	Max	Ref. (PM)
TS [N/mm²]	1.06 ± 0.04	1.24 ± 0.03	0.89 ± 0.04	0.53 ± 0.03	1.21 ± 0.05	0.24 ± 0.04	4.12 ± 0.09	4.61 ± 0.09	-	4.24 ± 0.19	4.81 ± 0.16	-
SF [-]	0.809 ± 0.003	0.821 ± 0.003	0.780 ± 0.004	0.780 ± 0.051	0.815 ± 0.003	0.768 ±0.002	0.921 ± 0.004	0.928 ± 0.003	-	0.921 ± 0.007	0.941 ± 0.032	-

As given in the Table above, ranges for F1 were smaller for TS and SF at the different CPs compared to F2 indicating that variation of process parameters for TSG had higher impact on tableting behaviour for F2 than for F1. Comparing the values to the ungranulated physical mixture (PM), especially F2 showed a strong improvement of TS values for tablets made out of granules (2.2 – 5 times better TS values).

Furthermore, for F2 the granules produced at high PFR and low ML could only be compressed to a maximum CP = 281 MPa because of high ejection forces during tableting process.

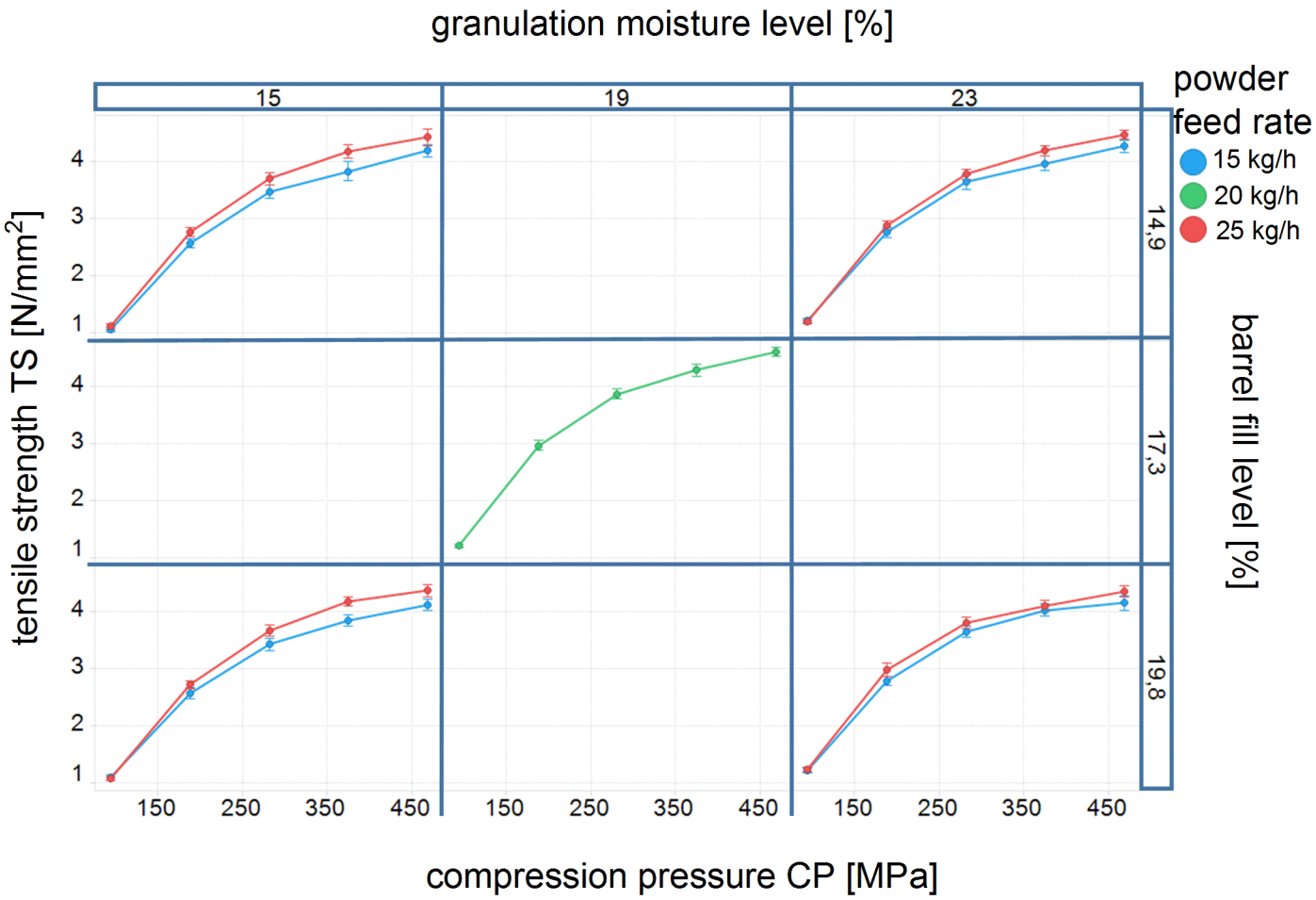

Figure 19 Tensile strength TS [N/mm²] plotted against compression pressure CP [MPa] for formulation 1 (F1); columns: different granulation ML [%]; rows: different barrel FL [%]; different colours: PFR [kg/h]; error bars: +/- 1 SD

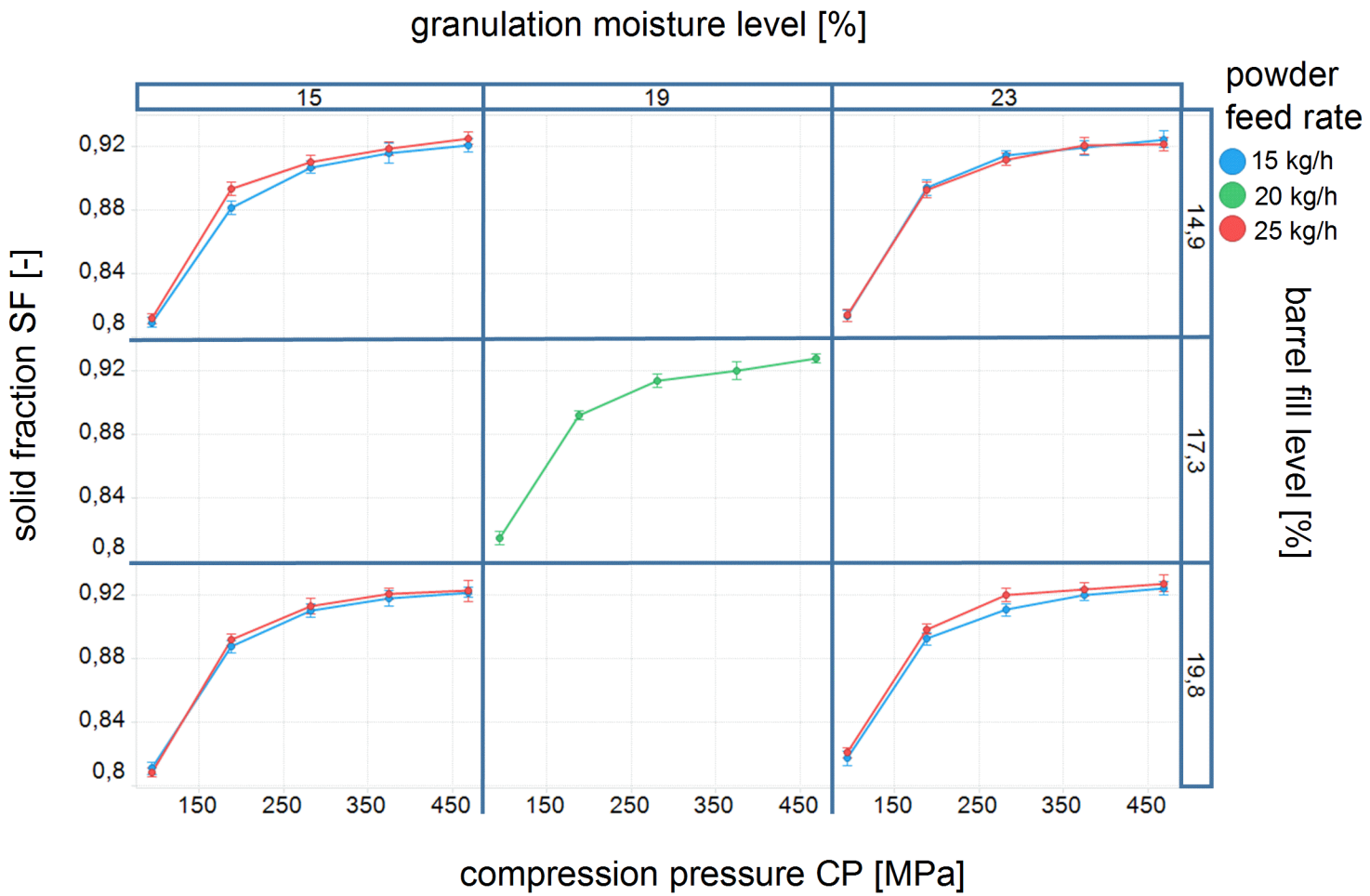

Figure 20 Solid fraction SF [-] plotted against compression pressure CP [MPa] for formulation 1 (F1); columns: different granulation ML [%]; rows: different barrel FL [%]; different colours: PFR [kg/h]; error bars: +/- 1 SD

Impact of **powder feed rate PFR [kg/h]**:

Influence of PFR on tabletability and compressibility behaviour was different for both formulations. Increasing PFR lead to a slight increase of TS and had no influence on SF for F1 whereas increasing PFR resulted in a lower TS and SF especially at low granulation ML = 10 % for F2.

Impact of **granulation moisture level ML [%]**:

Granulation ML had no influence on tabletability and compressibility for F1 and for the experiments of F2 performed at a low PFR = 10 kg/h. The experiments of F2 conducted at a high PFR = 30 kg/h resulted in a higher TS and a slightly higher SF at higher granulation ML. This indicates that PSD had different influence on tabletability and compressibility behaviour for both formulations. As a higher ML resulted in a lower particle fine fraction for both formulations a higher particle fine fraction lead to no effect on tableting behaviour for F1 and a decreased tabletability for F2.

Impact of **barrel fill level FL [%]**:

F1 showed no influence of barrel FL on tabletability and compressibility. For F2 barrel FL had impact on tabletability at specified process parameter settings. Increasing FL lead to a slight increase of TS at a high PFR = 30 kg/h.

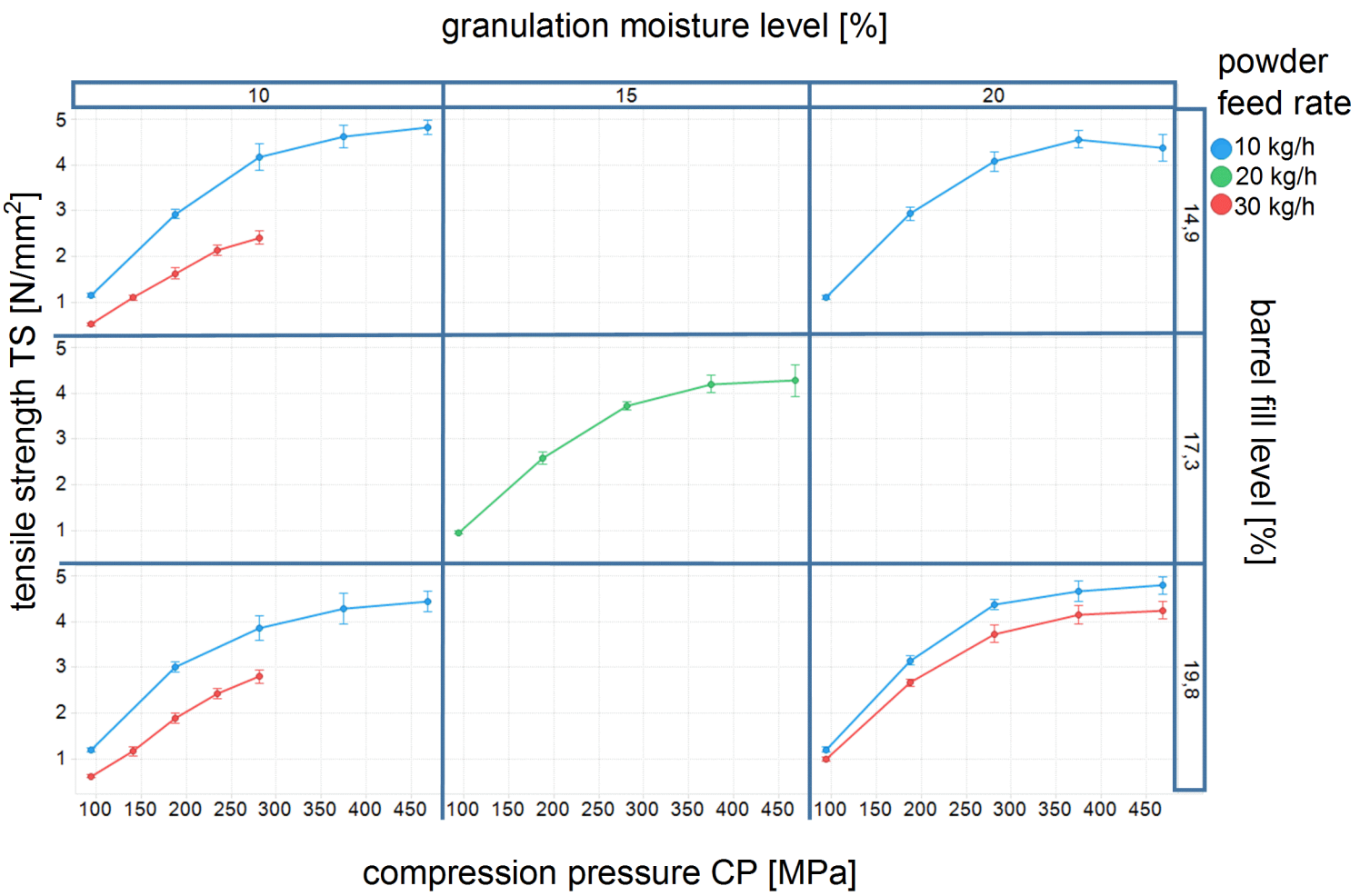

Figure 21 Tensile strength TS [N/mm²] plotted against compression pressure CP [MPa] for formulation 2 (F2); columns: different granulation ML [%]; rows: different barrel FL [%]; different colours: PFR [kg/h]; error bars: +/- 1 SD

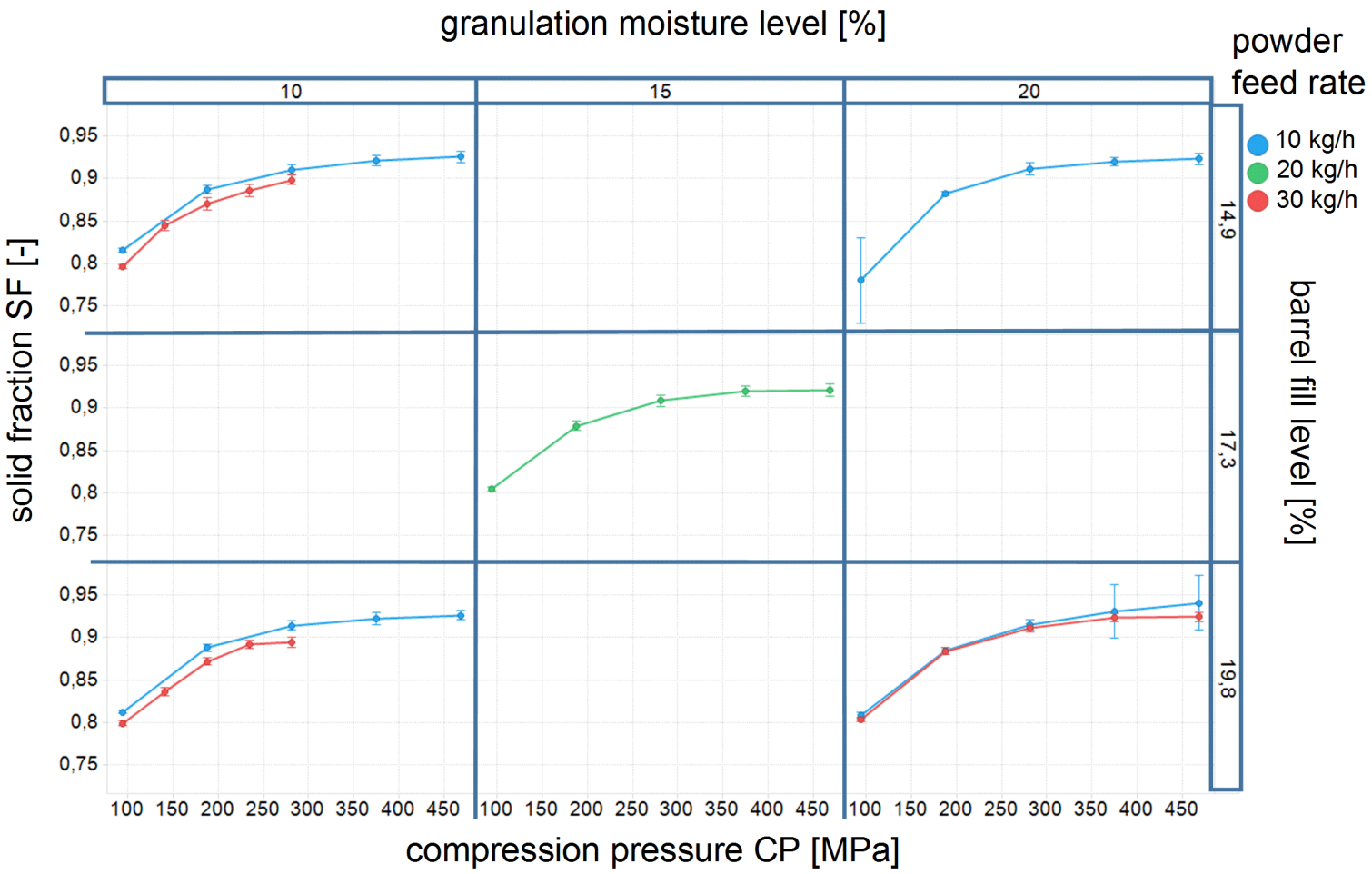

Figure 22 Solid fraction SF [-] plotted against compression pressure CP [MPa] for formulation 2 (F2); columns: different granulation ML [%]; rows: different barrel FL [%]; different colours: PFR [kg/h]; error bars: +/- 1 SD

All in all, with regard to tablet properties it could be figured out that PFR had impact on tableting behaviour for both formulations but in a contrary way. Furthermore, it could be found that granulation ML and barrel FL had only impact on tabletability and compressibility for F2 but not for F1. So, F1 was in total more independent of applied granulation process parameter settings but leading also to an adequate tableting behaviour in terms of tensile strength and solid fraction.

5.3 INVESTIGATION ON BINDER ADDITION MODES FOR FORMULATION 1

As granulation behaviour was evaluated to be worse for F1 compared to F2 with regard to particle size distribution and reduction of particle fine fraction during granulation (fine fraction > 20 % for all experiments using F1), it was decided to conduct additional experiments for F1 using the 24 mm TSG incl. the Modcos drying equipment (M-line scale equipment) again. This observation has also already been described in literature where the benefits of Copovidone compared to HPMC in terms of granule strength and particle agglomeration were figured out [89, 113].

Therefore, experiments were performed with different binder addition modes and for three different granulation MLs. Binder was either added to powder preblend (as in all previous experiments; see 5.2) or to the granulation liquid (see Figure 23).

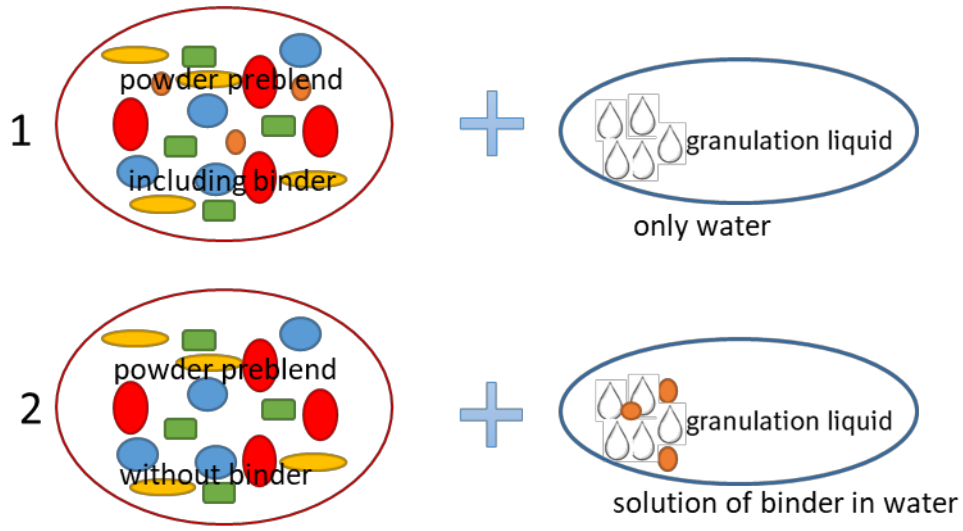

Figure 23 Binder addition modes: 1 – binder added to powder preblend; 2 – binder added to granulation liquid

Aim of this investigation was to evaluate whether granulation behaviour could be improved by adding the binder to the water und preparation of a granulation liquid. All other granulation process parameters were kept constant to guarantee comparability (PFR = 15 kg/h; screw speed = 175 rpm). An overview on all relevant process parameters (granulation and drying unit) for these experiments can be found in Table 37 in the appendix.

5.3.1 Granule properties

Resulting particle size distributions and particle fine and coarse fractions for the performed experiments are depicted in Figure 24 and Figure 25. Adding the binder to the granulation liquid resulted in an enlargement of particles going along with a decrease of particle fine fraction compared to the experiments where the binder was added to the powder preblend. Furthermore, for the experiments where a granulation liquid was prepared, the granulation ML had a higher impact on enlargement of particles.

Particle fine fraction ranged between 46 % and 51 % for the experiments where the binder was added to the powder preblend and between 14 % and 30 % for the experiments where the binder was added to the granulation liquid dependent on granulation ML. Addition of binder to the granulation liquid led to the reduction of particle fine fraction below the predefined specification limit < 20 % at least for the two higher granulation MLs of 19 % and 23 %.

With regard to particle coarse fraction, it could be stated that increasing ML lead to a decrease of coarse fraction for the experiments with addition of binder to the prebelend and to an increase of coarse fraction for the experiment with addition of binder to granulation liquid.

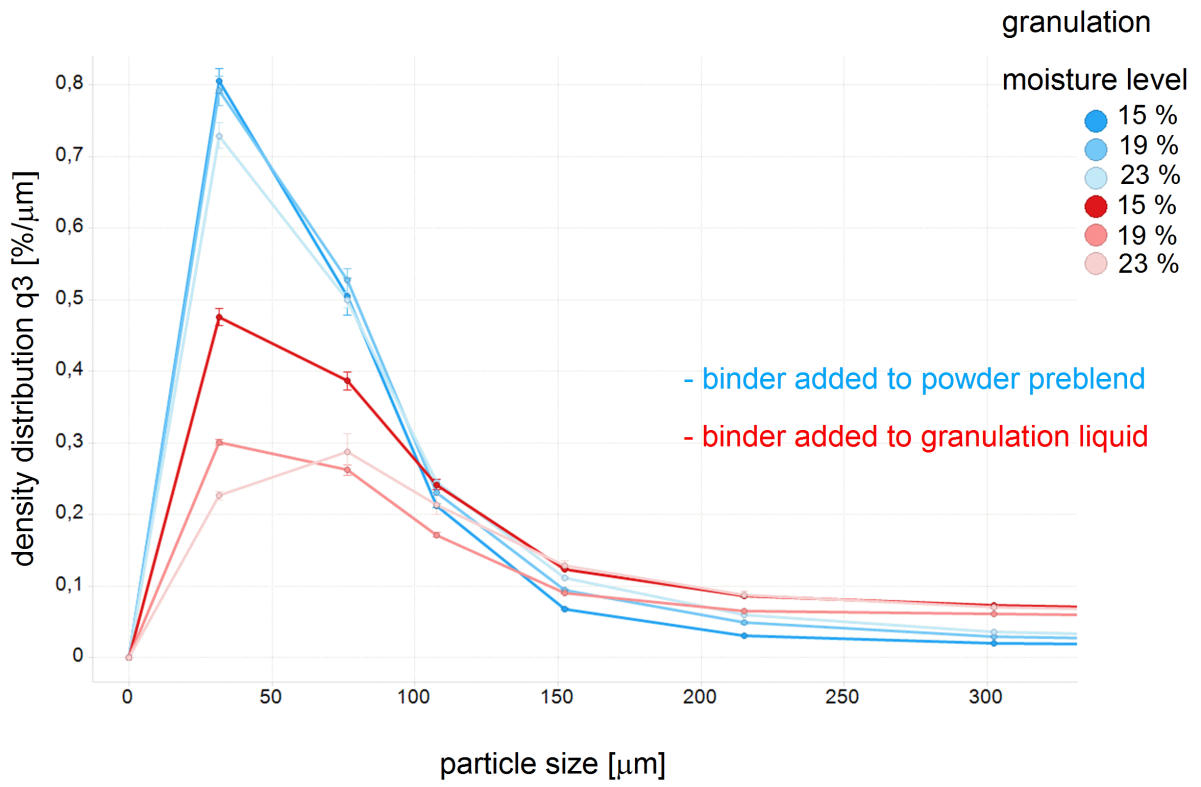

Figure 24 Density distribution q3 [%/µm] plotted against particle size [µm] from dynamic image analysis (Camsizer) for formulation 1 (F1), different colours: granulation ML [%] and binder addition method; n=3; error bars: +/- 1 SD

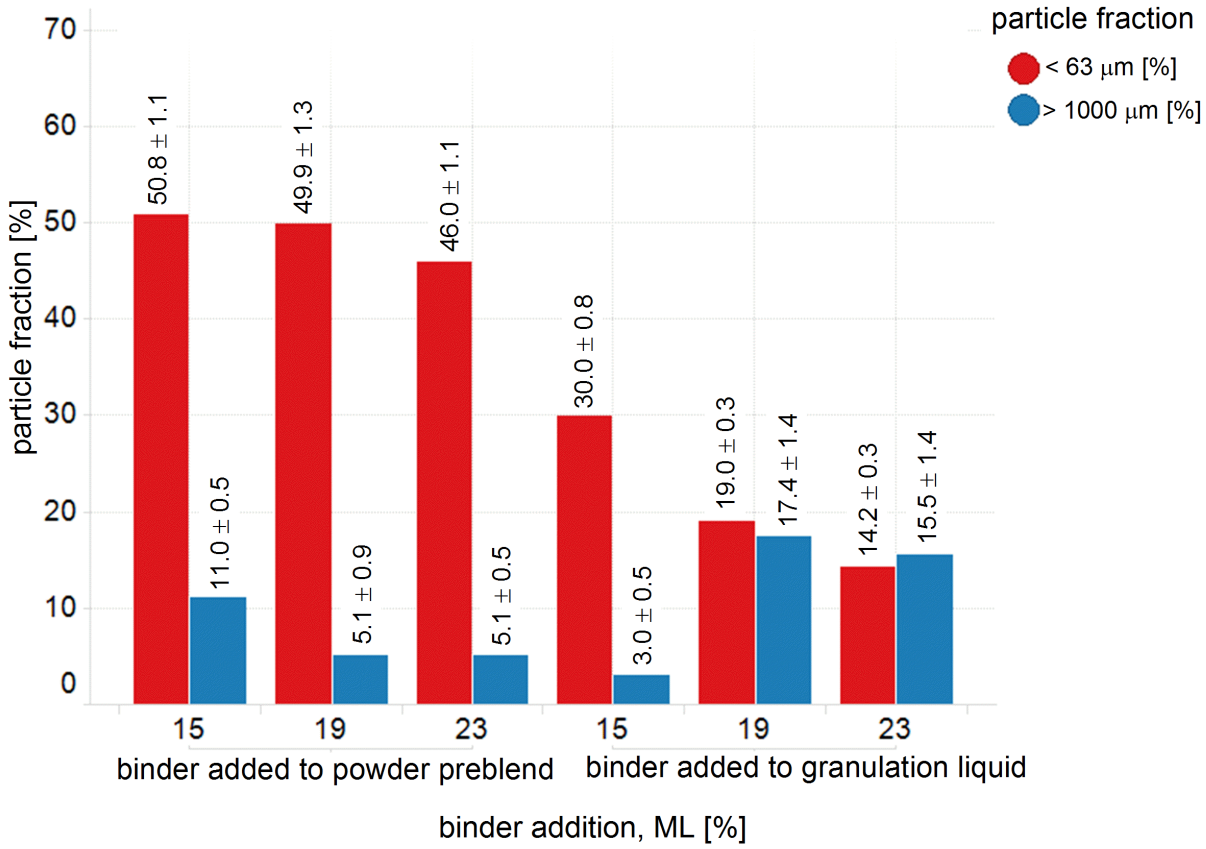

Figure 25 Particle fine fraction (< 63 µm; red bars) and particle coarse fraction (> 1000 µm, blue bars), sorted by binder addition method and granulation ML [%], formulation 1 (F1); n=3

Comparing flowability value FFC and residual water content of the dried granules (LoD) for the two binder addition modes, no big differences could be observed (see Figure 26). FFC value was in the range of an easy flowability (4 < FFC < 10) and LoD < 1.5 % independent of the applied binder addition mode and granulation ML.

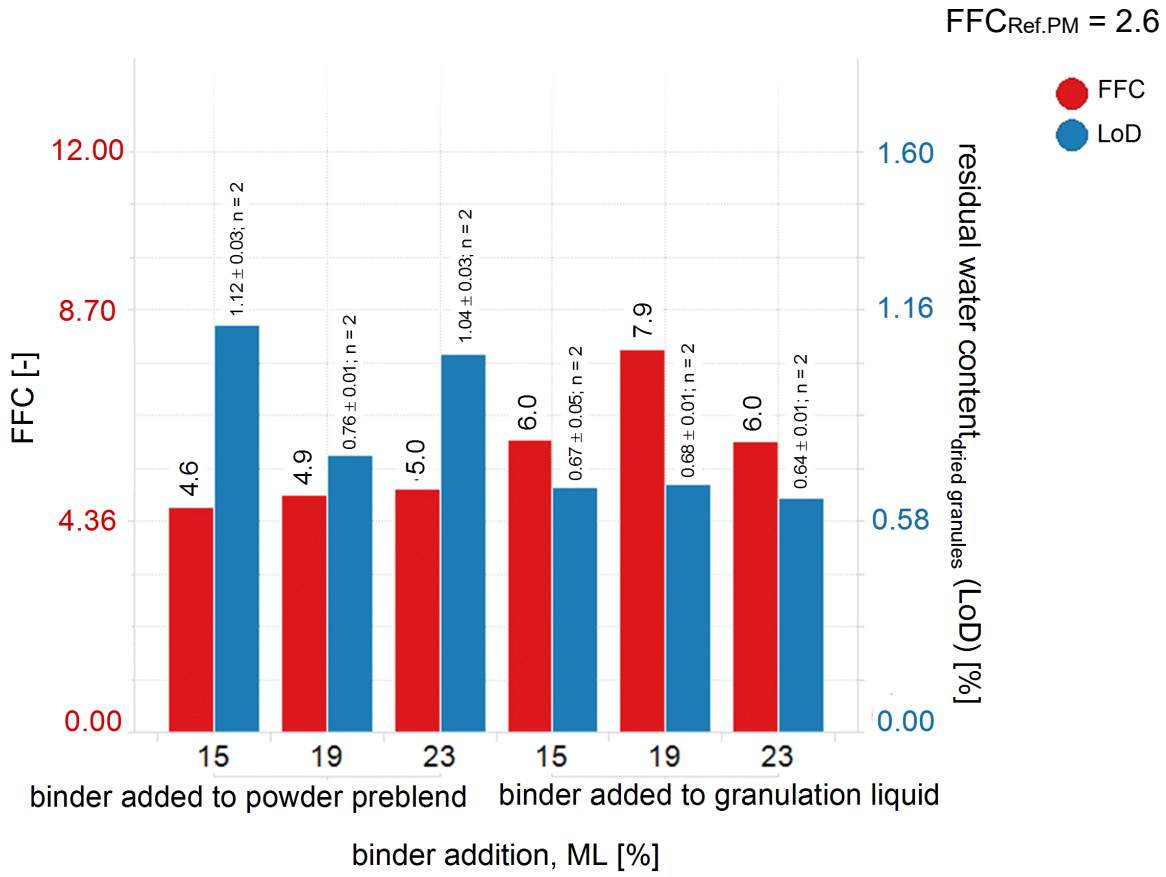

Figure 26 Flowability value FFC ([-]; red bars) and residual water content of dried granules ([%]; blue bars), sorted by binder addition method and granulation ML [%], formulation 1 (F1)

To sum up, adding the binder to the granulation liquid had major impact on particle size. Agglomeration of particles was more sufficient when the binder was already solved in the water and could immediately be available for agglomeration of particles as soon as powder preblend and granulation liquid got in touch.

5.3.2 Tablet properties

Experiments for the different binder addition modes were evaluated according to their tabletability and compressibility behaviour (see 5.2.2). The results of that evaluation are depicted in Figure 27 (tabletability) and Figure 28 (compressibility).

It became visible that binder addition mode had no impact on solid fraction SF but lead to an increase of TS when binder was added to the granulation liquid.

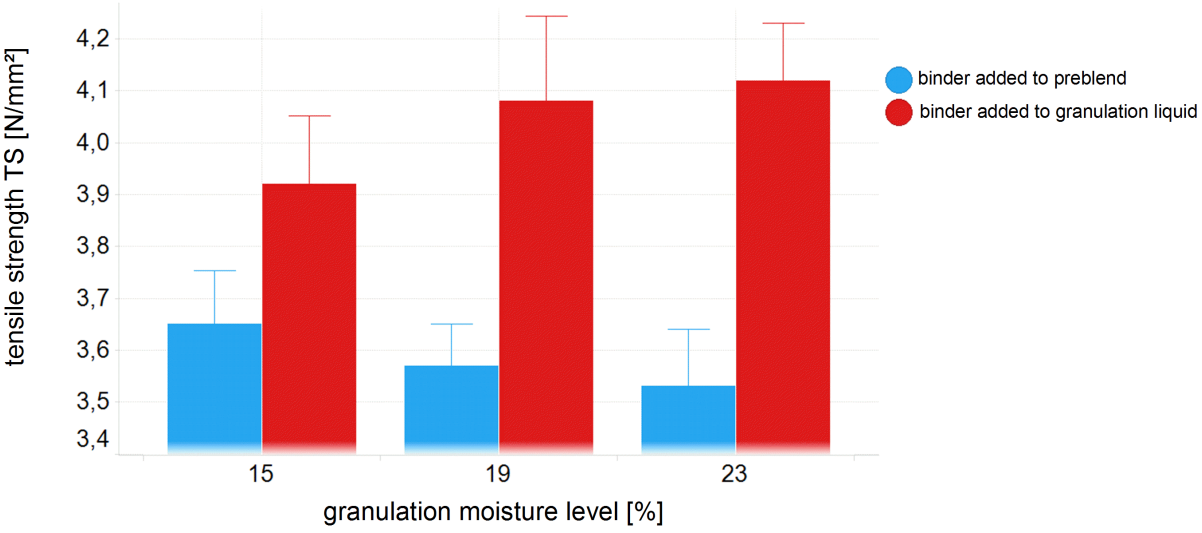

Figure 27 Tensile strength TS [N/mm²] at CP = 281 MPa plotted against granulation ML [%], different colours: binder addition method; error bars: +1 SD

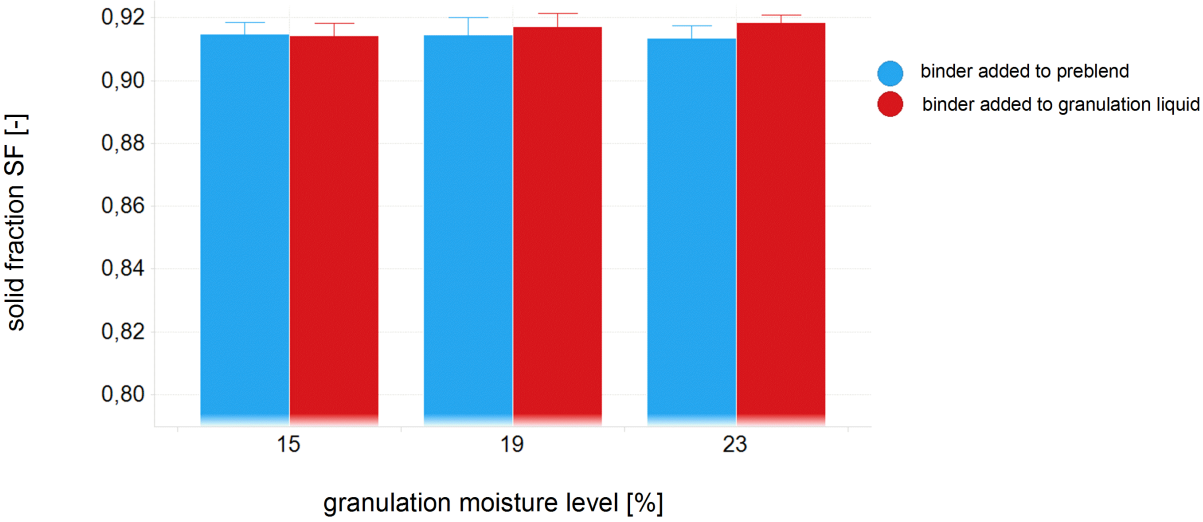

Figure 28 Solid fraction SF [-] at CP = 281 MPa plotted against granulation ML [%], different colours: binder addition method; error bars: +/- 1 SD

5.4 SUMMARY & QBD LEARNING

The comparison of the two presented formulations, one including cellulose (F1) and one avoiding cellulose (F2) with regard to their behaviour in twin screw wet granulation process by variation of the process parameters powder feed rate PFR [kg/h], moisture level ML [%] and barrel fill level FL [%] was investigated. The summary of this investigation for granules particle size distribution and tablets attributes is given in Table 5.

It was shown that granulation moisture level ML [%] had the highest impact on granules particle size with in general decreasing particle size at increasing granulation ML. In detail this general effect resulted in a decrease of particle fine fraction for both formulations at increasing ML and an increase of the coarse particle fraction for F2, too. That observation is in very good agreement with results in literature, where the impact of L/S-ratio (directly connected to granulation ML) on granules particle size was also investigated [14, 16, 49, 53, 54, 61, 64, 69, 70, 71, 88, 89, 90, 123, 129]. All that papers showed the effect of decreasing particle sizes at increasing granulation ML for very different formulations and process parameter settings.

Looking at the influence of granulation ML on tableting behaviour in terms of tabletability (TS [N/mm²]) and compressibility (SF [-]), it can be concluded that increasing granulation ML led to a slight increase of both, tabletability and compressibility, for F2. Especially F2 showed a much more better tabletability and also compressibility behaviour compared to the ungranulated physical mixture (2.2 – 5 times better, see Table 4) which indicated that a proper agglomeration behaviour is key for a good tableting performance. As agglomeration was better at higher granulation ML it is quite logical that increasing ML led to an improved tabletability and compressibility. Furthermore, according to Liu et al. (2017) [61] this effect results out of the reason that good deformable and porous granules are built at higher L/S-ratio.

Table 5 Summary of impact of TSG process parameters (PP) on granule and tablet material attributes (MA) for both formulations; arrow up - increasing MA at increasing PP; arrow down - decreasing MA at increasing PP; equivalent bar - no impact of PP on MA; arrow diagonally upwards - slight increase of MA at increasing PP (partly dependent on other PPs)

		PFR [kg/h]	ML [%]	FL [%]
Formulation 1 (including cellulose)	particle fine fraction (< 63 µm) [%]	↑	↓	↓
	particle coarse fraction (> 1000 µm) [%]	–	–	↓
	tabletability (TS [N/mm²])	↗	–	–
	compressibility (SF [-])	–	–	–
Formulation 2 (including starch)	particle fine fraction (< 63 µm) [%]	↗ – high ML, ↑ low ML	↓	↓
	particle coarse fraction (> 1000 µm) [%]	↗ – high ML, ↑ low ML	↗ – high PFR, ↑ low PFR	↗ – high PFR, ↑ low PFR
	tabletability (TS [N/mm²])	↓	↗ – ↑ high PFR, – low PFR	↗ – ↑ high PFR, – low PFR
	compressibility (SF [-])	↓	↗ – ↑ high PFR, – low PFR	–

Powder feed rate PFR [kg/h] affected also both formulations by increasing particle fine fraction at increasing PFR. The formulation without cellulose could compensate the increase of PFR by adaption of granulation ML quite well, so that particle fine fraction was only increasing for the experiments performed at low granulation ML. That should the benefit of the formulation without cellulose in terms of scaling as scaling by throughput for that formulation seemed more feasible to result in similar granular material attributes during scaling. Adaption of barrel fill level FL by decreasing of screw speed at a specified PFR lead to a decrease of fine fraction for both formulations and a decrease of coarse fraction for F1 and in contrast to that, to an increase of particle coarse fraction for F2 at low PFR. The impact of PFR, screw speed and barrel fill level FL on granule material attributes was investigated by several research papers [14, 21, 30, 34, 49, 50, 53, 68, 69, 70, 107, 129]. Based on formulation-dependent differences and differences on how PFR and/or FL were varied during the experimental setup, different effects of PFR and FL on granule PSD became visible. Increasing particle sizes at increasing PFR and FL simultaneously were found by several researchers [68, 69, 70, 129]. The effect of increasing

particle fine fraction and/or coarse fraction by increasing screw speed (combined with an increase of PFR in some cases) was also figured out by Djuric et al. (2010) [21], Keleb et al. (2004) [49], Kim et al. (2017) [50] and Kumar et al. (2016) [53].

In terms of tableting behaviour, surprisingly the formulation including cellulose showed no impact of FL and PFR (only a slight increase of tabletability with increasing PFR). That lead to the statement, that this formulation was figured out to be quite robust in terms of tableting behaviour according to changes during twin screw wet granulation process. The tableting behaviour of formulation 2 was effected by changes in PFR and FL. As PFR increase resulted either in an increase of particle fine fraction or residual water content, that lead to a decrease of both, tabletability and compressibility. Increasing FL (which came along with a decrease of screw speed at a certain PFR) had only minor effect on tableting behaviour of F2. That observation is in good agreement with the findings of Tan et al. (2011) [107] who also evaluated screw speed variation to have only minor effect on tablets' tensile strength.

So in general, formulation 2 (without cellulose) showed more dependence of tableting behaviour on granules material attributes than formulation 1 where the cellulose might be able to better mask changes in granules material attributes as that excipient shows high plastic deformation behaviour resulting in good tableting performance.

All in all, for the investigation of twin screw wet granulation unit, it can be stated, that granulation moisture level is the critical process parameter having the highest impact on resulting granule and material attributes (cMAs and cQAs) independent of the used formulation. The other two investigated process parameters (barrel fill level and powder feed rate) have been identified to have only minor impact on cMAs and cQAs and to show more formulation-dependent effects. In terms of comparison of the two formulations, either including cellulose or not, better agglomeration behaviour at lower granulation moisture level was observed for the formulation without cellulose whereas tableting behaviour was not influenced by the poor granulation behaviour of the formulation including cellulose. Nevertheless, proper agglomeration of particles is not only key to result in good QAs of final tablet, but also important for further processability of granules at production scale.

The summary of the evaluation of the two binder addition modes for F1 (see chapter 5.3) is given in Table 6. Adding binder to granulation liquid lead to an improvement of particle

agglomeration in terms of reduction of particle fine fraction. Furthermore, particle fine fraction could be decreased by increasing granulation ML. This reduction of fines had impact of tableting behaviour as tabletability was best for the experiment performed with binder added to granulation liquid and at highest granulation ML. No impact on compressibility was observed.

Table 6 Summary of impact of binder addition mode and ML (PP) on granule and tablet material attributes (MA) for formulation 1; arrow up - increasing MA at increasing PP; arrow down - decreasing MA at increasing PP; equivalent bar - no impact of PP on MA

	binder addition mode		ML [%]	
	binder added to powder preblend	binder added to granulation liquid	binder added to powder preblend	binder added to granulation liquid
particle fine fraction (< 63 µm) [%]	↑	↓	–	↓
particle coarse fraction (> 1000 µm) [%]	–	–	↓	↑
tabletability (TS [N/mm²])	↓	↑	–	↑
compressibility (SF [-])	–	–	–	–

Comparing these results with findings described in literature, the results can be explained very well. El Hagrasy et al. (2013) [22] found the same relationship of reduction of fines when the binder HPMC was solved in the granulation liquid for a Lactose:Cellulose based formulation. A decreasing fine fraction with increasing binder amount and granulation ML was figured out by Dhenge et al. (2012) [16]. In contrast to the finding within this thesis, Saleh et al. (2015) [97] resulted in more narrow particle size distributions when the binder was added to the powder preblend. Nevertheless, in contrast to the here described investigation where 1.5 % (m/m) of binder was used, they used a much higher amount of 5 % HPMC. That may be an explanation for the different behaviours on binder addition mode. Very well comparable to the here described findings, are the result of Portier et al. (2020) [89]. He even suggested to reduce L/S ratio when adding the binder to the granulation liquid, as the agglomeration behaviour was much better for this binder addition mode compared to the dry binder addition.

To sum up, the investigation of different binder addition modes showed that adding the binder to the granulation liquid resulted in a better agglomeration of particle for F1 at same moisture levels compared to the dry binder addition mode. So, adding the binder to the granulation liquid can help to avoid high granulation moisture levels. That is an important point as drying capacity within a continuous drying step (see chapter 6) is always limited.

6. CONTINUOUS FLUID BED DRYING: IMPACT OF PROCESS PARAMETERS ON MATERIAL ATTRIBUTES

Wet granules produced via twin screw wet granulation process are continuously fed into a fluid-bed dryer for drying process. The continuous fluid-bed dryer being mainly used in this thesis is the Modcos M system based on the Glatt GPCG10 (see 11.1.4.3 and 11.1.4.3.3). Several set process parameters (dryer rotation speed, inlet air temperature, inlet air flow rate) and response parameters (granule particle size, granule residual water content, drying time, fluidization, mass per chamber) can be defined for drying process as described in Figure 29.
The aim of this chapter is to evaluate the impact of set process parameters and their response parameters for continuous fluid bed drying process on the material attributes for resulting granules as well as tablets using the Modcos M-line equipment.

6.1 THEORETICAL ASPECTS

There are several (semi-) continuous drying systems discussed in literature to dry the wet granules after continuous twin screw wet granulation in a continuous mode. Different systems are offered by e.g., L.B. Bohle, Lödige, Gea or Glatt [115].
This thesis focuses on the system provided by Glatt GmbH, the Modcos continuous fluid bed drying system.
The Modcos dryer consists of a carousel dividing the fluid bed chamber into then small fluid bed chambers. Via a slow rotation of that carousel the chambers can be charged with wet granules, the drying process can take place during the rotation of the chamber and the dried granules are being discharged from the dryer after 8/10 of a full rotation of the dryer. As these three steps happen simultaneously over time, the drying principle can be stated as a continuous principle (see Figure 1).
An overview on set process parameters and the response parameters for the continuous fluid bed dryer is given in Figure 29. Logically, the drying mode is a design aspect of a certain dryer equipment. Fluidization and as a result drying efficiency are impacted by inlet air flow rate and inlet air temperature.

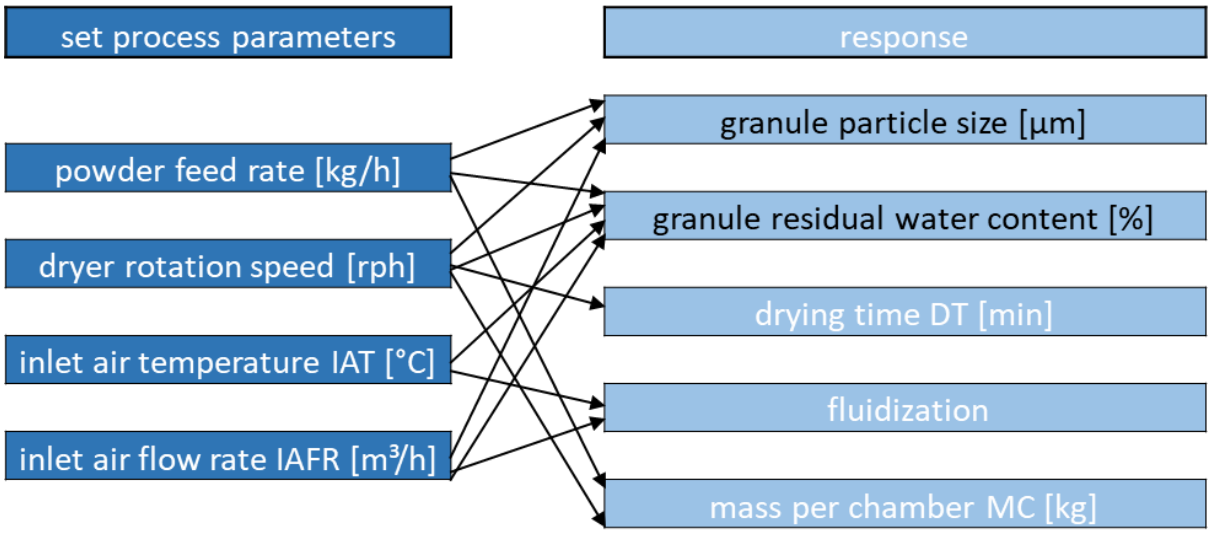

Figure 29 Set process parameters for continuous fluid bed drying process and their response parameter; black written response parameter: granule material attribute; white written response parameter: process condition

The mass per chamber is being defined by the powder feed rate and the dryer rotation speed. Drying time is dependent only on the dryer rotation speed. The formula according to Pauli et al. (2018) [80] for both parameters are given in equations (5) and (6).

$$MC\ [kg] = \frac{PFR\ [\frac{kg}{h}]}{DRS\ [rph] * 10} \quad (5)$$

$$DT\ [min] = \frac{60}{DRS\ [rph]} * 0.8 \quad (6)$$

A higher dryer rotation speed results in a lower mass per chamber and in a lower drying time simultaneously.

6.2 EXPERIMENTAL SETUP

The same formulations being investigated according to their twin screw wet granulation behaviour in the previous chapter (see chapter 5; compositions see Table 22 and Table 23) were also investigated according to their drying behaviour in the continuous fluid-bed dryer using the M-line scale equipment (24 mm TSG in combination with Modcos M continuous fluid bed drying system). As the preparation of a granulation liquid was evaluated to be beneficial for formulation 1 (see 5.3), this procedure was conducted for the investigation of drying behaviour of F1.

The two drying process parameters inlet air temperature IAT [°C] and dryer rotation speed DRS [rph] and the granulation process parameter moisture level ML [%] were varied on different levels (see Table 7). Granulation ML was included in the process experimental setup, because ML was known to be of high impact on material attributes based on previous experiments (see chapter 5). As drying behaviour should be investigated for a broad range of granules in terms of different material attributes, it was decided to add granulation ML as one parameter to these experiments.

Table 7 Overview on experiments conducted for the evaluation of the drying unit (M-line scale) for formulation 1 (F1) and formulation 2 (F2); blue = low level, green = middle level, red = high level

exp. no	ML*$_1$ [%] (F1 / F2)	IAT*$_2$ [°C] (F1 / F2)	DRS*$_3$ [rph] (F1 / F2)	IAFR*$_4$ [m³/h] (F1 / F2)
1	25 / 20	80 / 70	30	380 / 360
2	25 / 20	80 / 70	10	380 / 360
3	15 / 10	80 / 70	30	340 / 320
4	15 / 10	80 / 70	10	340 / 320
5	20 / 15	87 / 80	20	360 / 340
6	25 / 20	94 / 90	30	380 / 360
7	25 / 20	94 / 90	10	380 / 360
8	15 / 10	94 / 90	30	340 / 320
9	15 / 10	94 / 90	10	340 / 320

*$_1$ derived parameter

*$_2$ process parameter

*$_3$ process parameter

*$_4$ process parameter

Differences in experimental setup existed with regard to granulation moisture level. Out of the same reasons explained in chapter 5.2 the formulation containing cellulose needed a higher amount of granulation liquid added as water to result in a proper agglomeration of particles compared to formulation 2 without cellulose. Because of that, granulation ML were higher for F1 than for F2 (F1: ML1 = 15 %, ML2 = 25 %; F2: ML1 = 10 %, ML2 = 20 %). Out of that reason inlet air temperature IAT was set to a higher level for formulation 1 compared to formulation 2 (F1: IAT1 = 80 °C, IAT2 = 94 °C; F2: IAT1 = 70 °C, IAT2 = 90 °C). The investigated dryer rotation speeds DRS were the same for F1 and F2 (DRS1 = 10 rph,

DRS2 = 30 rph). A detailed overview on all important process parameters for the granulation and drying unit is given in Table 40 in the appendix.

6.3 GRANULE PROPERTIES

Granules of all performed experiments were analysed according to their particle size distribution. The density distribution function of particle size plotted against the particle size and coloured by granulation ML is depicted in Figure 30 (F1) and Figure 31 (F2).

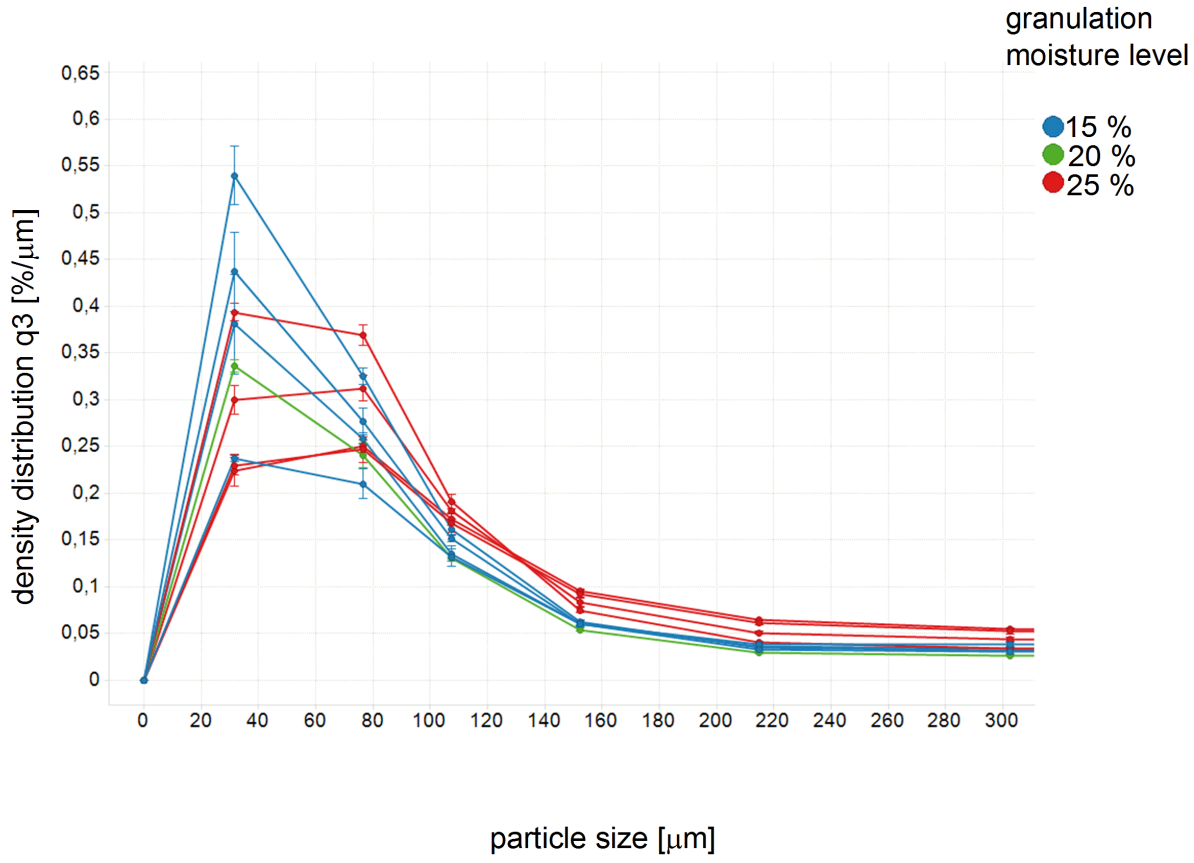

Figure 30 Density distribution q3 [%/µm] plotted against particle size [µm] from dynamic image analysis (Camsizer) for formulation 1 (F1), different colours: granulation ML [%]; n=3; error bars: +/- 1 SD

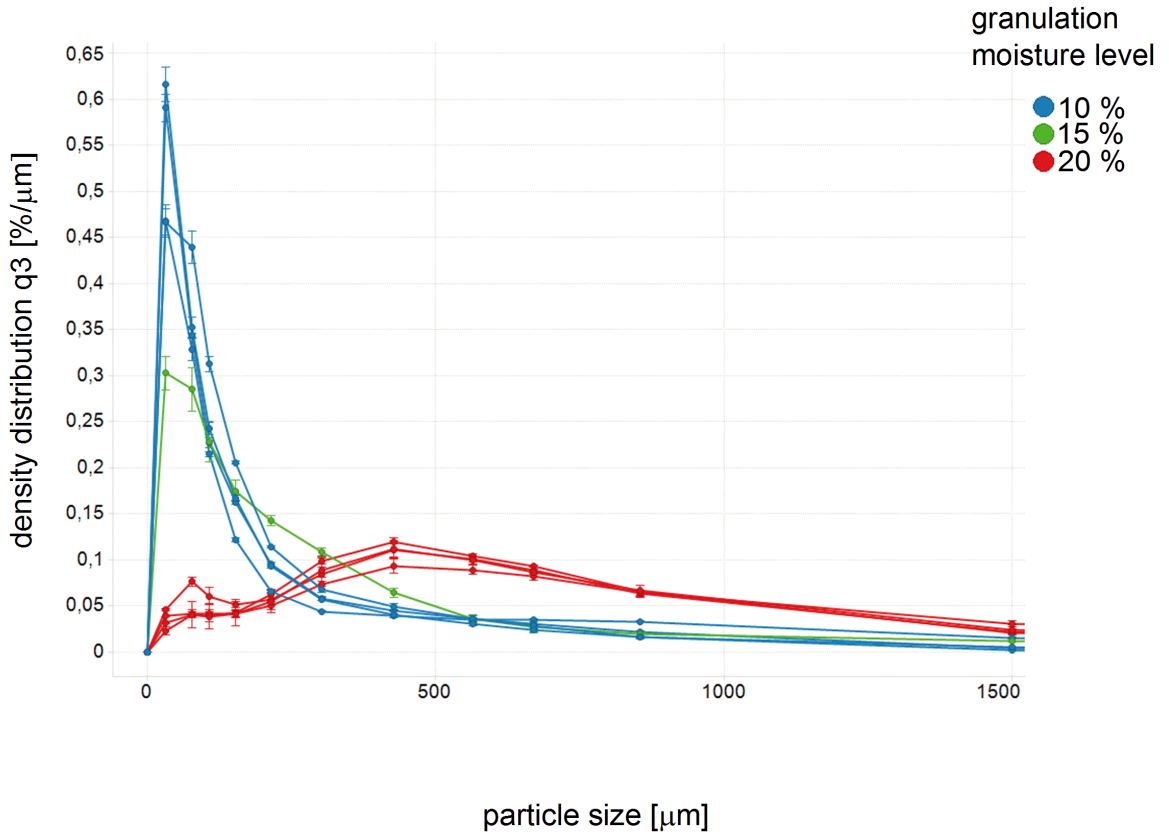

Figure 31 Density distribution q3 [%/µm] plotted against particle size [µm] from dynamic image analysis (Camsizer) for formulation 2 (F2), different colours: granulation ML [%]; n=3; error bars: +/- 1 SD

With regard to F1 no big differences in density distribution of particle size of granules produced at different granulation MLs became visible. F2 showed a clear relationship between particle size of resulting granules and applied granulation ML with increasing particle size at increasing ML (see 5.2.1).

A more detailed depiction of the impact of all three investigated process parameters (ML, DRS and IAT) on the resulting particle size distributions (particle density function and particle fine and coarse fractions) is given in Figure 32 (particle density function) and Figure 33 (particle fine and coarse fraction) for F1 and in Figure 34 (particle density function) and Figure 35 (particle fine and coarse fraction) for F2.

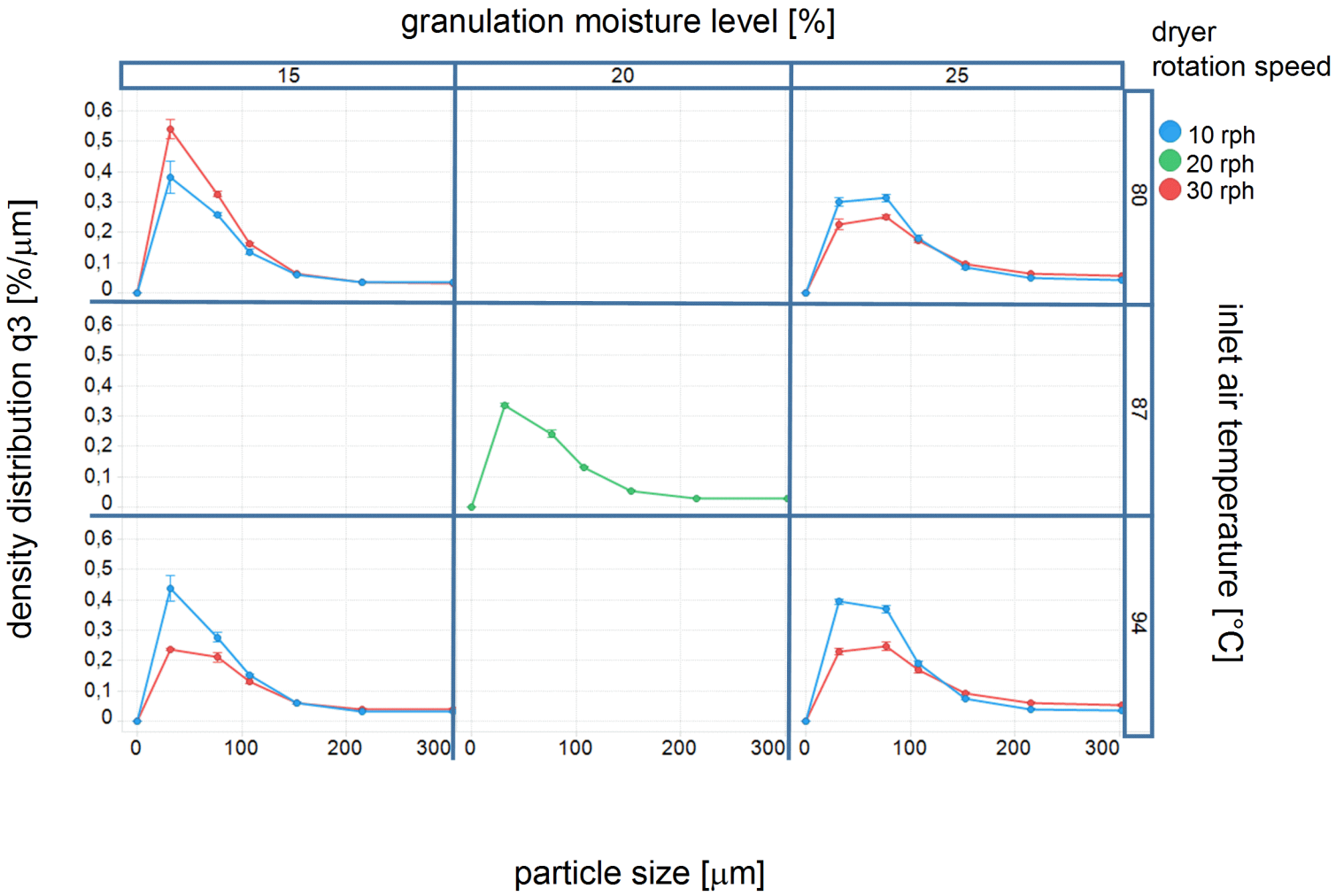

Figure 32 Density distribution q3 [%/µm] plotted against particle size [µm] for formulation 1 (F1); columns: different granulation ML [%]; rows: different IAT [°C]; different colours: DRS [rph]; n=3; error bars: +/- 1 SD

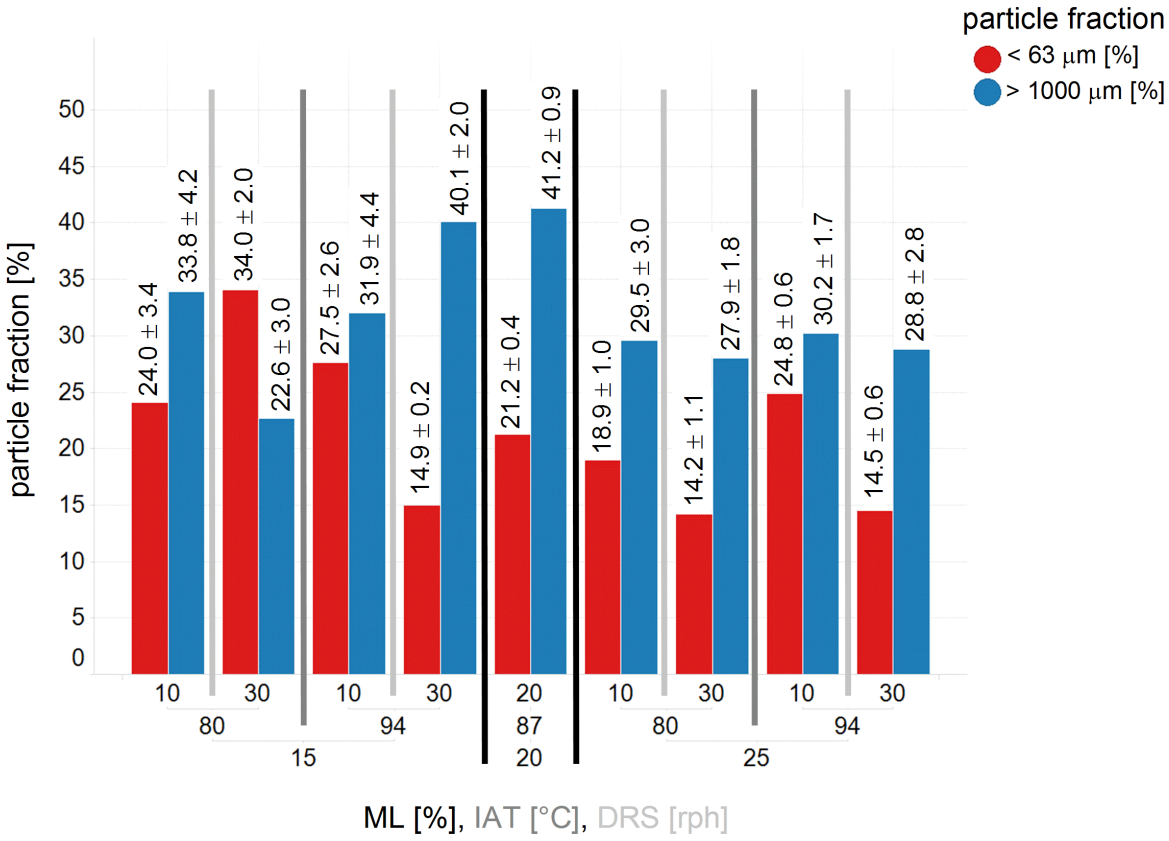

Figure 33 Particle fine fraction (< 63 µm; red bars) and particle coarse fraction (> 1000 µm, blue bars), sorted by granulation ML, IAT and DRS, for F1

Ranges for particle fine fraction were between 14.2 % and 34.0 % for F1 and between 1.5 % and 38.8 % for F2. Coarse particle fraction ranged between 22.6 % and 41.2 % for F1 and between 2.4 % and 30.8 % for F2. Comparing these results to the ranges investigated for the evaluation of the twin screw wet granulation process (see 5.2.1), they are quite similar. Formulation 1 resulted in particle fine and coarse fraction > 10 % for all investigated process parameter settings indicating the tendency of F1 to build heterogeneous particle size distributions. For formulation 2 process parameter settings were found where particle fine fraction and/or coarse fraction could be kept below a 10 % limit.

The influence of the three investigated process parameters within this experimental setup on the particle size distribution and particle fine and coarse fraction will be discussed in the following.

Impact of **granulation moisture level ML [%]**:

Comparing samples dried at the same DRS and IAT, a slight decrease of particle fine fraction with increasing granulation ML became visible for F1. For the impact of granulation ML on coarse particle fraction no clear tendency could be detected for F1 (see Figure 33).

In contrast to F1, formulation 2 showed a very strong influence of granulation ML on both, particle fine fraction and particle coarse fraction. With increasing ML a strong decrease of particle fine fraction and a strong increase of particle coarse fraction could be found at the same time (see Figure 35). These observations are in good agreement with the findings of the impact of granulation ML as described in the previous chapter 5.2.1.

Impact of **dryer rotation speed DRS [rph]**:

Both formulation showed the effect of decreasing particle fine fraction at increasing DRS comparing samples granulated at the same granulation ML and the same IAT (see Figure 33 and Figure 35). As DRS is directly linked to drying time and mass per chamber (see equations (5) and (6)), an increasing DRS results in a shorter drying time and a lower mass per chamber at the same time. Therefore, a shorter drying time seemed to be beneficial in terms of shorter shearing and abrasion of granules inside the dryer resulting in a lower particle fine fraction.

With regard to particle coarse fraction, no clear impact of DRS could be figured out for neither of the two formulations.

Impact of **inlet air temperature IAT [°C]**:

Density distribution function of particle size for both formulations produced at same DRS and granulation ML but at different IAT showed no differences as depicted in Figure 32 and Figure 34. Therefore, no impact of IAT on PSD could be found.

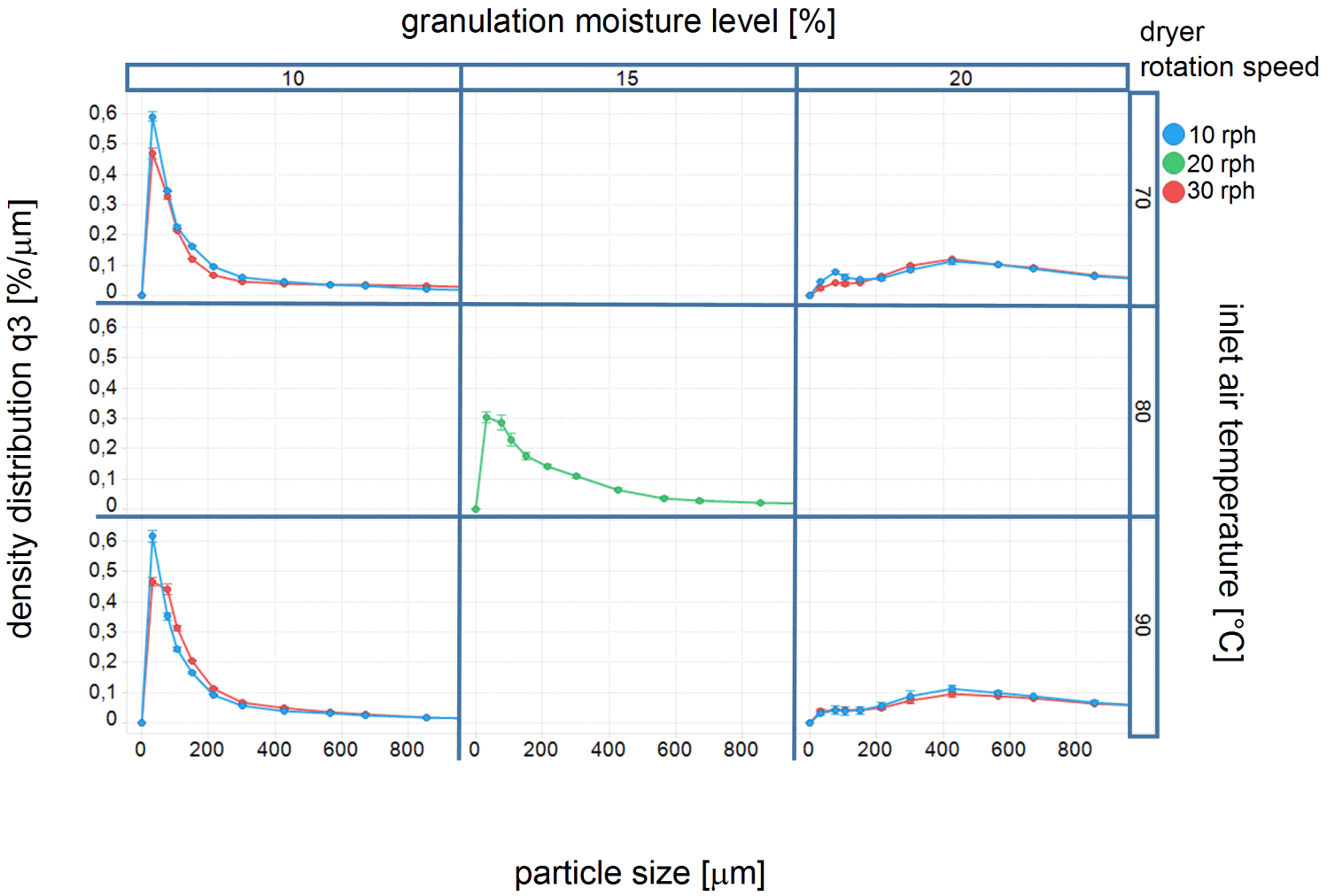

Figure 34 Density distribution q3 [%/µm] plotted against particle size [µm] for formulation 2 (F2); columns: different granulation ML [%]; rows: different IAT [°C]; different colours: DRS [rph]; n=3; error bars: +/- 1 SD

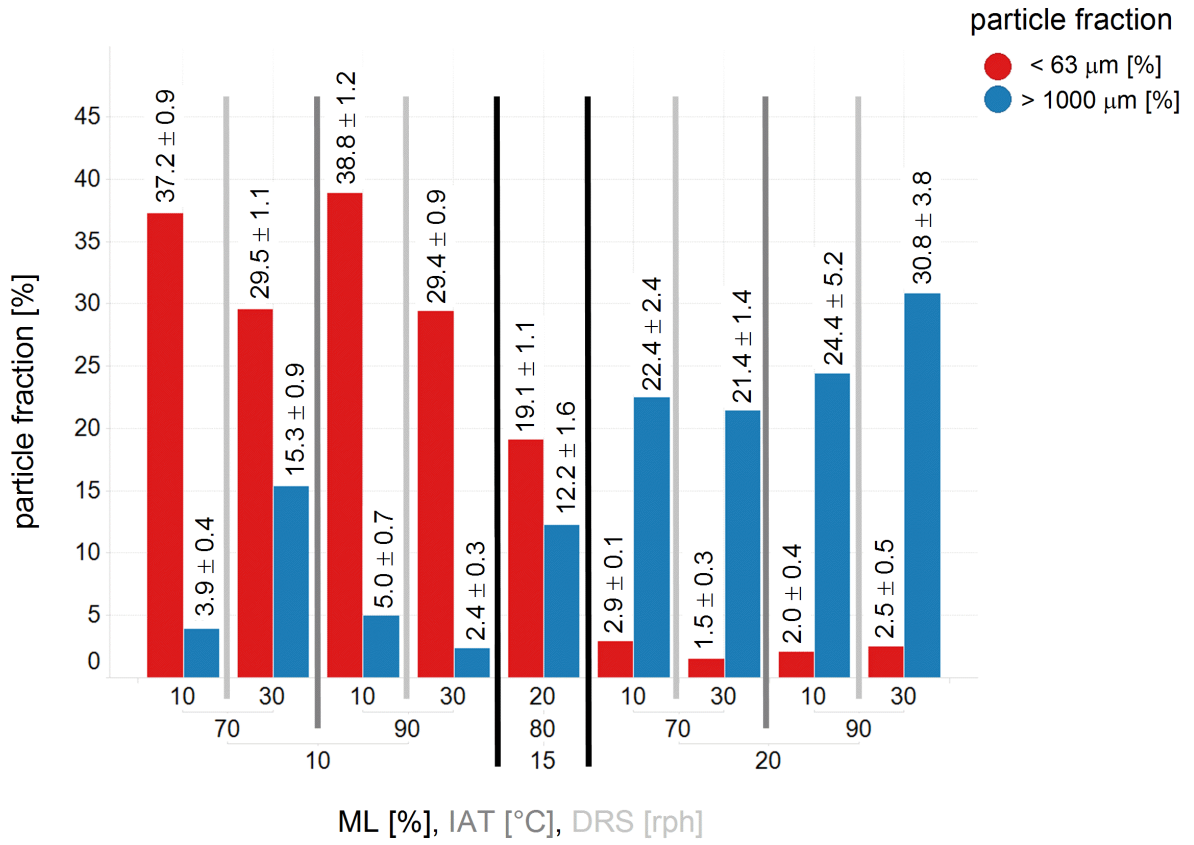

Figure 35 Particle fine fraction (< 63 µm; red bars) and particle coarse fraction (> 1000 µm, blue bars), sorted by granulation ML, IAT and DRS, for F2

The influence of all three process parameters on the flowability value FFC [-] and residual water content (LoD) of resulting granules is depicted in Figure 36 for F1 and in Figure 37 for F2.

Both formulations showed process parameter independent a good flowability indicated by the values ranging between FFC = 4 and FFC = 10. Two outliers of this observation occurred, one for each formulation. For F1 one sample resulted in a FFC value < 4 (3.7) and for F2 one sample resulted in a FFC value > 10 (19.0). All in all, no clear tendency of the impact of process parameters on flowability of resulting granules could be given.

Having a look at the residual water content of dried granules produced at different process parameter settings, better relationships between PPs and the granule material attribute could be figured out.

Impact of **granulation moisture level ML [%]**:

Both formulations showed the effect of increasing residual water content for the granules produced at a higher granulation ML compared to the ones produced at a lower granulation ML. For F1 this effect was especially pronounced for the granules produced at a lower IAT. The drying efficiency of the continuous fluid-bed dryer is driven by the inlet air flow rate, the inlet air temperature and the wet granule mass that has to be dried. As wet granule mass and therefore also the amount of water to be dried out increases with increasing granulation ML, the observation indicated that lower residual water contents could be achieved by either increasing inlet air temperature IAT and/or inlet air flow rate IAFR.

Impact of **dryer rotation speed DRS [rph]**:

Increasing residual water content at increasing DRS was found for both formulations. For F1 this effect became visible for the samples produced at a low granulation ML, whereas for F2 this effect was especially pronounced for the samples produced at a high granulation ML. A higher DRS implicates a shorter drying time and a lower mass per chamber at the same time. Therefore, a shorter drying time was for the observed samples the reason to result in a higher residual water content compared to the samples which had a longer drying time (= lower DRS).

Impact of **inlet air temperature IAT [°C]**:

As expected and also described for the effect of granulation ML on residual water content, an increasing IAT resulted in a lower residual water content of dried granules. IAT had a positive influence on drying efficiency and out of that reason, it is logical that IAT had directly impact on residual water content.

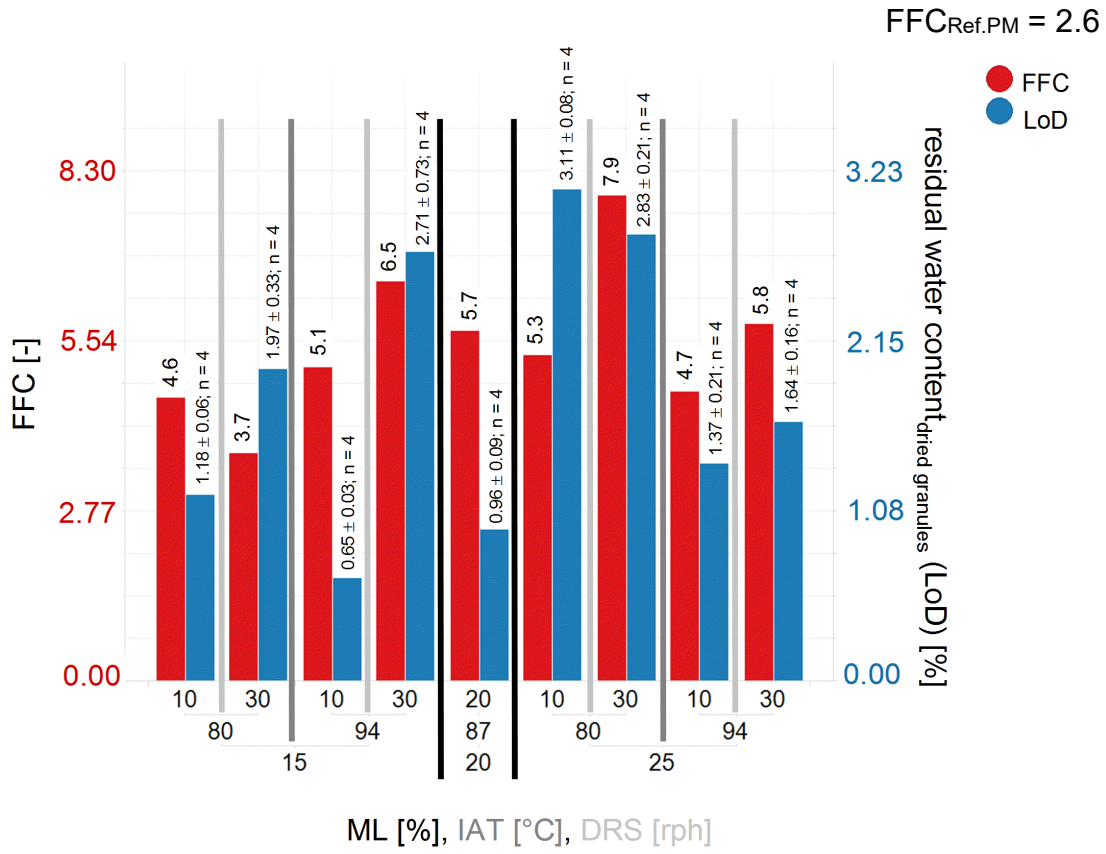

Figure 36 Flowability value FFC ([-]; red bars) and residual water content of dried granules ([%]; blue bars), sorted by granulation ML, IAT and DRS, for F1

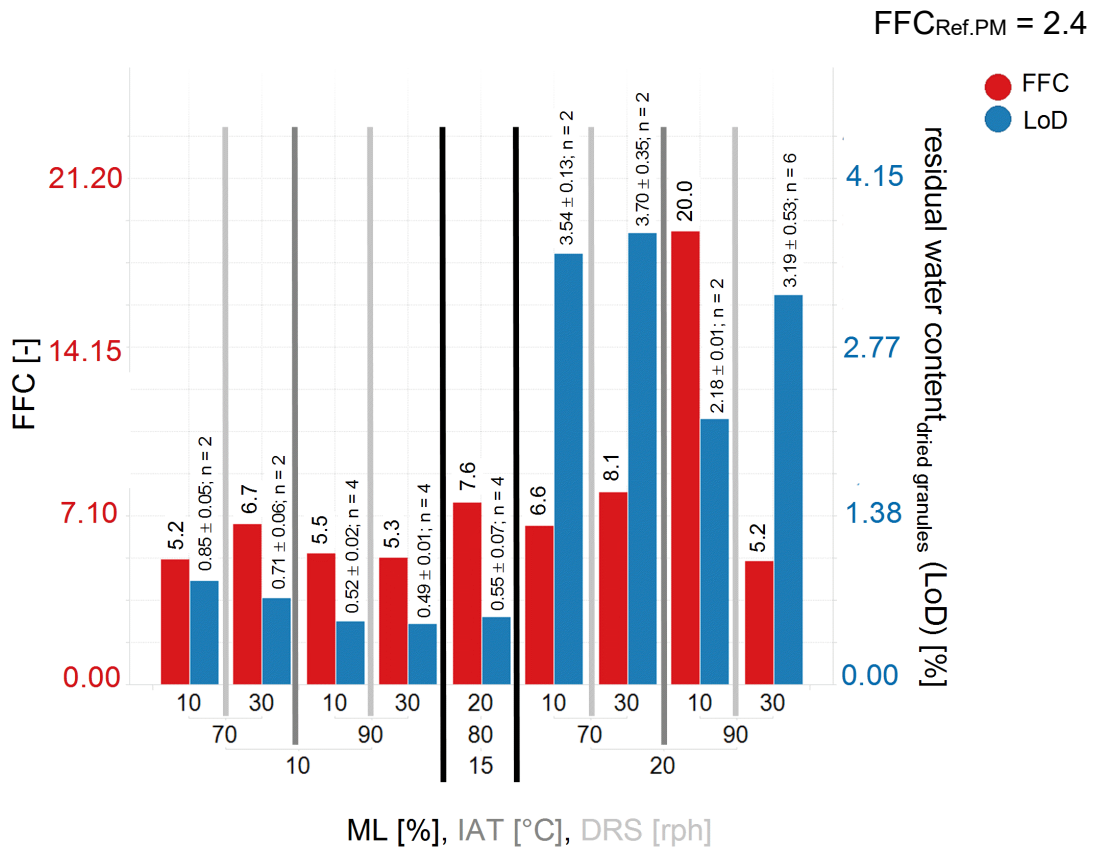

Figure 37 Flowability value FFC ([-]; red bars) and residual water content of dried granules ([%]; blue bars), sorted by granulation ML, IAT and DRS, for F2

6.4 TABLET PROPERTIES

All granules for both formulations and all different process parameter settings were compressed to tablets according to the description given in chapter 11.1.6. Tablets were analysed with regard to their dimensions, mass and crushing strength which enabled to calculate tensile strength TS [N/mm²] and solid fraction SF [-]. Tensile strength TS and solid fraction SF were plotted against compression pressure CP [MPa] (tabletability and compressibility graphs, explanation see chapter 5.2.2) and sorted by the three different varied process parameters granulation ML, DRS and IAT in Figure 38and Figure 39 for formulation 1 (F1) and in Figure 40 and Figure 41 for formulation 2 (F2).

The minimum and maximum TS [N/mm²] and SF [-] values for both formulations at lowest and highest applied compression pressure CP [MPa] and compared to the ungranulated physical mixture (PM) at lowest CP = 94 MPa are given in Table 8.

Table 8 Minimum and maximum TS [N/mm²] and SF [-] values for both formulations at lowest and highest applied compression pressure CP [MPa]; comparison to ungranulated premixture (PM) at lowest CP = 94 MPa

	CP = 94 MPa						**CP = 468 MPa**					
	F1			**F2**			**F1**			**F2**		
	Min	Max	Ref. (PM)	Min	Max	Ref. (PM)	Min	Max	Ref. (PM)	Min	Max	Ref. (PM)
TS [N/mm²]	1.18 ± 0.04	1.43 ± 0.05	0.89 ± 0.04	0.55 ± 0.02	1.62 ± 0.04	0.24 ± 0.04	4.66 ± 0.12	5.02 ± 0.10	-	2.13 ± 0.13	4.14 ± 0.13	-
SF [-]	0.797 ± 0.002	0.825 ± 0.005	0.780 ± 0.004	0.797 ± 0.007	0.835 ± 0.004	0.768 ± 0.002	0.920 ± 0.004	0.936 ± 0.005	-	0.885 ± 0.005	0.943 ± 0.003	-

Comparing these ranges for both formulations, the same conclusions can be drawn than already done in chapter 5.2. Ranges for F1 were smaller for TS and SF at the different CPs compared to F2 indicating that variation of process parameters for TSG had higher impact on tableting behaviour for F2 than for F1.

As also described previous in chapter 5.2, high ejection forces, arising during tableting of the granules produced at low and middle granulation ML for F2, limited the tableting process to a maximum CP = 281 MPa.

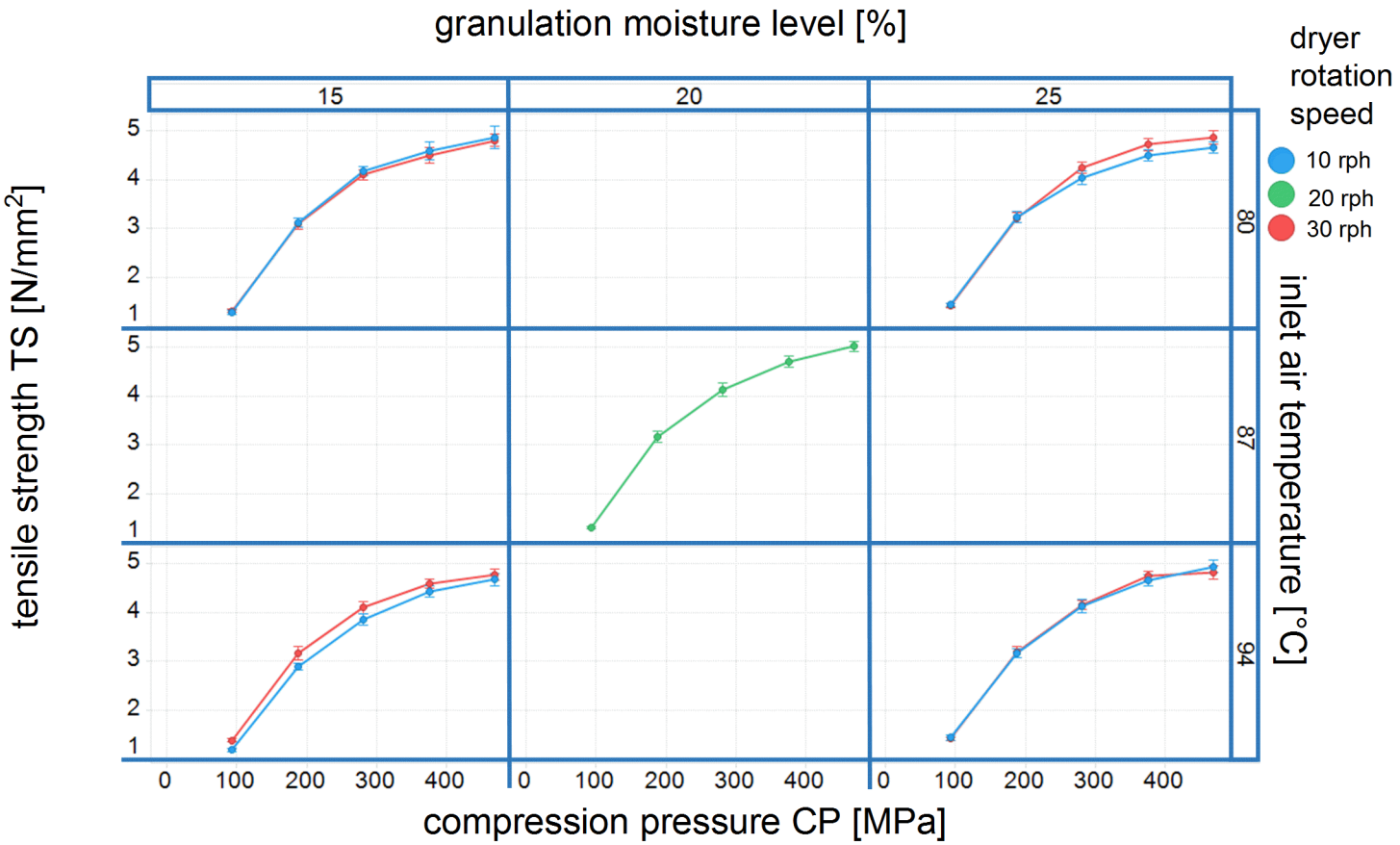

Figure 38 Tensile strength TS [N/mm²] plotted against compression pressure CP [MPa] for formulation 1 (F1); columns: different granulation ML [%]; rows: different inlet air temperature IAT [°C]; different colours: DRS [rph]; error bars: +/- 1 SD

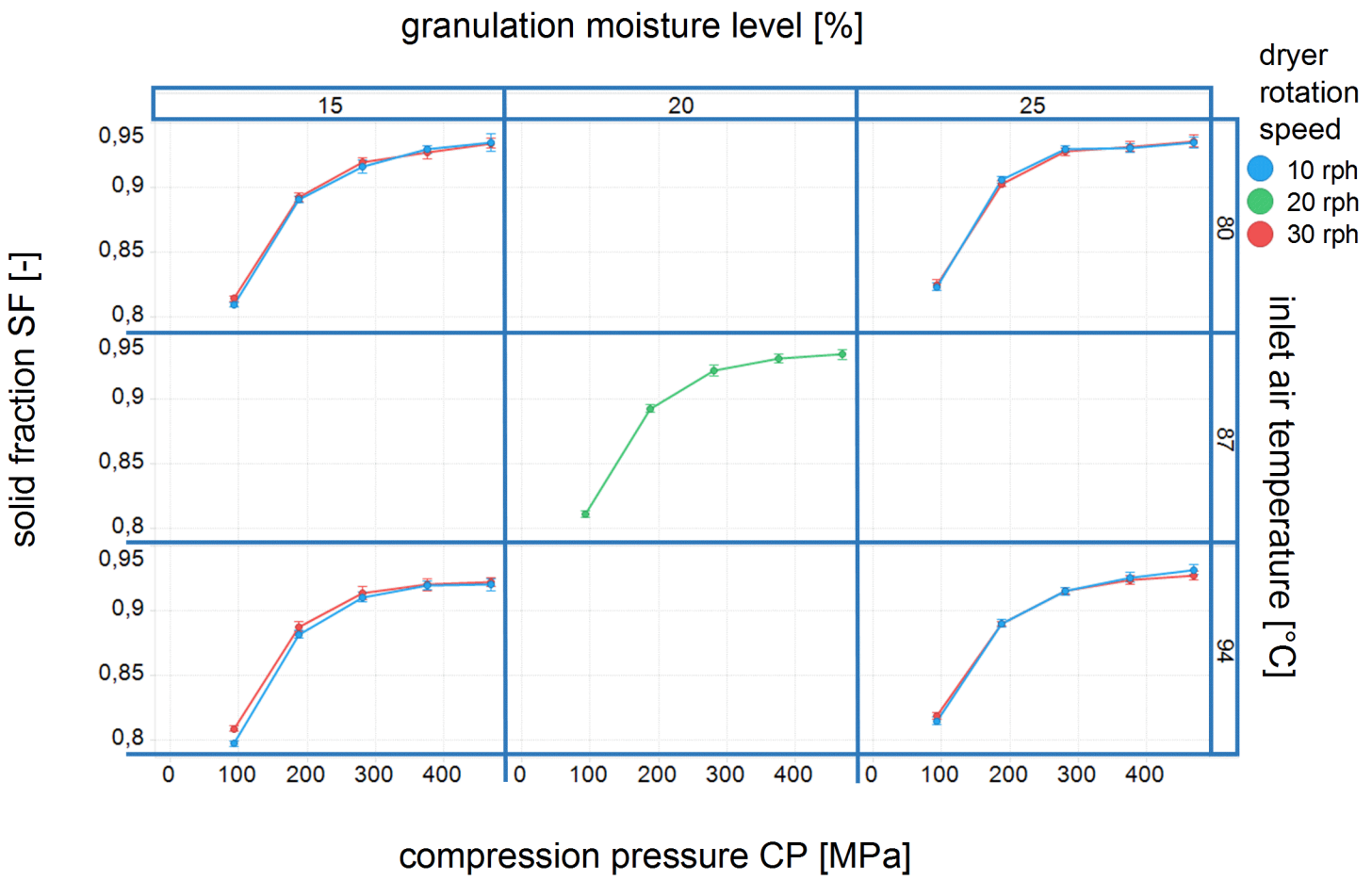

Figure 39 Solid fraction SF [-] plotted against compression pressure CP [MPa] for formulation 1 (F1); columns: different granulation ML [%]; rows: different inlet air temperature IAT [°C]; different colours: DRS [rph]; error bars: +/- 1 SD

Impact of **granulation moisture level ML [%]**:

With regard to tabletability, F1 showed no impact of granulation ML, whereas F2 showed an increasing tabletability at higher granulation ML. This result for F2 is in good agreement with the conclusions drawn in chapter 5.2.2. A decreasing particle fine fraction caused by a higher granulation ML and a better agglomeration of particles at a result, lead to an increased tabletability for F2. Having a look at the compressibility behaviour, it can be stated that for F2 within this dataset no clear tendency could be found. For F1 a slightly higher SF was found with increasing granulation ML for the tablets produced at CP < 281 MPa.

Impact of **dryer rotation speed DRS [rph]**:

DRS showed no impact on tabletability as well as compressibility behaviour for F1. Influences of DRS on tabletability and compressibility became visible for F2 for the experiments performed at the higher granulation ML = 20 %. For these experiments a higher DRS resulted in a higher tabletability despite the outliers which could be identified to be the ones, which resulted in a higher residual water content (> 2.5 %). Like described previous a higher DRS resulted in a lower particle fine fraction. This lower fine fraction influenced tabletability in a positive manner. For the compressibility behaviour differences in SF became visible but no clear tendency could be figured out.

Impact **of inlet air temperature IAT [°C]**:

The impact of IAT on tabletability and compressibility behaviour was different for both formulations. For F1, no impact on tabletability became visible but a decrease of SF at increasing IAT could be evaluated. In contrast to that, formulation 2 showed increasing SF (compressibility behaviour) at increasing IAT. This effect was especially pronounced for the experiments performed at high granulation ML. Furthermore, for the experiments conducted at high granulation ML, a higher TS (tabletability behaviour) at increasing IAT could be found. These relationships made clear that a low residual water content which was achieved at a higher IAT (see 6.3) was very relevant for a good tabletability and compressibility for F2.

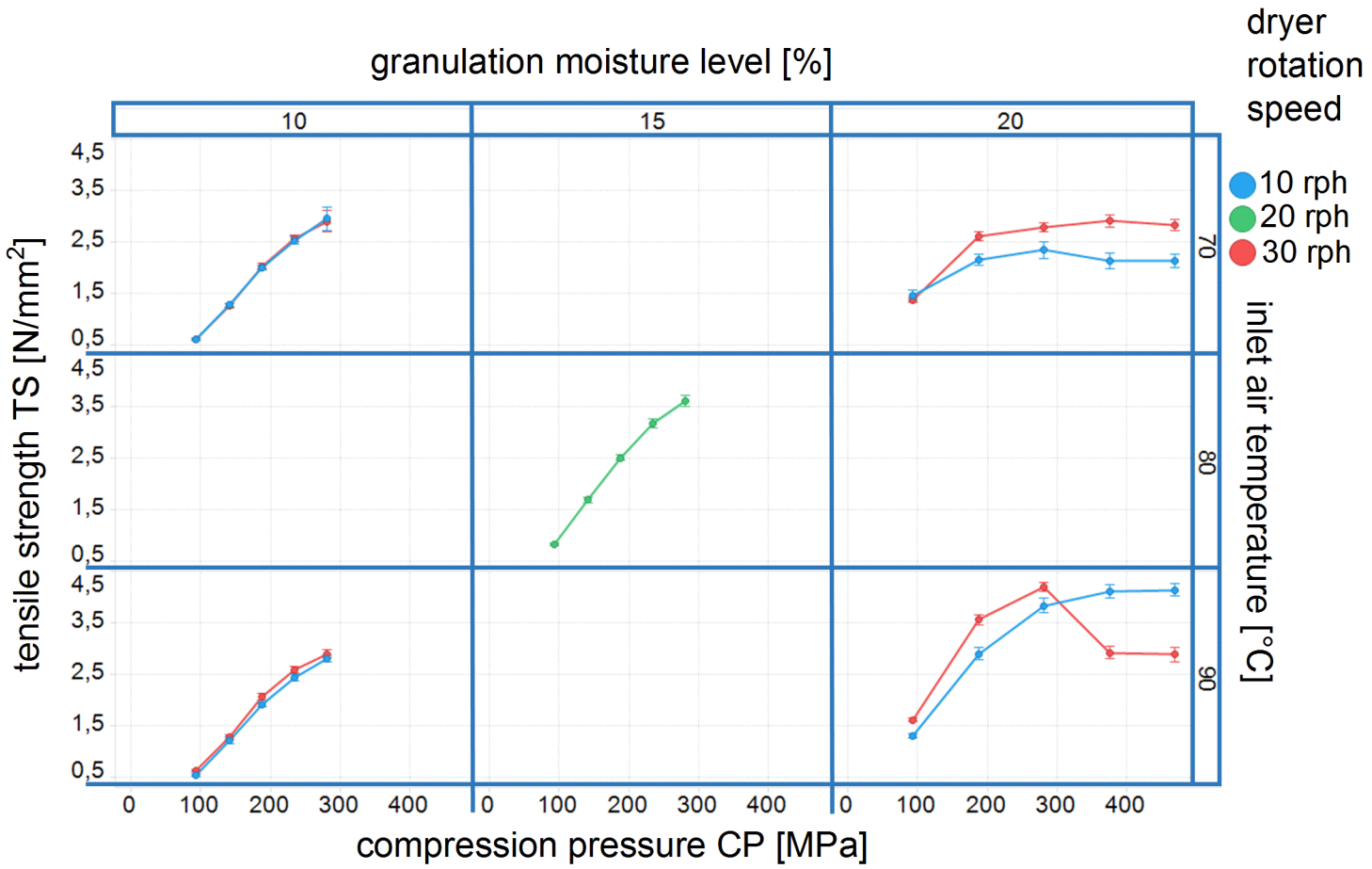

Figure 40 Tensile strength TS [N/mm²] plotted against compression pressure CP [MPa] for formulation 2 (F2); columns: different granulation ML [%]; rows: different inlet air temperature IAT [°C]; different colours: DRS [rph]; error bars: +/- 1 SD

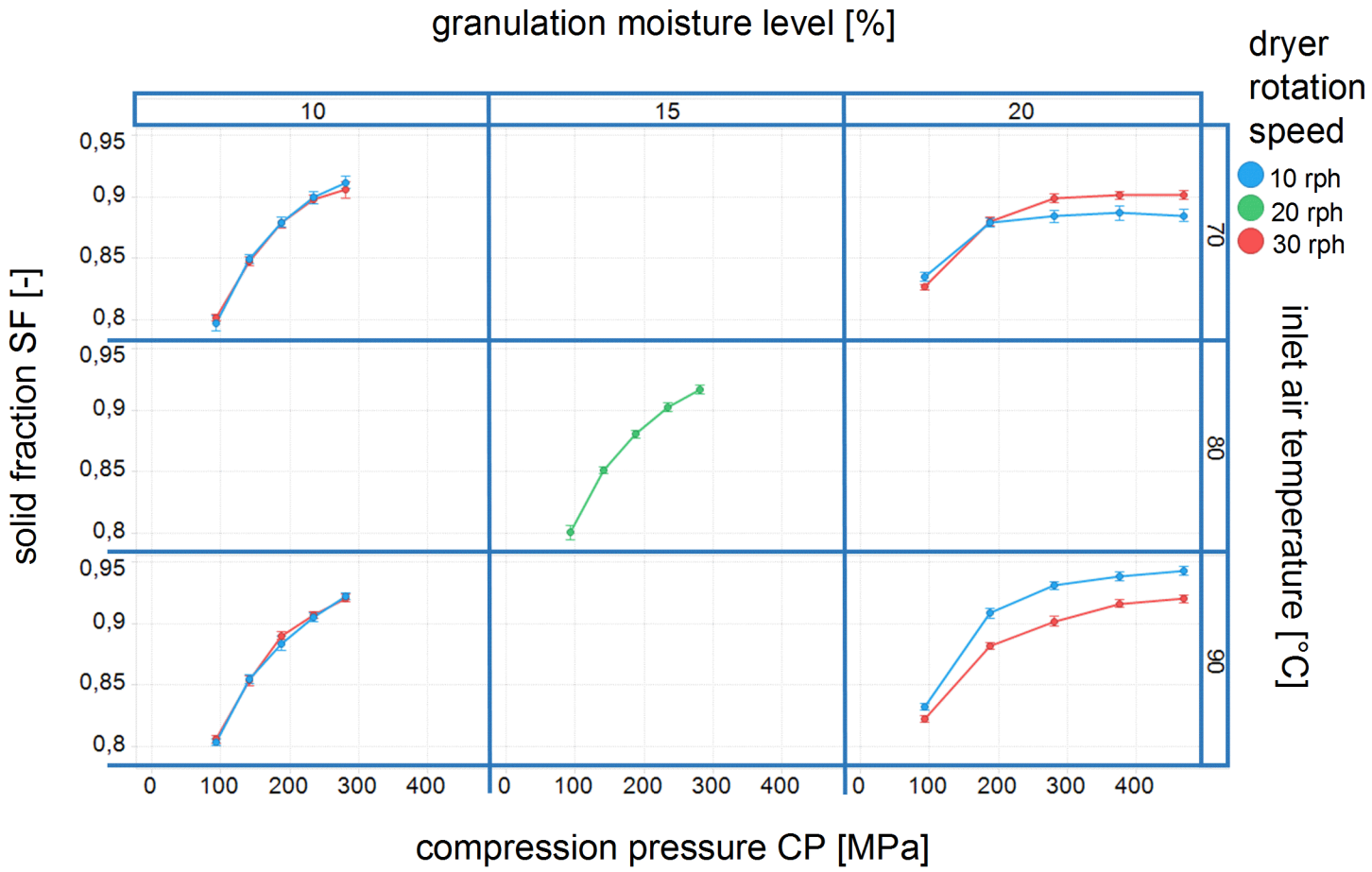

Figure 41 Solid fraction SF [-] plotted against compression pressure CP [MPa] for formulation 2 (F2); columns: different granulation ML [%]; rows: different inlet air temperature IAT [°C]; different colours: DRS [rph]; error bars: +/- 1 SD

6.5 SUMMARY & QBD LEARNING

The summary table of the impacts of the three investigated parameters on granule MAs and tablet QAs is given in Table 9. As explained and described in the previous chapter, granulation ML was of high impact on resulting attributes of granules and tablets. Therefore, it was confirmed to state granulation ML as a cPP. Furthermore, the evaluation presented in that chapter showed that increasing granulation ML lead to an increase of residual water content as well at the chosen drying conditions.

Table 9 Summary of impact of TSG process parameters (PP) on granule and tablet material attributes (MA) for both formulations; arrow up - increasing MA at increasing PP; arrow down - decreasing MA at increasing PP; equivalent bar - no impact of PP on MA; arrow diagonally upwards/downwards - slight increase/decrease of MA at increasing PP (partly dependent on other PPs)

		ML [%]	DRS [rph]	IAT [°C]
Formulation 1 (including cellulose)	particle fine fraction (< 63 µm) [%]	↘	↓	–
	particle coarse fraction (> 1000 µm) [%]	–	–	–
	residual water content (LoD [%])	↗ – high IAT / ↑ low IAT	↗ – high ML / ↑ low ML	↓
	tabletability (TS [N/mm²])	–	–	–
	compressibility (SF [-])	↗	–	↓
Formulation 2 (including starch)	particle fine fraction (< 63 µm) [%]	↓	↓	–
	particle coarse fraction (> 1000 µm) [%]	↑	–	–
	residual water content (LoD [%])	↑	↗ ↑ high ML / – low ML	↓
	tabletability (TS [N/mm²])	↑	↗ ↑ high ML / – low ML	↗ ↑ high ML / – low ML
	compressibility (SF [-])	–	–	↗ ↑ high ML / – low ML

With regard to dryer rotation speed DRS and inlet air temperature IAT, especially the influences on particle fine fraction and residual water content of granules are important to look at. Reason for that is that they also determine the tableting behaviour at the end. Further investigation of the tableting performance of the produced granules will be given in chapter 7.5 where also the here presented dataset is included. It was found that increasing DRS lead to a

decrease of particle fine fraction. As increasing DRS lead to a shorter residence time inside the granulator, that finding seemed reasonable as the granules at lower DRS were exposed shear stresses for a longer time. Nevertheless, the major impact on particle fine fraction was determined by the applied granulation ML.

With regard to residual water content, it was found that increasing DRS and decreasing IAT resulted in an increase of residual water content of the granules. That finding is in good agreement with the results of De Leersnyder et al. (2018) [12] who found decreasing residual water content of granules at increasing inlet air temperature, drying time and inlet air flow rate and the results of Pauli et al. (2018) [80] who found a linear relationship between DRS and residual water content. Pauli et al. (2020) [82] used that knowledge to define a startup procedure for the continuous fluid bed drying process where a ramp of dryer rotation speeds is applied to result in a residual water content within the applied. As shown here and also described in literature, the residual water content is of high impact for further processing of granules and therefore can be also considered as a cMA. Different papers describe model-based approaches to predict and control the residual water content for continuous fluid bed drying processes [31, 33, 83, 93].Within this thesis a simple drying capacity parameter is presented to estimate dryer performance at different equipment scales (see chapter 7.4).

To sum up, within this chapter residual water content and particle fine fraction were evaluated to be cMAs. Particle fine fraction is mostly influenced by the cPP granulation ML, whereas residual water content is also impacted by the cPPs dryer rotation speed and inlet air temperature. A further discussion of the here presented dataset will be conducted in the next chapter 7 where the scaling approach including three different equipment scales is evaluated.

7. A MECHANISTIC SCALING APPROACH FOR CONTINUOUS GRANULATION AND DRYING [73]

One advantage often mentioned in terms of continuous manufacturing is the option of easy scale-up, as scaling by time, scaling by throughput, and scaling by operating with parallel processing lines are possible [57]. Nevertheless, the lack of drug substance in early development stages necessitates the transition from smaller scale equipment to larger scale equipment with a limited number of experiments during drug product development. One equipment size cannot cover the throughput amounts from lab scale over pilot scale to full scale. A remaining advantage of continuous manufacturing, even if scale up is necessary, was stated by Mort [75]. He claimed scale-up from a small scale batch process to a continuous process to be more robust than scaling batch vessel processes.

Therefore, this chapter introduces a scaling approach established by investigating three equipment scales for continuous twin screw wet granulation and fluid bed drying based on the Glatt Modcos systems (XS-, S- and M-line) with the aim to result in equally good processability in terms of tabletability and compressibility for all three scales. Based on a Design of Experiment (DoE) performed on each equipment scale, the feasibility of the scaling approach was evaluated. To the knowledge of the authors there are two publications available dealing with the topic of scaling of twin screw wet granulation process [20, 79] and one publication comparing two different equipment scales of a continuous granulation and drying line, namely the Gea Consigma systems [122].

Osorio et al. (2017) [79] as well as Vercruysse et al. (2015) [122] used in their work formulations including cellulose. Other publications even investigated the effect of different grades of cellulose for twin screw wet granulation process [32, 41]. The authors of the here presented work consciously avoided cellulose in their formulation. The reason for that is the “sponge effect” of cellulose with regard to water uptake capacity [10, 29]. Therefore, relativly high liquid-to-solid-ratios LSR are necessary, when cellulose is part of the formulation to result in a proper agglomeration of particles.

The formulation without cellulose (formulation 2) used to evaluate the scaling approach guarantees two important aspects: On the one hand, it allows the manufacture of granules and tablets with a very broad range of resulting material attributes, as a wide range of process

parameters can be applied, while the resulting statistical models are sensitive for process parameter variation. On the other hand, the resulting throughput for the largest production scale based on the scaling approach reaches an adequate value. This is the key for the presented scaling approach to be reasonable and relevant for development of a NCE within the pharmaceutical industry.

7.1 THEORETICAL ASPECTS

7.1.1 Initial scaling approach

Aim of a scaling approach is always to result in equal material attributes over all equipment scales. Therefore, the process parameters have either to be adapted or to be kept constant when switching from scale to scale.

An initial scaling approach for the continuous granulation and drying line over three different equipment scales (XS – lab scale; S – pilot scale, M – production scale) is given in Table 10.

Table 10 Overview on initial scaling approach

	process parameter	initial scaling approach
GRANULATION	moisture level ML [%]	XS = S = M
	filling level FL [%]	XS = S = M
	screw speed [rpm]	XS = S = M
	powder feed rate PFR [kg/h]	XS < S < M
	liquid feed rate LFR [kg/h]	XS < S < M
	screw configuration	XS = S = M
	L/D ratio (processing and granulation zone)	XS = S = M
	barrel temperature [°C]	XS = S = M
DRYING	drying mode	XS ≠ S = M
	dryer rotation speed DRS [rph]	XS ≠ S = M
	drying time DT [min]	XS = S = M
	mass per chamber MC [kg]	XS = S < M
	inlet air temperature IAT [°C]	XS = S = M
	inlet air flow rate IAFR [m³/h]	XS < S < M

For the granulation unit, moisture level and screw speed were kept constant over all three scales within this approach. Powder feed-rate was adapted according to equipment scale to result in equal barrel filling level over all three scales. The design aspects screw configuration, L/D ratio and barrel temperature were kept constant, too.

Regarding the drying unit, the dryer rotation speed was a constant parameter except for the XS-line scale, as the XS-line scale has a lotwise and not a continuous drying mode. Drying time and inlet air temperature were the same for all three scales. The mass per chamber was the same for the lotwise XS-dryer and one chamber of the S-dryer as they are of the same size. MC

was higher for the M-line scale. Inlet air flow rate was adapted according to the applied powder feed rate and granulation moisture level per scale.

7.1.2 Enhanced scaling aspects

Several scaling parameters for twin screw wet granulation processes have been described in literature [20, 79] namely Froude number FR (see Eq. (7)), Powder feed number PFN (see Eq. (8)) and liquid-to-solid-ratio LSR (see Eq. (9)). The LSR is directly linked to the granulation moisture (see Equation (3)). Equation (10) shows, how ML and LSR are connected.

$$Froude\ number\ FR\ [-] = \frac{(screw\ speed\ [rps])^2 * diameter_{screw}[m]}{gravitational\ constant\ g\ [\frac{m}{s^2}]} \quad (7)$$

$$Powder\ feed\ number\ PFN\ [-] = \frac{PFR\ [\frac{kg}{s}]}{density_{powder}\left[\frac{kg}{m^3}\right] * (diameter_{barrel}[m])^3 * screw\ speed\ [rps]} \quad (8)$$

$$liquid - to - solid - ratio\ LSR\ [-] = \frac{LFR\ [\frac{kg}{h}]}{PFR\ [\frac{kg}{h}]} \quad (9)$$

$$moisture\ level\ ML\ [-] = \frac{LSR\ [-]}{1 + LSR\ [-]} \quad (10)$$

FR increases with increasing screw speed and increasing equipment scale (screw diameter), and therefore gives a hint on the applied shear energy of the twin screw granulator at fixed FL. PFN also depends on both, equipment scale and screw speed, but in contrast to FR, PFN decreases with increasing screw speed and equipment scale at a given PFR and is therefore a parameter similar to filling level FL (see equation (4)).

7.2 DESIGN OF EXPERIMENT BASED ON INITIAL SCALING APPROACH

The initial scaling approach presented in the theoretical section of this chapter (7.1) was used for evaluation of the three different equipment sizes. The process parameters per scale for the center point settings are given in Table 11.

Table 11 Initial scaling approach with resulting process settings for the center point settings

	process parameter	initial scaling approach	resulting process setting		
			XS	S	M
GRANULATION	moisture level ML [%]	XS = S = M	for center point settings: 15	15	15
	filling level FL [%]	XS ≅ S ≅ M	23 %	24 %	24 %
	screw speed [rpm]	XS = S = M	250	250	250
	powder feed-rate PFR [kg/h]	XS < S < M	1.5	5	20
	liquid feed-rate LFR [kg/h]	XS < S < M	for ML = 15 %: 0.26	0.88	3.53
	screw configuration	XS = S = M	conveying	conveying	conveying
	L/D-ratio (= processing length)	XS ≅ S ≅ M	26	29	27
	L/D ratio (granulation zone)	XS ≅ S = M	21	23	23
	barrel temperature [°C]	XS = S = M	20	20	20
DRYING	drying mode	XS ≠-S = M	batchwise	continuous	continuous
	dryer rotation speed DRS [rph]	XS ≠ S = M	no rotating dryer	20	20
	drying time DT [min]	XS = S = M	2.4	2.4	2.4
	mass per chamber MC [kg]	XS = S < M	0.025	0.025	0.1
	inlet air temperature IAT [°C]	XS < S = M	for center point settings: 70	80	80
	inlet air flow rate IAFR [m³/h]	XS < S < M	for center point settings: 19	150	340

To challenge and evaluate the described initial scaling approach, experiments on each equipment scale (XS, S & M) were performed based on a design of experiment (s. Figure 42). For each scale a 3-factorial, 2-level full factorial design including a center point was chosen. The three independent factors were moisture level ML, dryer rotation speed DRS and inlet air temperature IAT. The levels for ML were ML1 = 10 % and ML2 = 20 %, for DRS they were DRS1 = 10 rph and DRS2 = 30 rph and for IAT they were for XS scale IAT1 = 60 °C and IAT2 = 80 °C and for S scale and M scale IAT1 = 70 °C and IAT2 = 90 °C. The setting of

center (0) and extreme (+1 / -1) levels of the DoE of the IAT for the XS dryer was adjusted to a 10 K lower value compared to S scale and M scale. These three process parameters were chosen to cover process parameters of both, granulation and drying unit. Based on the short process times and low throughput rate for the XS equipment, additional experiments could be conducted at this smallest scale (see Figure 42).

In addition to that design of experiment, additional experiments were performed where the center point settings were repeated at two additional higher screw speeds (center point screw speed 1 = 250 rpm; screw speed 2 = 270 rpm; screw speed 3 = 300 rpm). The purpose of these experiments was to check also the influence of screw speed as scaling parameter. The results of that evaluation are discussed in the next chapter 7.3.

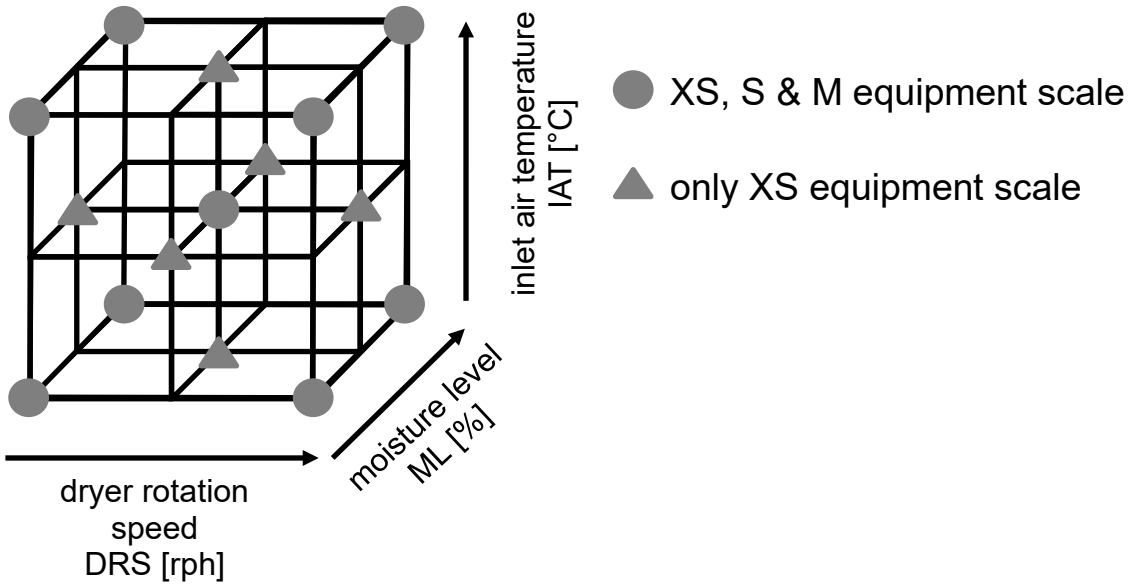

Figure 42 Design of experiment performed on each scale

7.3 ENHANCED SCALING PARAMETERS FOR TWIN SCREW WET GRANULATION

Table 12 gives an overview on Froude number FR, powder feed number PFN and filling level FL for the experiments performed at different screw speeds and on all three equipment scales as described in chapter 7.1.2. Comparing these experiments per scale, a decrease of FL, a decrease of PFN, and an increase of FR could be observed with increasing screw speed. Looking at every scale separately, PFN increased with increasing FL following a linear correlation.

The applied scaling approach lead to an increase of FR with increase of the equipment size at identical screw speed and constant FLs.

Table 12 Enhanced scaling parameters for twin screw wet granulation process for the three equipment scales for the additional performed experiments

scale	diameter screw [m]	powder feed rate PFR [kg/h]	exp.no.	screw speed [rpm]	filling level barrel FL [%]	Froude number FR [-]	powder feed number PFN [-]
XS	0.011	1.5	1	250	23.2	1.95E-02	1.50E-01
			2	270	21.5	2.27E-02	1.39E-01
			3	300	19.3	2.80E-02	1.25E-01
S	0.016	5	1	250	23.9	2.83E-02	1.63E-01
			2	270	22.2	3.30E-02	1.51E-01
			3	300	19.9	4.08E-02	1.36E-01
M	0.024	20	1	250	23.8	4.25E-02	1.93E-01
			2	270	22.0	4.95E-02	1.79E-01
			3	300	19.8	6.11E-02	1.61E-01

One result of the evaluation of the different scaling parameters at different screw speeds is depicted in Figure 43 where the effect of the Froude number FR on the coarse particle size fraction (> 1000 µm) is shown.

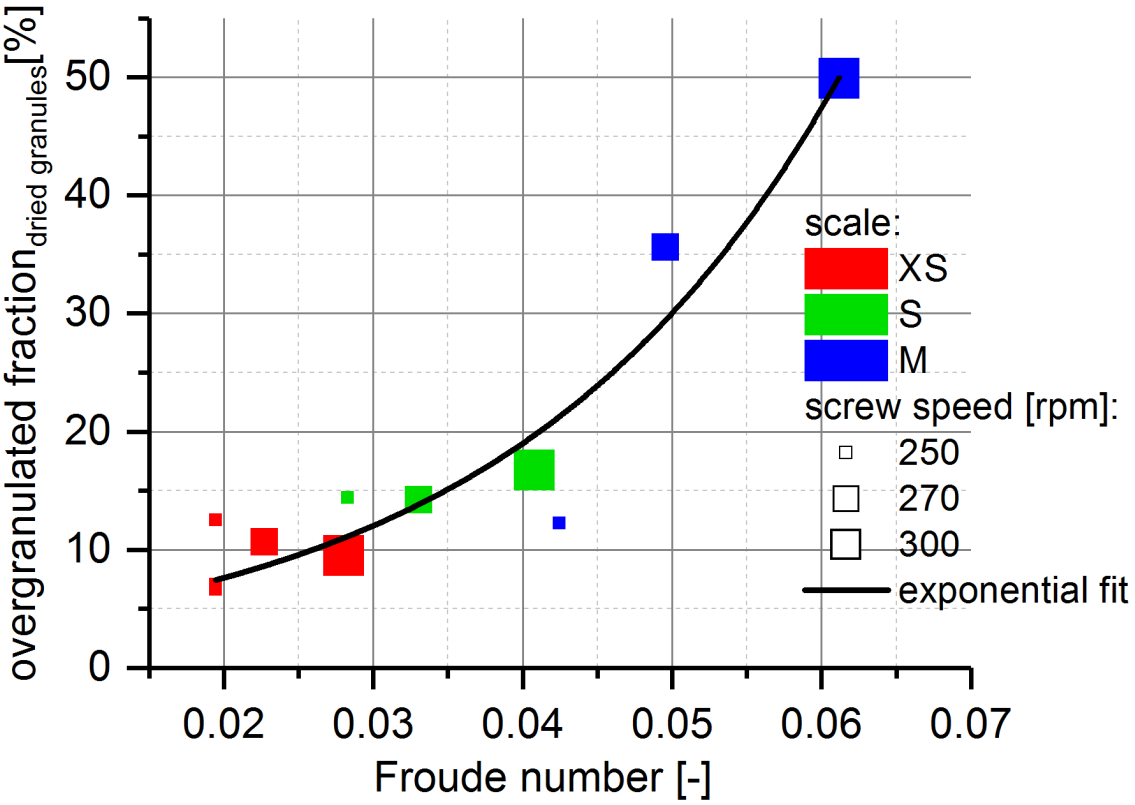

Figure 43 Effect of Froude number [-] on overgranulated fraction [%] at different equipment scales and screw speeds at ML = 15%; different colours of squares: equipment scale; different sizes of squares: screw speed; solid black line: exponential fit, for illustrational purpose

The highest coarse particle size fraction of approx. 50 % was obtained for the biggest scale M and the highest screw speed of 300 rpm. No increase of the coarse particle size fraction could be observed at FR below approximately 0.045. Experiments which were performed with a higher shear stress, namely at a FR above approximately 0.045 resulted in a strong increase of the coarse fraction. FR is directly connected to the diameter of the screws (scale) and to the screw speed. Both, equipment scale and screw speed can be covered with this parameter. Compensating high screw speed for experiments with smaller screws with a low screw speed for larger screws hence, leads to comparable FRs for at least some process conditions of the different equipment scales.

Applying the correlation presented in Figure 43, identical coarse particle fractions could be achieved by bridging the scales at settings where the process parameters resulted in similar Froude numbers.

7.4 DRYING PERFORMANCE PER SCALE

Figure 44 shows the residual water content of dried granules for all performed experiments of the process DoE sorted by applied moisture level ML during twin screw wet granulation and categorized by the used equipment scales. For the lower ML of 10 % and 15 % an average residual water content below 1 % could be reached at the chosen drying conditions for all three scales, due to the fact that no microcrystalline cellulose was used for the formulation, which offers the possibility to have proper particle agglomeration also at lower MLs. For a granulation ML of 20 % the water content exceeded 1 % for all three scales.

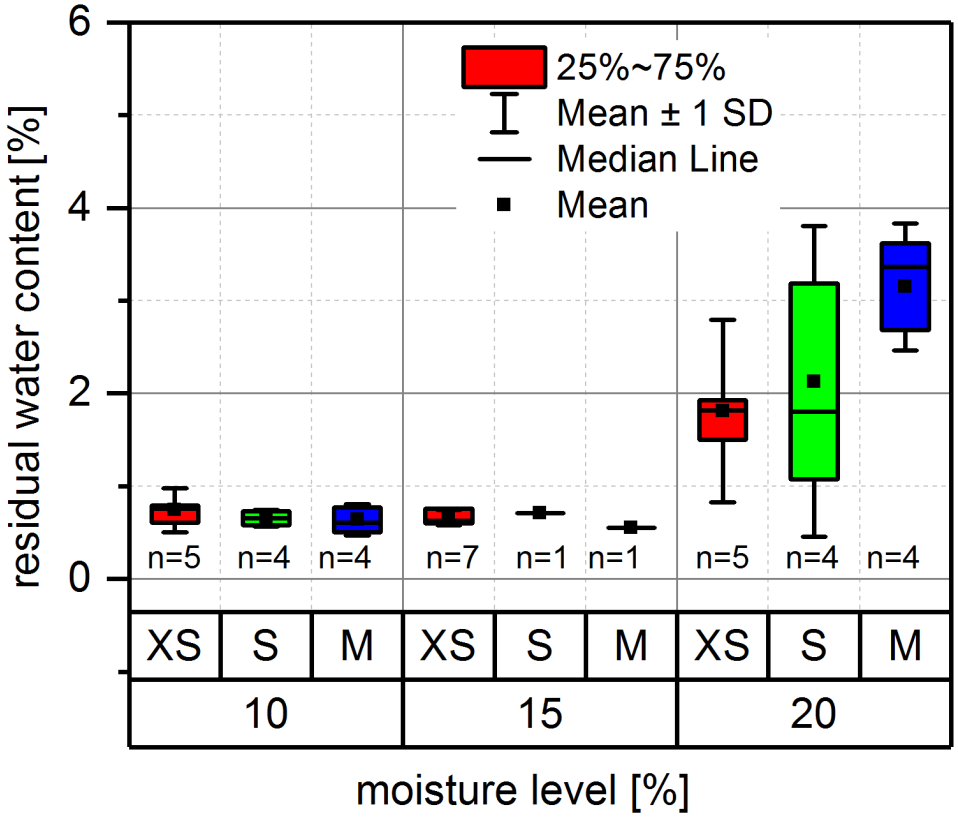

Figure 44 Residual water content of dried granules [%] for different moisture levels during wet granulation (ML) [%], categorized by equipment scales, boxes represent 25 – 75 % percentile

Furthermore, an increase in water content after drying with increasing equipment scale could be observed. For the XS-line and S-line scale experiments the residual water content of dried granules shows larger error bars compared to the M-line scale experiments. As granulation ML was not the only parameter, which was varied during the process DoE, the larger error bars reflect the additional variation of DRS and IAT, also. In chapter 7.6 the impact on residual water content is discussed in more detail. Nevertheless, the increase of the average water content gives a hint that drying capacity was decreasing with increasing scale for the chosen process settings. Mortier et al. (2014) [76] and Pauli et al. (2019) [81] used mass and energy balance models to investigate drying performance of fluid bed drying process. In this study a simple parameter (drying capacity parameter DCP) is presented to easily estimate drying performance of the Modcos fluid bed drying system.

In Figure 4 the average residual water content of granules produced at a moisture level ML = 20 % for each equipment scale is plotted against the average of this drying capacity parameter DCP per scale. DCP is defined as the applied air volume flow per granule mass that has to be dried. As the IAT for the XS-Line experiments was lower than for the M-Line and S-Line, a δT for temperature compensation was included in the drying capacity parameter DCP (see Eq. (11) and Eq. (12)).

$$drying\ capacity\ parameter\ DCP\ [\frac{m^3 * °C}{g}] = \frac{IAFR_{chamber}\left[\frac{m^3}{h}\right] * DT\ [h] * \delta T_{in-out}[°C]}{mass_{chamber}[g]} \quad (11)$$

$$\delta T_{in-out}[K] = IAT\ - IPT \quad (12)$$

$$with\ inlet\ product\ temperature\ IPT = 25\ °C = 298.15\ K = const$$

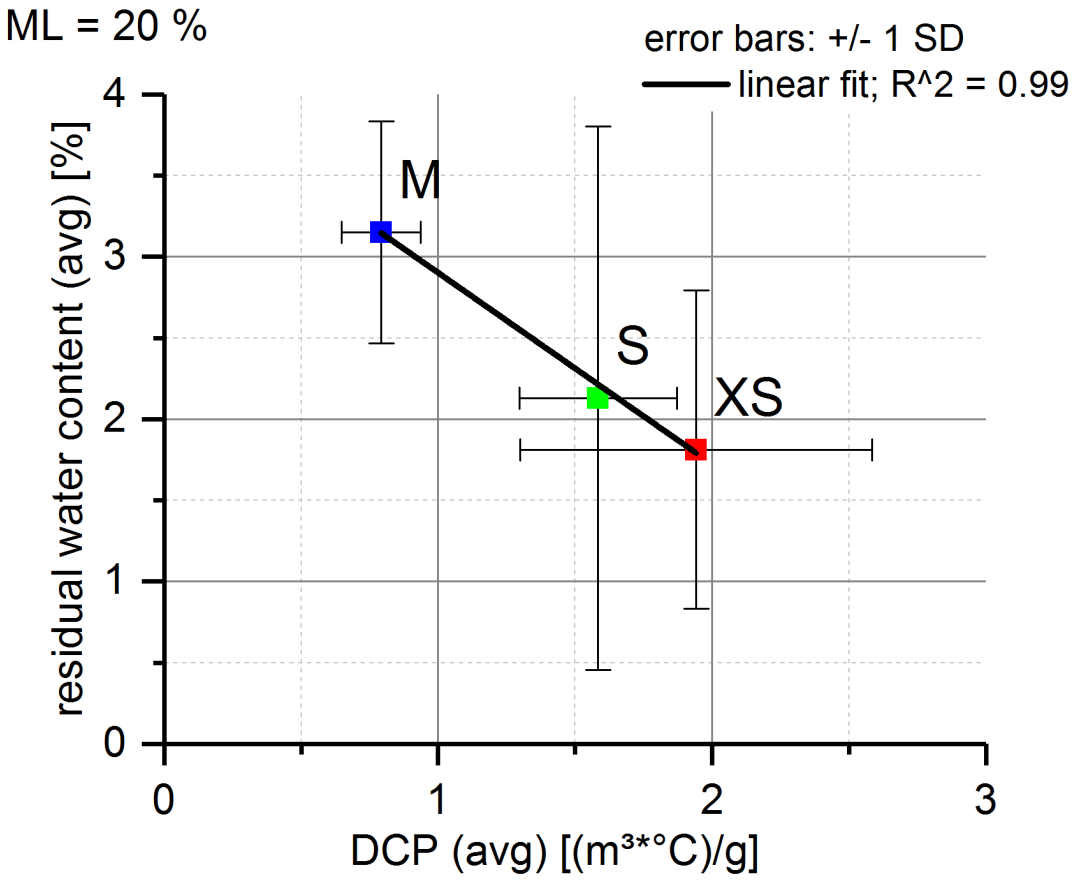

Figure 45 Correlation of average residual water content [%] and average drying capacity parameter DCP [(m^3*°C)/g] for the experiments performed at a moisture level ML = 20 %; coloured squares: different equipment scales; solid black line: linear fit with $R^2 = 0.99$; error bars (x/y): +/- 1 SD

As shown in Figure 45, a linear correlation of average residual water content at the highest applied ML = 20 % per scale and the average DCP per scale could be observed ($R^2 = 0.99$). The correlation in Figure 45 explains the observation above for Figure 44; as the XS-Line experiments were performed at the highest DCP (best drying capacity) the average residual water content was the lowest compared to the bigger scales. This result is in good agreement with the observations of De Leersnyder et al. (2018) [12] who also found lower residual water content at higher IAFR, DT and IAT for the Consigma system.

7.5 SCALE INDEPENDENT TABLETING PERFORMANCE

The influence of particle fine fraction (< 63 µm) of dried granules on tabletability is illustrated in Figure 46. Tabletability is the possibility of forming a tablet with a certain tensile strength TS at a defined compression pressure CP (Tye et al., 2005) [112]. Scale-independent, a linear correlation between TS at compression pressure CP = 281 MPa and particle fine fraction could be observed with rising TS at decreasing fine fraction despite of three outliers. These outliers could be identified as the ones having a relatively high residual water content for the dried granules (> 3.0 %). To have a deeper understanding of these outliers and especially, why not all samples with a residual water content > 3 % resulted in a decreased tabletability, investigations were conducted on tablets' compressibility (see Figure 47).

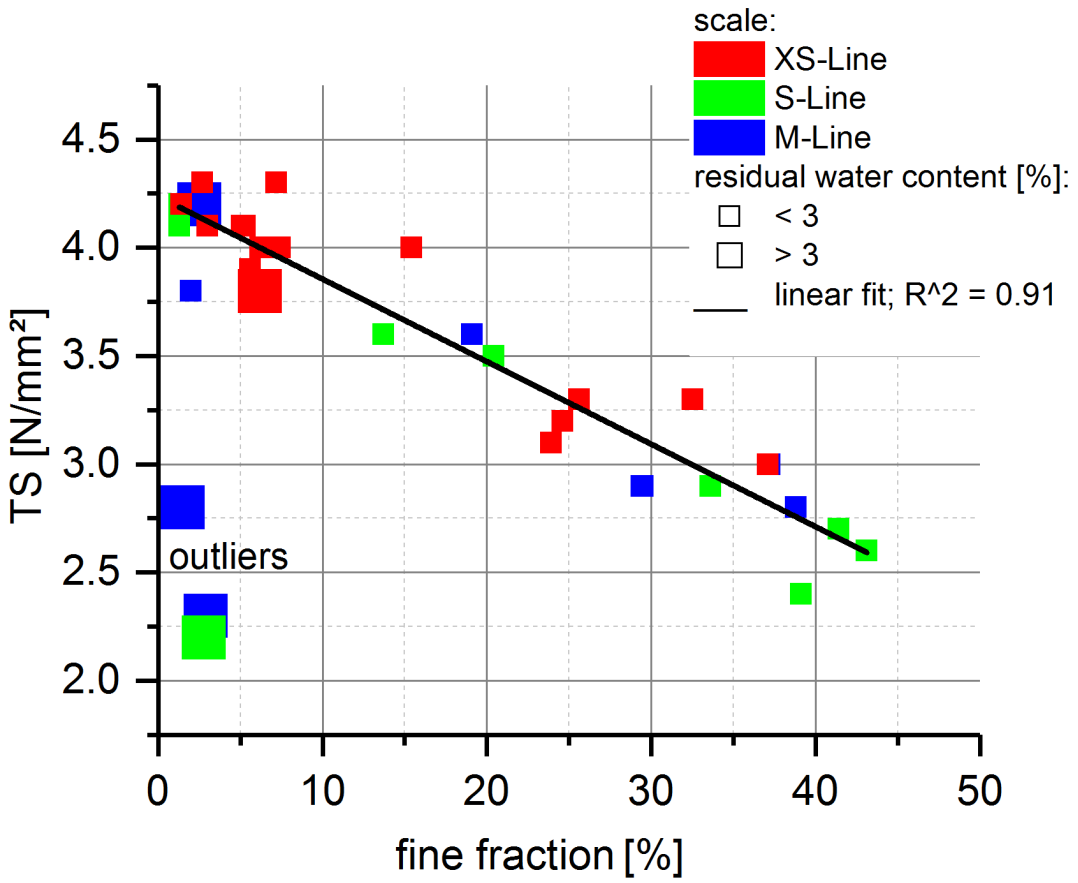

Figure 46 Correlation of tensile strength TS [N/mm^2] of tablets compressed at 281 MPa and fine particle fraction of dried granules for all three scales; different colours of squares: equipment scale; different sizes of squares: residual water content; solid black line: linear fit with R^2= 0.91

The compressibility of a tablet is defined as the ability of forming a tablet with a certain solid fraction SF at a defined compression pressure CP (Tye et al., 2005) [112]. The modified Kawakita equation (Schmidtke et al., 2017 [100]; see Eq. (13)) was used to calculate the Kawakita *a* parameter for each process setting and equipment scale. A linear fit was performed by plotting the quotient of compression pressure and solid fraction $\frac{CP}{SF}$ against the compression pressure CP. Kawakita *a* is defined as the reciprocal of the slope resulting from this linear regression. The meaning of Kawakita *a* is the maximum solid fraction, that is theoretically achievable (Schmidtke et al., 2017 [101]). Figure 47 shows that compressibility of tablets was getting worse (decreasing Kawakita *a)* for higher residual water content (> 2.5 %) for those experiments, which resulted in a particle fine fraction < 10 %.

$$\frac{CP}{SF} = \frac{CP}{a} + \frac{1}{a * b} \tag{13}$$

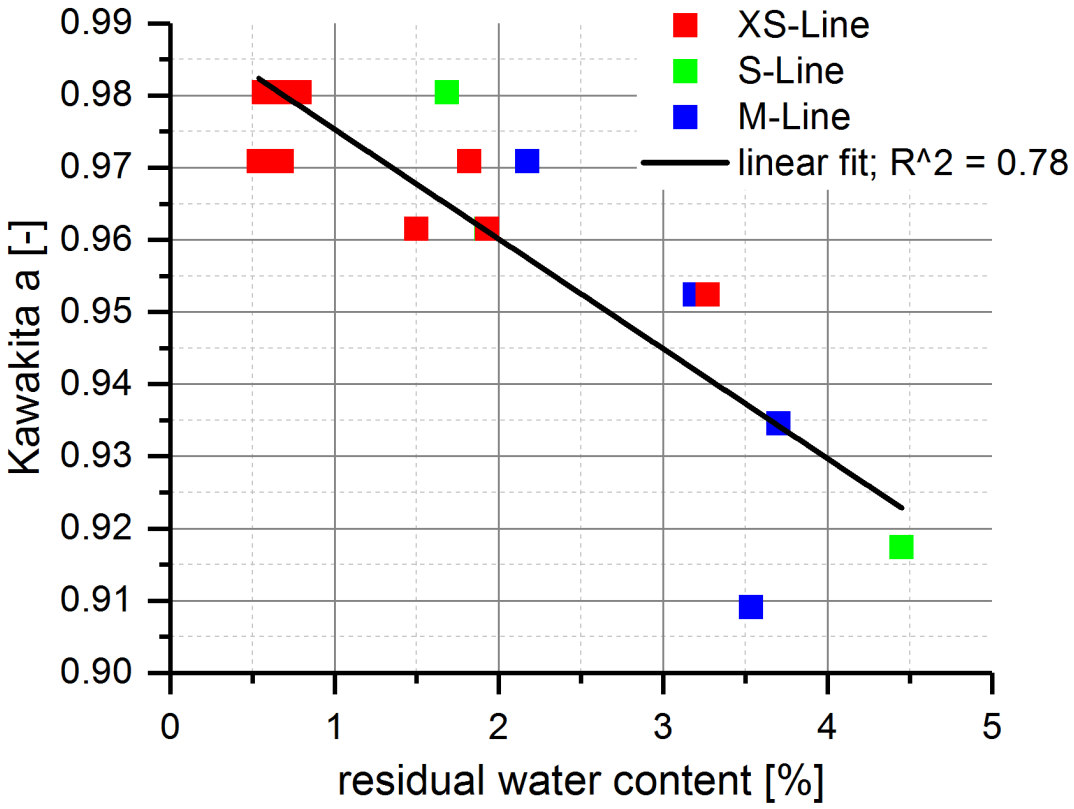

Figure 47 Influence of residual water content of dried granules with a fine fraction < 10 % on compressibility behaviour (Kawakita a) of tablets; solid black line: linear fit with $R^2 = 0.78$

Hence, regardless of the equipment scale, a low amount of particle fine fraction (< 10 %) and a low residual water content (< 2.5 %) of dried granules could be identified to be the most important material attributes of granules to result in a good tabletability and compressibility of the investigated product and therefore were defined to be the specification limits for further investigations.

7.6 CALCULATED PROCESS DESIGN SPACE PER SCALE BASED ON STATISTICAL EVALUATION

As particle fine fraction and residual water content of granules were identified to be of high impact on the quality of manufactured tablets in terms of tabletability and compressibility (see 7.5), statistical models for these two granule material attributes were generated for each equipment scale. The models were based on the test case described in 7.2 statistical modelling was performed with Statistica software. As expected, based on previous experience, the effect of ML on fine fraction and residual water content was significant for this formulation. The effect of ML on these two material attributes was also significant for all three equipment scales (except: residual water content model for S-line; confidence interval = 95 % and $p < 0.05$).

Good correlation was achieved for all three scales for the particle fine fraction models with coefficients $R^2 > 0.9$. Residual water content models resulted in slightly lower coefficients (XS and M: $R^2 > 0.8$ and S: $R^2 = 0.7$). Equations (19) – (24) in the appendix show the regression equations for all three scales and both material attributes.

Based on these models a process design space for each scale was calculated to reach a particle fine fraction < 10 % and a residual water content < 2.5 %. MLs were predicted at a defined IAT of 80 °C and for five different DRS in a range between 10 rph and 30 rph. As Keleb et al. (2004) [48] already showed, that increasing ML resulted in a decrease of particle fine fraction, the particle fine fraction models were used to calculate the lower limit of ML to still result in a particle fine fraction < 10 % for different DRS. Higher ML were shown to result in a higher residual water content irrespective of scale as well. Therefore, the residual water content models were selected to calculate the upper limit of ML to ensure a residual water content < 2.5 %.

In Figure 48 the results of the described calculation of ML limits per DRS are depicted per scale. Inside the coloured areas a particle fine fraction < 10 % and residual water content < 2.5 % can be obtained.

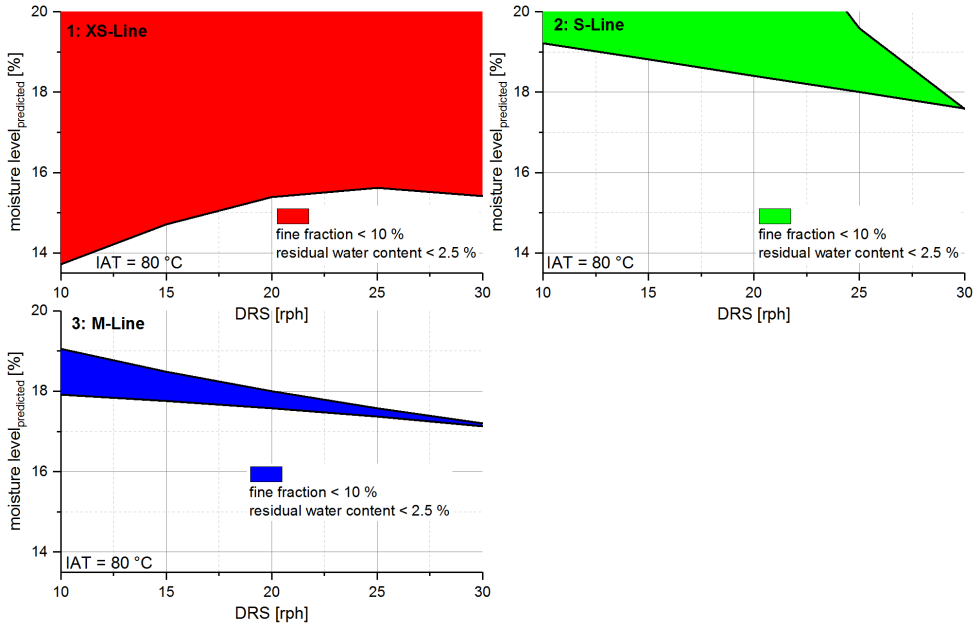

Figure 48 Predicted moisture level [%] based on statistical models for each equipment scale to achieve a particle fine fraction < 10 % and a residual water content < 2.5 % (inside coloured areas) at different dryer rotation speeds DRS [rph] and at an inlet air temperature IAT = 80 °C; 1: XS-Line; 2: S-Line; 3: M-Line

For XS-line the largest area is visible. As XS-line experiments showed higher fine fraction at higher DRS, the predicted ML increases with increasing DRS. Due to the fact, that the XS fluid bed dryer is a non-continuous dryer, a higher DRS means a shorter drying time as well as a lower amount of granule mass to be dried per batch. Residual water content was below 2.5 % for all XS experiments despite of one outlier at a residual water content of 3.27 %. Therefore, the upper ML limit defining the border to result in a residual water content < 2.5 % is not visible for the XS-line experiments at the depicted ML range between 14 % and 20 %.

Comparing the XS-line process design space with the ones of the S-line and M-line, reveals that the process design space areas are smaller for S-line and M-line than for XS-line. Two reasons for that observation can be mentioned. The first reason is that S-line experiments as well as M-line experiments generally resulted in a higher particle fine fraction compared to XS-line experiments. Therefore, a higher ML was needed for S-line and M-line compared to XS-line to result in a particle fine fraction < 10 % (lower limit of coloured areas in Figure 48).

As described above, drying performance for S-line and especially for M-line was lower compared to XS-line resulting in higher residual water contents specifically for ML = 20 %. Therefore, the second reason for the smaller areas for these two scales is the fact that the upper ML limit defining the border to result in residual water content < 2.5 % was at a ML level below 20 % for M-line and partially for S-line (DRS dependent).

The influence of DRS on particle fine fraction and residual water content for the continuous fluid bed dryers of S-line and M-line was the same overall. Increasing DRS resulted in lower particle fine fraction and higher residual water contents because higher DRS implicates shorter drying times. Pauli et al. (2018) [80] found a linear correlation of DRS and residual water content in their study. Nevertheless, based on the conducted experiments, no overall guidance for the correlation on all scales can be given. More significant correlations could possibly established at constant drying capacity.

7.7 SUMMARY & QBD LEARNING

A new scaling approach was predefined and successfully applied for three equipment scales and resulted in scale independent and well comparable material attributes for both, granules and the resulting tablets. The chosen formulation, that avoids microcrystalline cellulose allowed a broad range of process parameters settings to allow the evaluation of the drying performance and to generate a sensitive model. In addition to the selected initial scaling approach, further data were successfully used to depict a systematic influence of screw speed and filling level of the TSG on granules particle size distribution. Correlations of particle fine fraction and residual water content of the produced granules on the resulting tabletability and compressibility behaviour were identified. Within the presented case study these correlations were applied to define (specification) limits for the two critical granule MAs particle fine fraction and residual water content. Based on statistical models of the applied design of experiments and the granules attributes' specification limits, a process design space for continuous granulation and drying process could be defined for each scale. A limitation of the process design space by the equipment scale was observed and by a detailed investigation and comparison of the drying performance an explanation could be given. The investigation showed, that at higher moisture levels the drying performance decreased with increasing scale. For further evaluation, especially at larger scale, the drying performance will be improved by higher energy input through increasing the inlet air flow rate IAFR and/or the inlet air temperature IAT. However, further investigation will be performed to allow sound calculations that result in a more constant process design space across different scales.

Even with that limitation, the presented scaling approach offers the possibility for a smooth scaling during drug product development, saving time and money by selecting the most suitable process parameters based on a small set of experiments.

8. EVALUATION OF LONG-TERM RUNS

The aim of the previous chapters was to build a proper process understanding for all three investigated process units: continuous dosing (chapter 4), continuous twin screw wet granulation (chapter 5) and continuous fluid-bed drying (chapter 6). The relationship between process parameters for each process unit and the material attributes of incoming and resulting intermediates as well as the final drug product tablet was investigated. Furthermore, a scaling approach was evaluated to result in a smooth transition from lab over pilot to production scale during development of a NCE (chapter 7).

However, a proper process understanding as described and evaluated in these previous chapters is not the only key for success within continuous pharmaceutical manufacturing. Additionally, robustness and stability of continuous pharmaceutical processes have to be analysed within an evaluation of long-term effects.

Therefore, two long-term runs were conducted with a runtime of 5 hours per run using the M-line-scale equipment (see 11.1.4.3.3) for continuous granulation and drying to gain knowledge about process robustness and stability. An overview on important process parameter settings of both long-term-runs is given in Table 13.

Table 13 Overview on important process parameter settings for granulation and drying process unit and general aspects (runtime and used powder preblend) for long-term run #1 and long-term run #2

		long-term run #1	**long-term run #2**
Granulation	PFR [kg/h]	20	20
	screw speed [rpm]	250	250
	granulation ML [%]	appr. 15	appr. 15
	water temperature cooling system for barrel [°C]	20	18
Drying	IAT [°C]	70	75
	IAFR [m³/h]	300	290 / 300
	DRS [rph]	20	20
General aspects	runtime [hrs]	5	5
	preblend (formulation 2)	DL = 5 % ↓ DL = 25 % ↓ DL = 5 %	placebo ↓ DL = 5 %

Aim and focus of this chapter is to evaluate long-term-effects of the continuous dosing unit (see 8.1) as well as twin screw wet granulation process (see 8.2). For the dosing unit a refill regime of the hopper during running process was investigated whereas for TSG process heating effects along the barrel over time were under evaluation.

8.1 CONTINUOUS DOSING: REFILL REGIME OF HOPPER

With regard to the continuous dosing process unit, manual refilling of the hopper took place during running process. Drugload changes of formulation 2 (see 10.2.3) were introduced during refilling. For long-term run 1 a DL change from DL = 5 % to DL = 25 % and back to DL = 5 %

was introduced during running process. During long-term run 2 a switch from placebo preblend of F2 to verum preblend with DL = 5 % of F2 took place (see also Table 13).

The impact of the fill level of the hopper (see equation (1)) on the powder feed rate is depicted in Figure 49 for long-term run 1 and in Figure 50 for long-term run 2. It has to be considered that a 100 % fill level of the hopper was defined to coincide with a 100 % nominal fill in this case.

The blue coloured graphs in the upper part of both figures show the powder feed-rate PFR along the whole process time. Single PFR values exceeding a 10 % limit of the target PFR (upper limit: 22 kg/h, lower limit: 18 kg/h) were excluded from that depiction, because they occurred due to accidently touching the feeder by operator (especially during refilling) and do not reflect the resteering process of the gravimetric controller. The borders indicating a 1 % and 1.5 % deviation from the target PFR = 20 kg/h were added. For long-term run 1 it became visible, that the 1 % and even the 1.5 % deviation border for PFR were exceeded at time points, where refilling of the hopper took place at a fill level FL < 45 %. In the time range between process time T1 = 57 min and process time T2 = 213 min the 1 % deviation border was not exceeded. During this time period, the hopper was refilled at a fill level FL > 45 %.

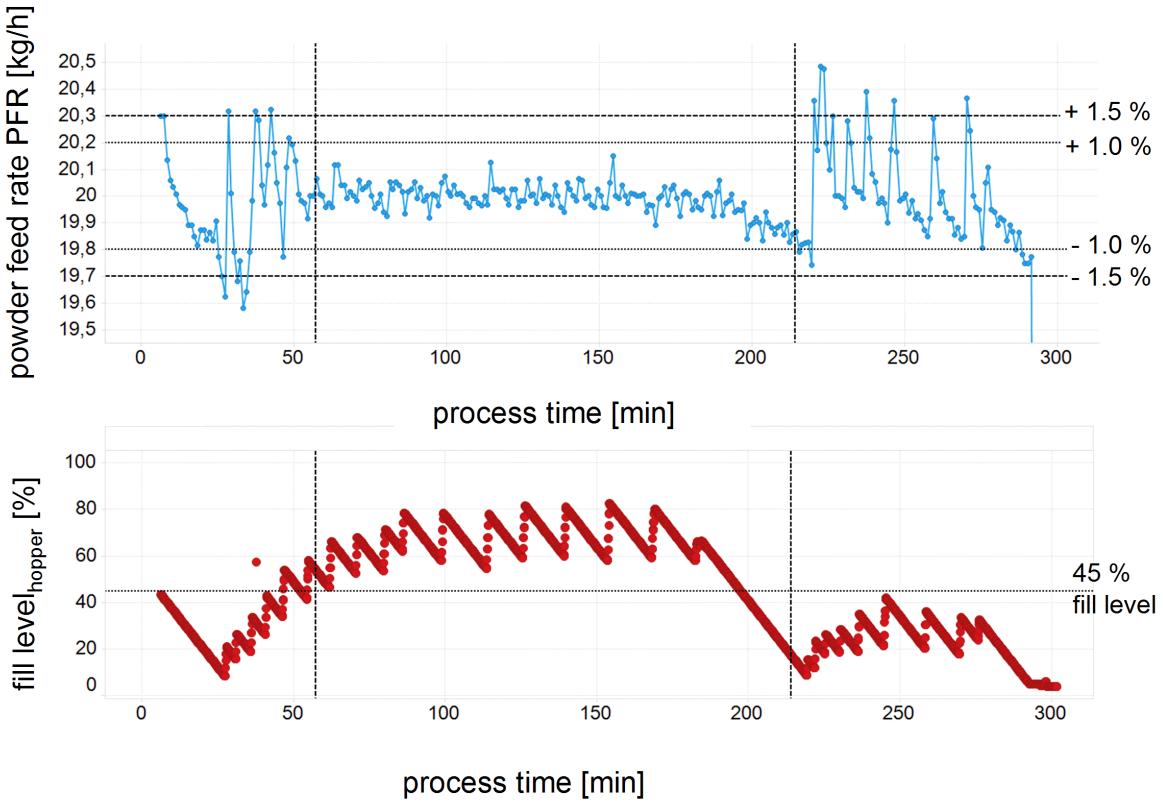

Figure 49 Impact of fill level of the hopper [%] on powder feed rate PFR [kg/h] for long-term run #1; blue coloured graph: powder feed rate PFR [kg/h] plotted against process time [min]; red coloured graph: fill level of the hopper [%] plotted against process time [min]

This observation regarding the gravimetric feeding mode during long-term run 1 is in line with the investigation of continuous volumetric dosing in chapter 4.3. Figure 6 showed the impact of the fill level of the hopper on dosed mass per revolution for a volumetric feeding mode. Therefore, it is reasonable that refilling at a higher fill level of the hopper (> 45 % in this case study and for the bigger hopper) lead to a more accurate PFR over time, as less resteering of the gravimetric controller was necessary.

This gained knowledge about refilling at the right fill level of the hopper was applied for long-term run 2 (see Figure 50).

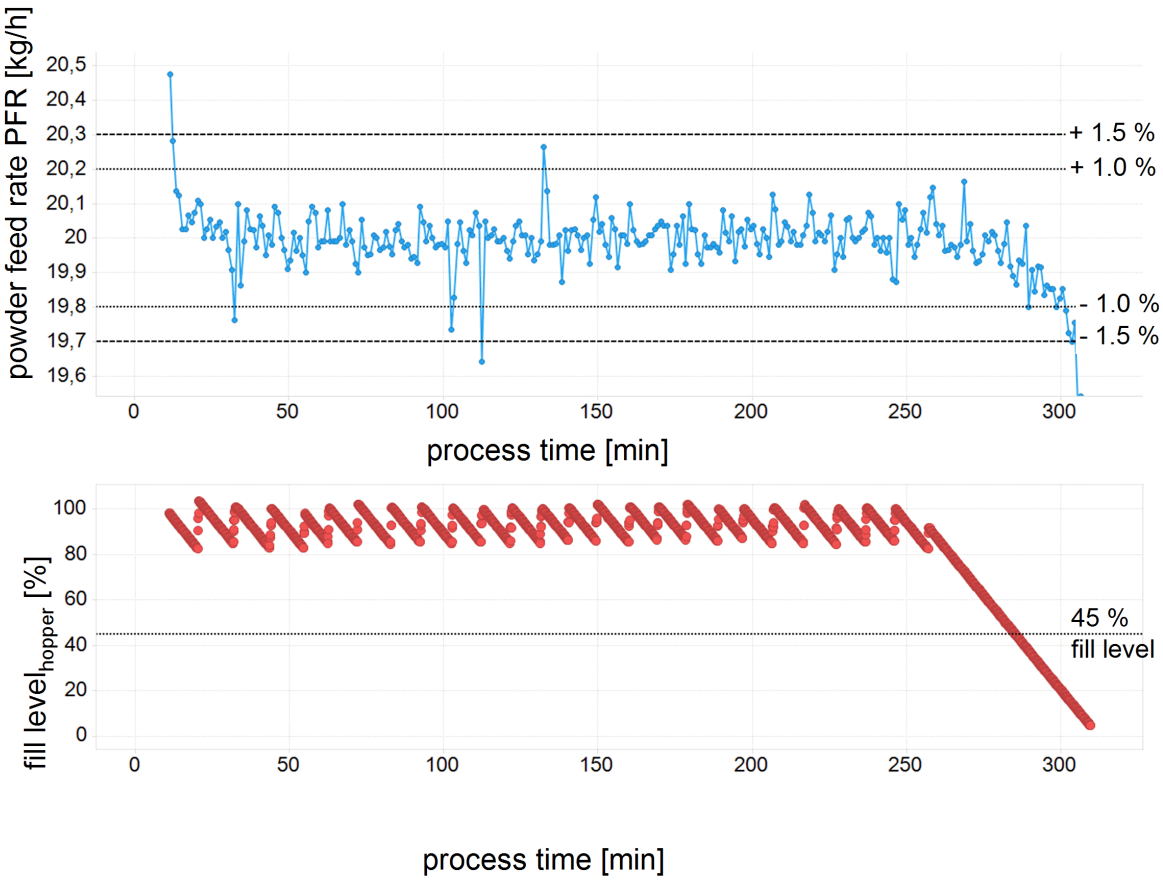

Figure 50 Impact of fill level of the hopper [%] on powder feed rate PFR [kg/h] for long-term run #2; blue coloured graph: powder feed rate PFR [kg/h] plotted against process time [min]; red coloured graph: fill level of the hopper [%] plotted against process time [min]

Refilling the hopper at a fill level FL > 45 % (even > 80 %) over the whole process time range, lead to an accurate powder feed-rate PFR with a deviation < 1.5 % of the target PFR as expected (except one outlier).

Thus, the long-term run 2 experiment proved the observations and conclusions drawn from long-term run 1. Furthermore, it emphasized the importance of more frequent refilling of a smaller amount of material as well as shorter refilling times for an accurate feedability [25]. These two approaches were applied at refilling during both long-term runs and were concluded from the results drawn in chapter 4. The results from investigation of volumetric feeding mode led to the additional conclusion that a more frequent refilling of a smaller amount of material as well as a shorter refilling time were beneficial in terms of an accurate powder feed rate over time. As a strong dependence between dosed mass per revolution and filling level of the hopper

was found in a volumetric feeding mode, it became clear that a more frequent refilling of a lower amount of material leads to less resteering necessity of the gravimetric controller as the difference between the dosed mass per revolutions between starting and endpoint of refilling can be kept low (see sketch in Figure 51).

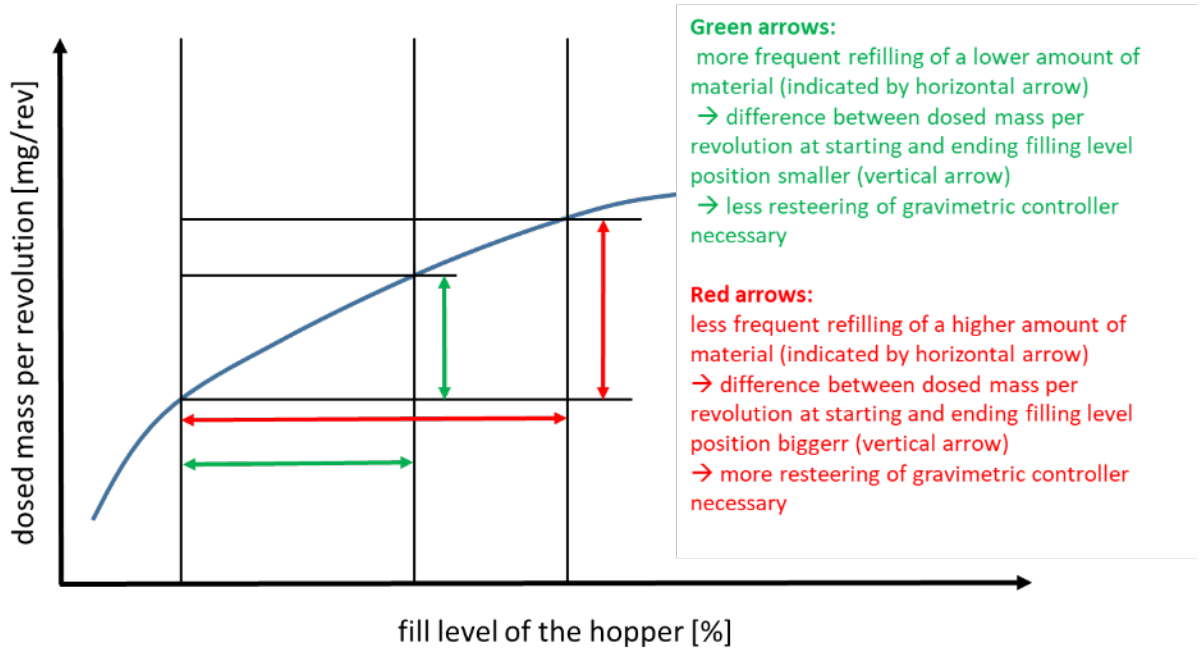

Figure 51 Rationale for a more frequent refilling of a lower amount of material based on the investigation of volumetric dosing in chapter 4

The rationale behind the short refilling times (< 1 min within this case study) is the fact that the feeder switches to run in a volumetric feeding mode during refilling. Therefore, during that period no resteering by the gravimetric controller is possible. This fact makes it logical to keep this period of time as short as possible to keep the overall time of the feeder running in a volumetric feeding mode without gravimetric controller to a minimum level.

8.2 TWIN SCREW WET GRANULATION: TEMPERATURE CONTROL OF BARREL AS KEY FOR PROCESS STABILITY

The temperature of the granulator barrel was controlled by a temperature control system during both long-term runs. Water temperature was set to a temperature T = 20 °C for long-term run 1. The water temperature during long-term run 2 was set to a T = 18 °C. In Figure 52 the temperature control system is depicted including the 5 temperature sensors along the barrel (T1 – T5) recording barrel temperature during process.

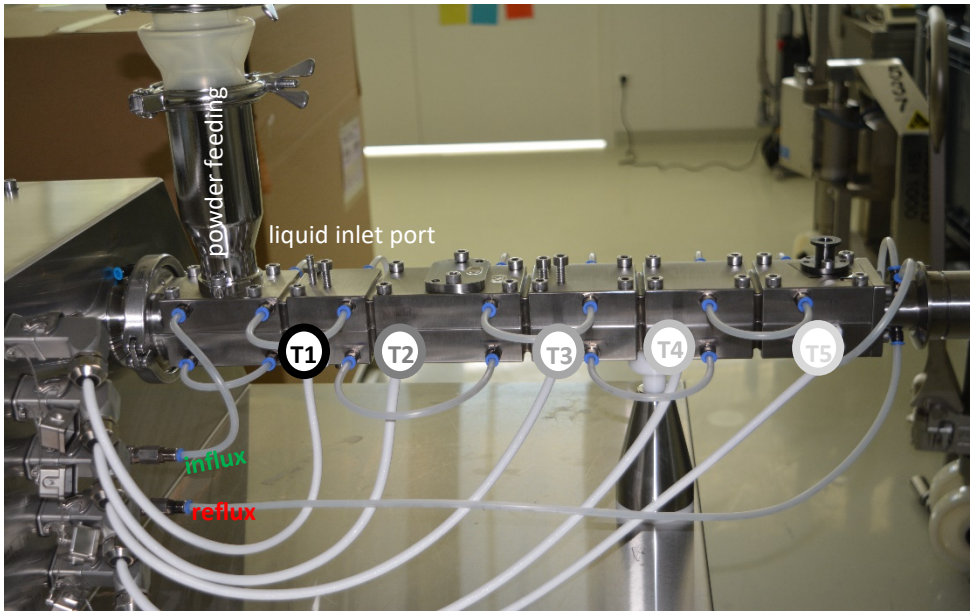

Figure 52 Photography of the granulator barrel (M-line) including description of powder feeding, liquid inlet port and the temperature control system (influx and reflux + 5 temperature sensors along the barrel [T1 – T5])

The resulting temperatures measured in zone 1 - 5 along the barrel were plotted against process time in the grey coloured graphs in Figure 53 for long-term run 1 and in Figure 54 for long-term run 2. Table 14 gives an overview of the ranges in barrel temperatures in zone 1 - 5.

Table 14 Overview of barrel temperatures zone 1-5 [°C] during long-term runs 1 and 2

temperatures	**long-term run #1**	**long-term run #2**
water temperature cooling system for barrel [°C]	20	18
barrel temperature zone 1 [°C]	19.8 - 23.7	18.8 – 21.2
barrel temperature zone 2 [°C]	21.7 – 32.9	19.5 – 28.3
barrel temperature zones 3-5 [°C]	21.1 – 26.0	18.9 – 24.0

Differences between the different zones along the barrel occurred. For both long-term runs, the barrel temperature in zone 1 was the lowest compared to the other zones. Zone 1 was the part along the barrel where the powder preblend was added to the granulator until the point where

granulation liquid was added. In contrast to this observation, barrel temperature in zone 2 was found to be the highest compared to the others. Zone 2 was the sector of the barrel where intermeshing between the granulation liquid and the powder preblend inside the granulator took place. The temperatures along the granulation zone of the barrel (zones 3 – 5) lay in-between the ones of zone 1 and zone 2.

An increasing temperature indicates shear and friction effects inside the granulator [121]. Therefore, the observed temperature levels showed that friction effects were especially pronounced for the barrel sector where the intermixing of powder preblend and granulation liquid (water in this case study) happened. Low friction effects became visible at the barrel sector where only the dry powder preblend was transported through the granulator until the point of addition of granulation liquid. These results are in very good agreement to the results evaluated in chapter 9 later on. Wall friction measurements with a ring shear tester showed the same trend of higher friction effects for wet granule masses compared to the dry powder preblends.

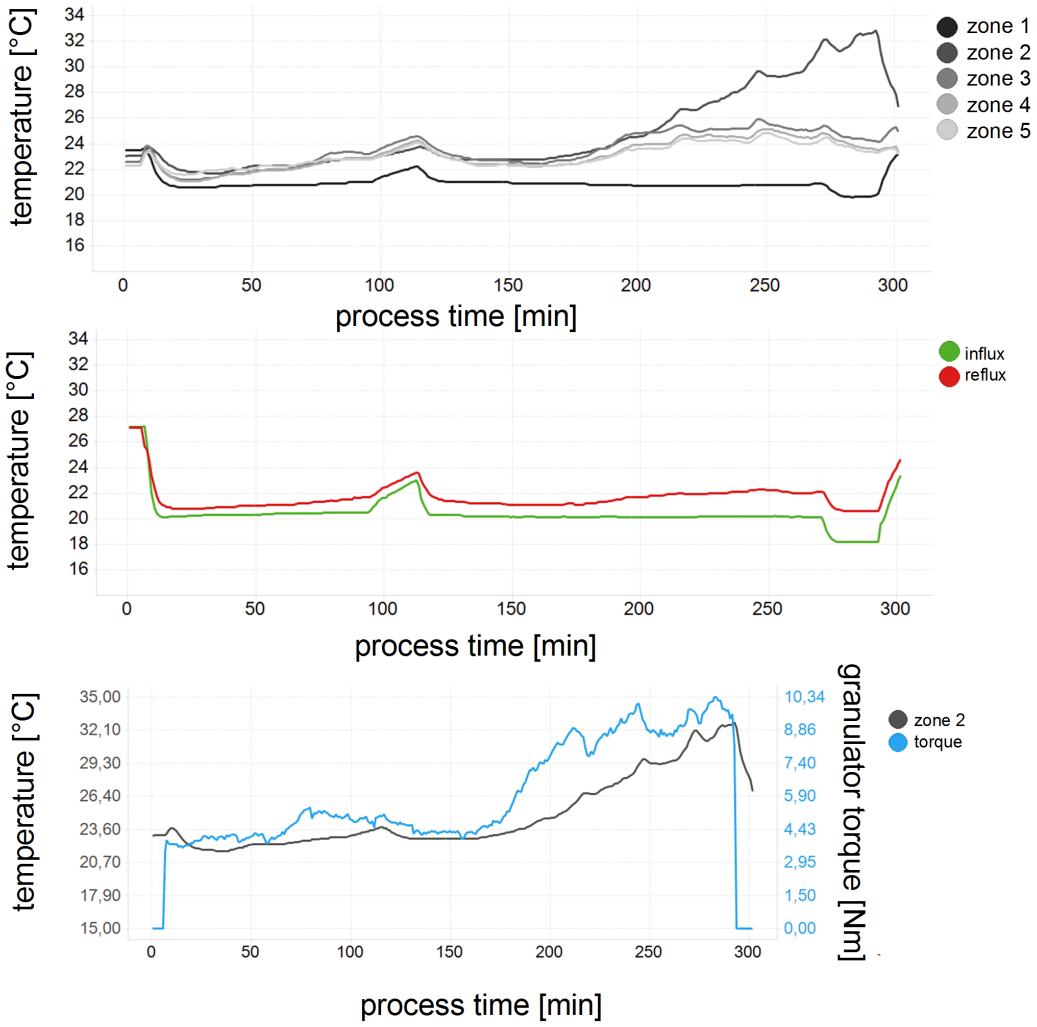

Figure 53 Barrel temperature sensors zone 1 – 5 [°C] (grey coloured graphs), influx and reflux temperature of cooling water [°C] (red and green coloured graphs), granulator torque [Nm] (blue coloured graph) and barrel temperature zone 2 [°C] (dark grey coloured graph) as a function of process time [min] for long-term run #1

Looking at the graphs showing the temperature values of influx and reflux water of the cooling system for long-term run 1 (see Figure 53) and long-term run 2 (see Figure 54), it can be stated that the reflux temperature was always higher than the influx temperature. This indicated that the energy arising during granulation due to shearing and friction effects (see explanation before) resulted in a temperature increase of reflux water compared to the influx water. A maximum difference of 2 °C between influx and reflux water temperature was found during both long-term runs. The efficiency of the cooling system was getting worse at one timepoint

during both long-term runs. For long-term run 1 that happened at timepoint t = 113 min. Influx temperature increased to a maximum value of T = 22.9 °C, reflux temperature reached a maximum value of T = 23.5 °C at the same timepoint (set temperature of cooling system T = 20 °C, see Table 14). In long-term run 2 the maximum influx temperature was T = 20.8 °C and the maximum reflux temperature T = 21.9 °C at timepoint t = 288 min (set temperature of cooling system T = 18 °C, see Table 14). By improving the ventilation resulting in improved efficiency of the cooling system, a decrease of the water cooling temperature to the particular set temperature was achieved.

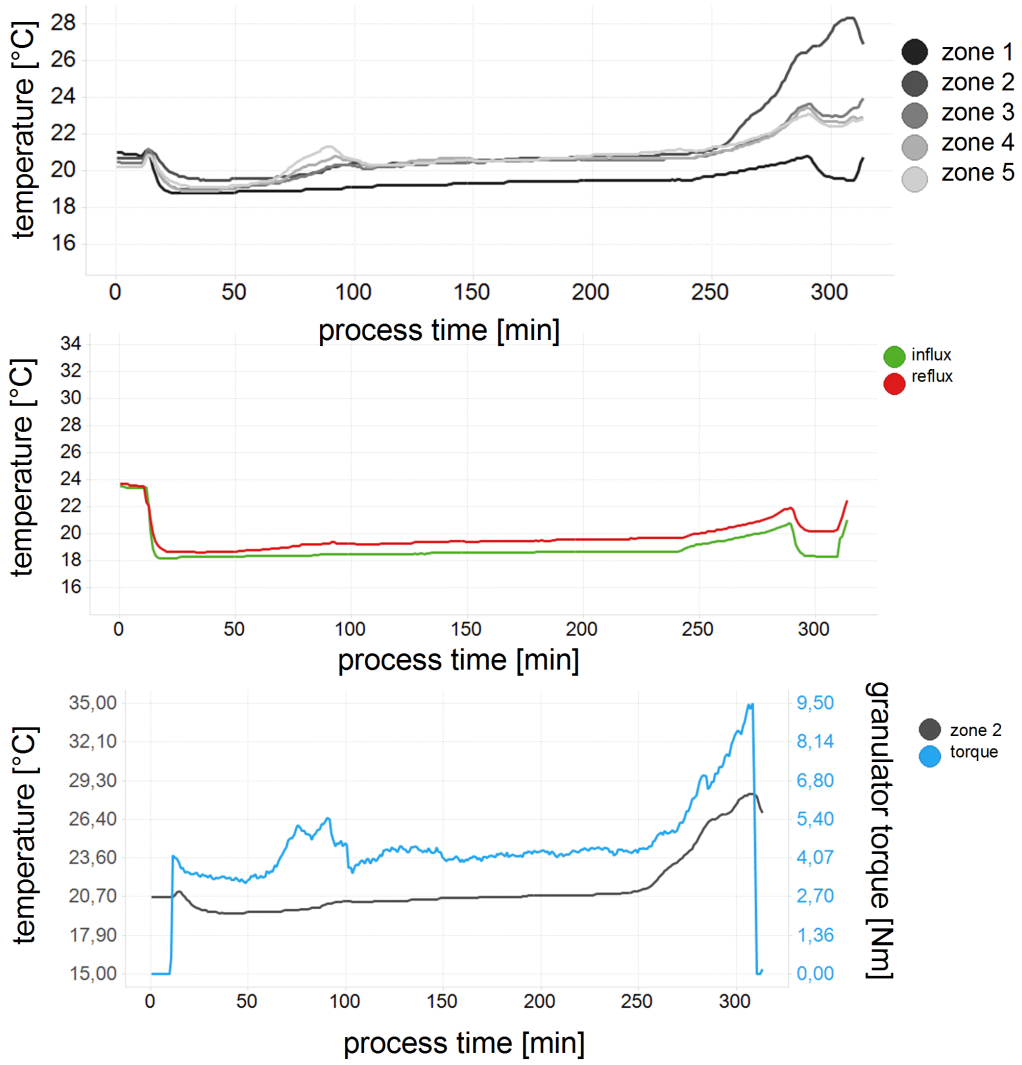

Figure 54 Barrel temperature sensors zone 1 – 5 [°C] (grey coloured graphs), influx and reflux temperature of cooling water [°C] (red and green coloured graphs), granulator torque [Nm] (blue coloured graph) and barrel temperature zone 2 [°C] (dark grey coloured graph) as a function of process time [min] for long-term run #2

Increasing influx and reflux temperature - as just described - lead to an increase of both, granulator torque [Nm] and temperature of zone 2 [°C], where the granulation liquid was added to the granulator. The relationship between temperature of zone 2 and granulator torque along the process time is depicted in the lower graphs of Figure 53 and Figure 54. During long-term run 1 the highest torque of 10.3 Nm was reached at the highest occuring temperature of zone 2, namely 32.7 °C. For long-term run 2 a similarly high torque of 9.5 Nm was reached at the highest temperature of zone 2 of 28.3 °C. For both long-term runs, these highest torque and

temperature values were found at the end of process time. The increase of torque and temperature in zone 2 from the stable base level started at appr. t = 175 min during long-term run, whereas for long-term run 2 the increase began later (appr. t = 250 min). After these described “starting points” of increasing torque and temperature in zone 2, no decrease of neither of the two parameters could be achieved anymore. Therefore, the importance of a constantly efficient temperature control system of granulator barrel during long-term runs became evident.

8.3 SUMMARY & QBD LEARNING

Within this chapter indicators for process robustness and stability were evaluated for the two process units continuous dosing and twin screw wet granulation.

Regarding continuous dosing using a gravimetric feeding mode, a refill regime was implemented by the evaluation of refilling at different hopper fill levels. More frequent, thus fast refilling of the hopper at a hopper fill level > 45 % guaranteed an accurate powder feed-rate PFR with a deviation < 1.5 % compared to the set PFR = 20 kg/h over time (see Table 15). This result is in good agreement with the findings of Engisch et al. [26]. As the PFR is an important process parameter influencing nearly all other derived process conditions, an accurate PFR is essential for a robust and stable process.

Table 15 Overview of indicators for process robustness and stability per process unit and how they can be influenced

process unit	**parameter indicating process robustness & stability**	**influenced by**
continuous dosing with gravimetric feeding mode	**accurate powder feed-rate PFR [kg/h]** (deviation < 1.5 %)	- refilling at hopper FL > 45 % - more frequent refilling of a lower amount of material - fast refilling
twin screw wet granulation	**low temperature in zone 2** (< 24 °C) and **low granulator torque** (< 5 Nm)	- efficient, stable temperature control system along the barrel

For the twin screw wet granulation process, the importance of a temperature control system for the granulator barrel was found during a long-term run. The temperature sensor position in zone 2 of the barrel was identified to be a key measurement position, as in that zone the highest temperature values occurred. These temperature values indicated the increasing shear and friction forces in the zone, where granulation liquid was added to the powder preblend inside

the granulator (= zone 2). The same relationship was found by Stauffer et al. [105, 106]. They identified that the temperature increase in the wetting zone gives information on wetting efficiency and that the temperature increase along the barrel is proportional to granulator power and friction forces. A further proof of the temperature indicating shear and friction forces inside TSG was the fact, that a relationship between granulator torque and temperature measurement in zone 2 was detected. Furthermore, it was found during the long-term runs that already a small increase of preflux water temperature of the water (appr. 3 °C) due to decreasing cooling efficiency lead to an increase of both important indicators, granulator torque and measurement of temperature in zone 2. A second important aspect was the fact that once an increase of granulator torque and temperature of zone 2 occurred, no decrease of both parameters could be achieved anymore.

Therefore, an efficient temperature control system and a careful observation of both mentioned indicators, temperature and torque, were found to be the key for a stable and robust twin screw wet granulation process in terms of minimization of shear and friction effects (see Table 15).

9. ASSESSMENT OF ABRASION INDUCED VISUAL DEFECTS IN TWIN SCREW WET GRANULATION PROCESS USING WALL FRICTION MEASUREMENTS

In the previous chapter 8 evaluation of long-term runs, arising effects and their impact on process robustness and stability were investigated for continuous dosing and twin screw wet granulation process. With regard to TSG process, it was stated that the control and measurement of granulator torque and temperature increase along the barrel were important indicators for shear and friction effects inside the granulator. Evaluation of such friction effects inside TSG is also content of this chapter. Friction arises out of the interaction of granule mass and the equipment surface, respective the barrel wall and the screws. An IPC method that is capable of friction effect measurement is wall friction measurement using a ring shear tester. Explanation of friction forces occurring inside the twin screw granulator at some equipment and process parameter settings of TSG as well as the understanding of the impact of different parameters on wall friction angle is the aim of this chapter. Therefore, wall friction measurements were performed using a Schulze ring shear tester, investigating different wall/screw materials, different powder preblends, different moisture levels of powder preblends, and different normal stress levels, respectively. Based on this dataset, an explanation on how equipment and process parameter changes of TSG processes could reduce abrasion effects is presented.

Despite of the TSG test case, there are several different purposes described in literature wall friction measurements are used to. To evaluate friction effects between powders and equipment in general, wall friction measurements are supposed by many authors [4, 7, 8, 28, 35, 36, 37, 38, 45, 46, 84, 91]. One application is the usage for the design of silos because knowledge about wall friction is essential to guarantee mass flow inside a hopper [8, 46, 91]. In addition, several authors have investigated the influence of either powder material or wall material attributes on the wall friction angle. Fekete et al. [28], Halford et al. [36] and Iqbal et al. [45] described the impact of powder moisture on resulting wall friction angle in their work. In general, they all found the effect of increasing wall friction at increasing moisture level of the powder. Additionally, Fekete et al. found a pronounced decrease of that relationship exceeding a certain moisture level [28] and Halford et al. found the described relationship especially at a lower normal pressure [36]. Bradley et al. could show the correlation of increasing relative

wear of different steel materials with increasing wall friction angle [7]. Han [37] found lower wall friction angles for polished steel compared to non-polished samples.

The interaction of powder and process dependence on friction, adhesion and cohesion phenomena are mostly described for the tableting process [13, 66, 78, 118].

Nakamura et al. used a shear stress measurement device for predicting the sticking tendency of powder to the punch using friction measurements [78], which might be mechanistically similar to phenomena observed in twin screw granulation.

9.1 THEORETICAL ASPECTS

Wall friction measurement is a method where the abrasion/friction effects between a powder bulk and a specific (equipment) surface is being investigated. The measured parameter describing the friction between a powder and a (equipment) surface is the wall friction angle, which is accessable by various wall friction testers described in literature [3, 4, 35, 84]. Amongst all the Schulze ring shear tester offers easy handling at reduced measuring periods [3] and was therefore seleceted to be used in this study.

The method of wall friction measurement for the Schulze ring shear tester was described by Schulze [103], too. A small layer of powder is being sheared is shifted across the respective wall material sample. The shear cell is rotated slowly with a certain angle velocity ω while applying a certain normal stress σ_w [Pa] applied on the system (see Figure 55).

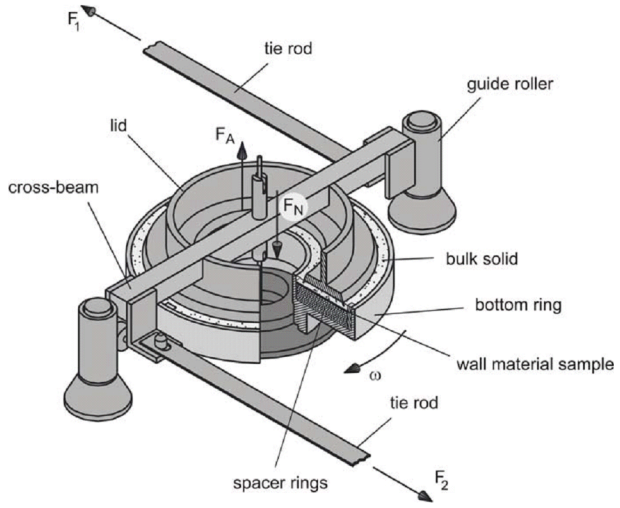

Figure 55 Setup of Schulze ring shear tester for wall friction measurement [102]

Two force sensors record the the forces *F1* and *F2* resulting in the shear stress τ_w [Pa]. By plotting the shear stress τ_w [Pa] against normal stress σ_w [Pa], a wall yield locus is obtained (see Figure 56); finally, the wall friction angle φ (WFA) is calculated according to Equation (15) as described by Behres [3].

$$WFA\ \varphi = arctan\frac{\tau_w}{\sigma_w} \tag{15}$$

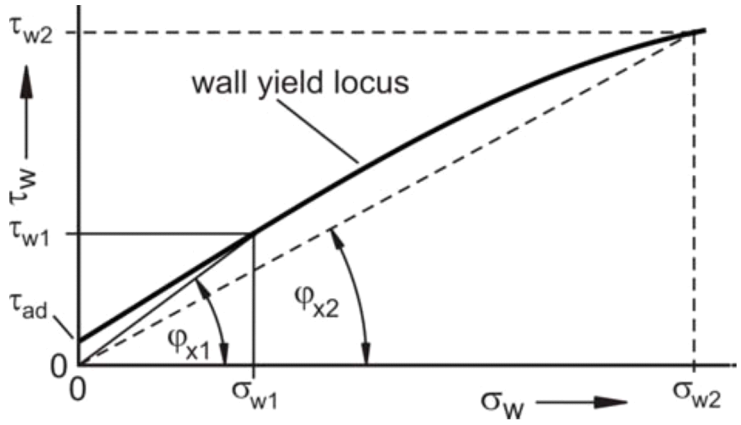

Figure 56 Relationship between shear stress τ_w and normal stress σ_w resulting in a wall yield locus [103]

Hancock [38] mentioned the typical correlation of normal stress σ_w [Pa] and WFA φ [°] for pharmaceutical bulks where WFA increases at decreasing normal stress (see also Figure 56).
Within this chapter wall friction angles WFA were measured for the different formulations (F1 placebo and verum (see 10.2.2), F2 placebo and verum (see 10.2.3) and BIxx1 verum formulation (see 10.2.4)) and their interaction with different wall/screw materials. Furthermore, not only dry powder preblends of the different formulations were tested for their friction effects for different wall and screw materials, but also wet granules (wetted powder preblend).
Two different sets (named “set 1” or “set 2” in the following) of wall material samples were tested in the ring shear tester with regard to their interaction with different formulations.
Three different materials with varying surface treatments were chosen to be included into set 1. Background of the choice was the ability to evaluate whether wall friction measurements can differentiate between the different wall materials for different formulations and moisture levels of granules. Surface roughness of all wall materials (set 1 and set 2) was measured using a MahrSurf M 300 (Mahr GmbH, Germany). The measured roughness Ra was chosen as reference parameter for the surface roughness of each wall material. Table 16 gives an overview of the wall material samples of set 1.

Table 16 Wall material samples of set 1 with material specification, surface treatment and surface roughness [µm]

sample no.	**material specification**	**surface treatment**	**surface roughness [µm]**
1	glass	smooth	Ra: 0.006
2		rough	Ra: 2.299
3	plastic: PEEK	smooth	Ra: 3.548
4	steel type 1.4301	cold-rolled	Ra: 0.171
5		polished	Ra: 0.163

Wall material sample set 2 consisted of different screw materials being under current evaluation for twin screw wet granulation process within the NCE development unit of Boehringer Ingelheim Pharma GmbH & Co.KG. Five different wall material samples had therefore been manufactured by Three Tec GmbH, Switzerland. These five samples were made of two

different steel types (1.4404 or 1.4542) which then underwent either a special surface treatment or a special hardening treatment. Each of the five samples had an unpolished side and a polished side (exemplary shown for one sample in Figure 57). Table 17 shows the complete list of wall/screw material samples for set 2.

Table 17 Wall/screw material sample description of set 2 with material specification, special surface or hardening treatments and the roughness of the final surface [µm] per sample

sample no.	material specification	surface / hardening treatment	roughness of final surface [µm]
1	steel type 1.4404	unhardened	polished – Ra 0.053
			unpolished – Ra 0.782
2		HARD-INOX®-S hardened	polished – Ra 0.091
			unpolished – Ra 0.531
3	steel type 1.4542	unhardened	polished – Ra 0.531
			unpolished – Ra 0.570
4		precipitation hardened	polished – Ra 0.053
			unpolished – Ra 0.610
5		TiN layered	polished – Ra 0.283
			unpolished – Ra 0.812

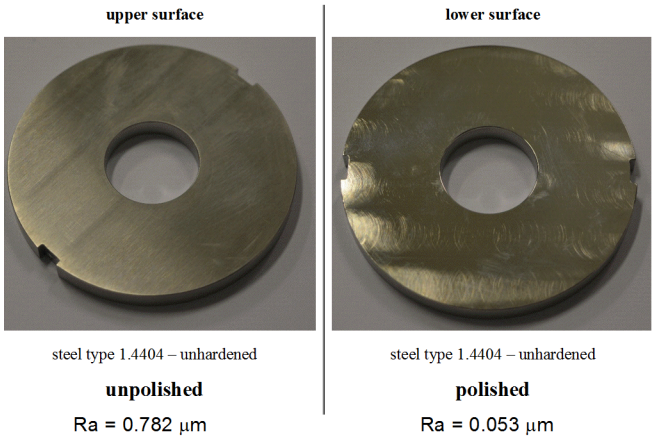

Figure 57 Visual difference between unpolished and polished surface for steel type 1.4404 unhardened sample (exemplary for all samples) of wall/screw material sample set 2

9.2 WALL FRICTION MEASUREMENT METHOD – PROOF OF FEASIBILITY

In the first part of the WFA evaluation the effect of different formulations at different granulation MLs on different wall materials (set 1, see Table 16) was investigated. Purpose was to see whether differences in resulting WFA occurred.

Figure 58 shows the interaction of placebo formulation 2 with the different wall materials of set 1 (see Table 16) at different granulation moisture levels [% (m/m)] and normal stresses σ_w [Pa]. A decrease of the average WFA φ [°] with increasing normal stress σ_w [Pa] could be observed. Furthermore, an increase of average WFA φ [°] with increasing moisture level [%] – compared at defined normal stresses σ_w [Pa] – was obtained. These two effects are especially pronounced for steel with the two different surface treatments (polished and cold-rolled) and glass with a smooth surface. The plastic wall material PEEK and the glass material with roughened surface did not show a comparable strong effect of normal stresses σ_w [Pa] and moisture level [%] on average WFA φ [°]. Additionally, differences in average WFA φ [°] were observed between the different wall materials and surface treatments at fixed normal stress σ_w [Pa] and comparable moisture level [%]. For example, at a normal stress σ_w = 200 Pa and a moisture level ML = 15 %, the lowest WFAs (φ = 37 ° to 40 °) were measured for the wall materials glass with roughened surface, the plastic PEEK, and the polished surface of the 1.4301 steel. A medium WFA (φ = 55 °) was measured for the cold-rolled surface of the 1.4301 steel. The highest WFA (φ = 77 °) was obtained for the glass material with a smooth surface.

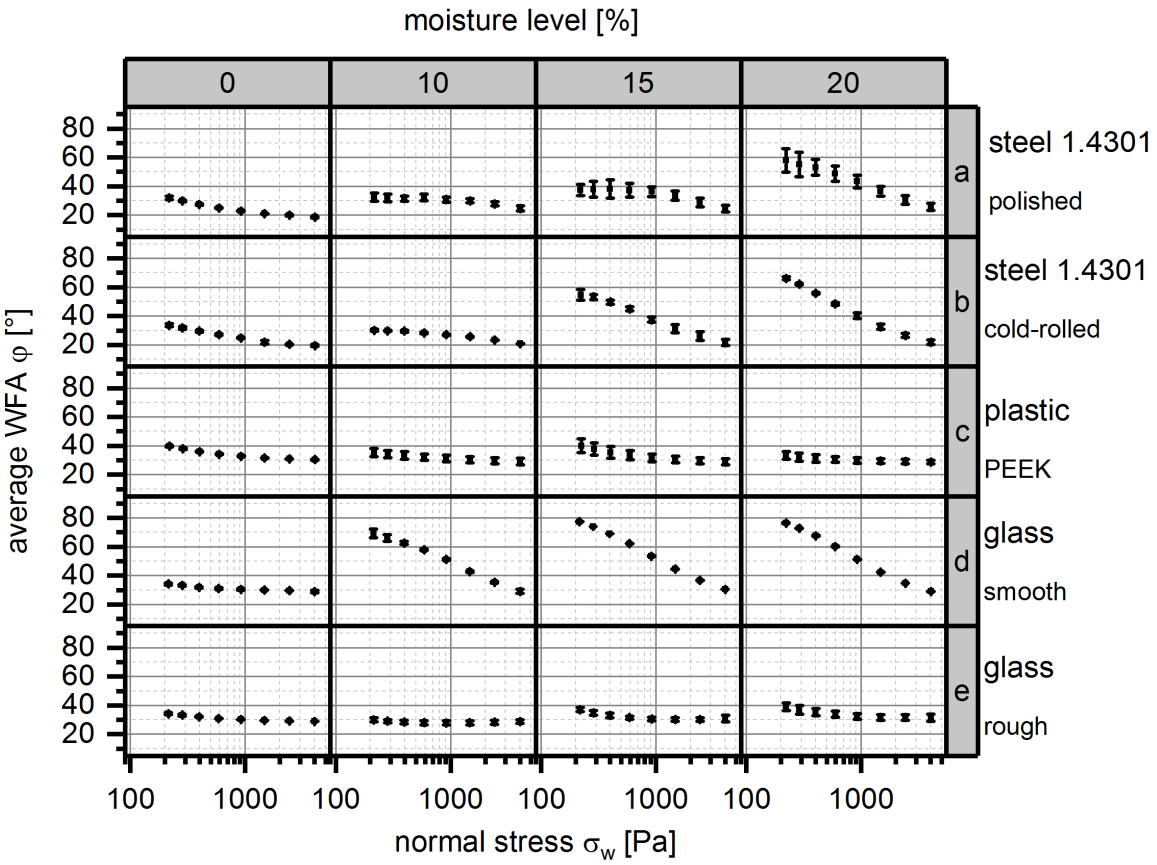

Figure 58 Relationship between average wall friction angle WFA φ [°] and normal stress σ_w [Pa] for different moisture levels [%] (columns) and different wall materials (rows) for placebo formulation 2; error bars: +/- 1 SD (n=4)

Using an exemplary wall material (glass – roughened and smooth surface), Figure 59 illustrates how differences in formulations affected the measured WFA φ [°].

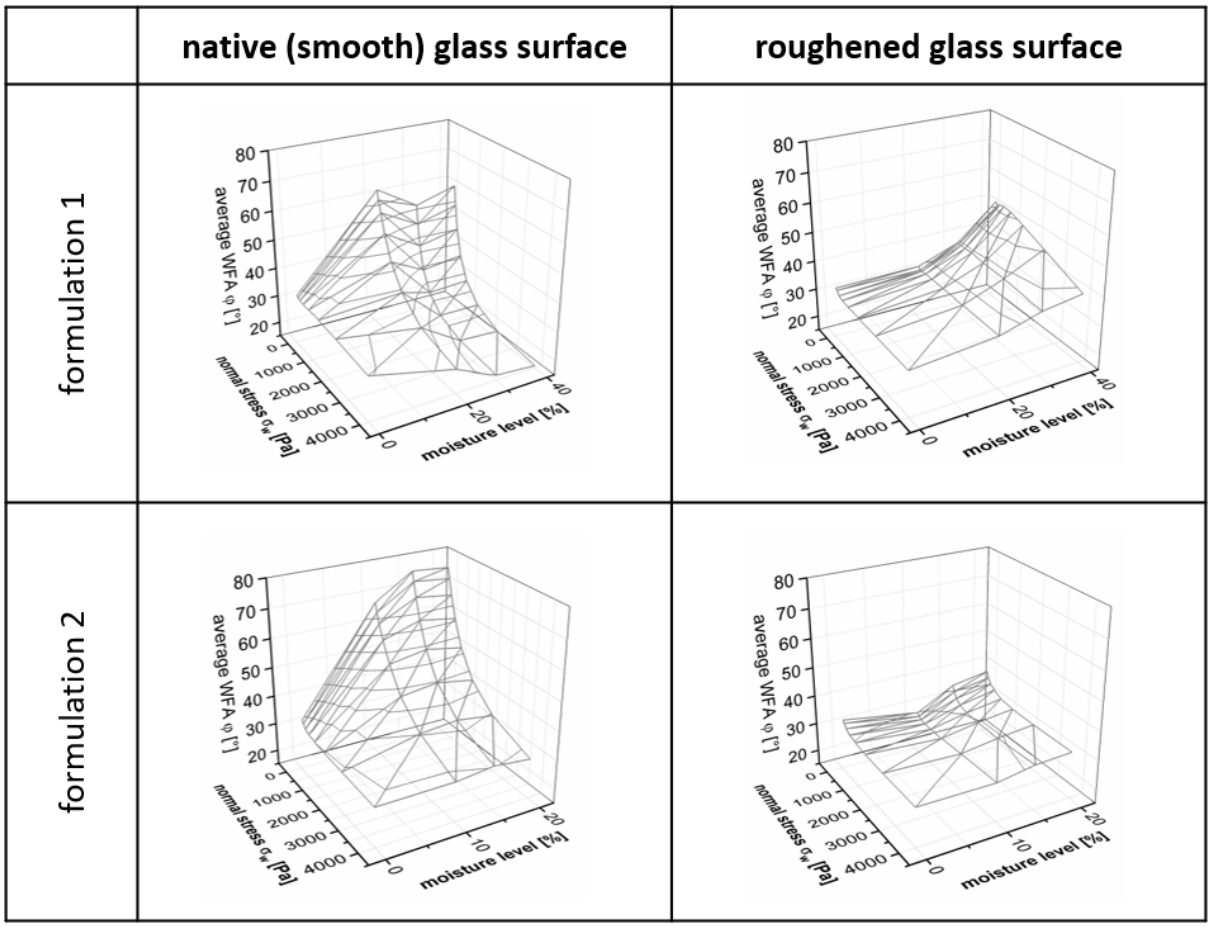

Figure 59 Relationship between average wall friction angle WFA φ [°] and normal stress σ_w [Pa] and different moisture levels [%] for different glass surfaces and placebo formulations

Looking at the results of the average WFA φ [°] at different moisture levels [%] and normal stresses σ_w [Pa] on smooth glass surface and roughened glass surface for both placebo formulations showed that average WFAs φ [°] were lower on the roughened surface compared to the smooth surface irrespective of the investigated formulation. Furthermore, average WFAs φ [°] were very similar for both formulations with regard to friction on the roughened glass surface. In contrast to that, strong differences between formulation 1 and formulation 2 were visible for the experiments performed on the smooth surface. Starting at ML = 0 %, formulation 1 showed a maximum of WFA at a ML = 20 %; at higher MLs lower WFA values were observed again. In contrast to that, formulation 2 showed a strong correlation of WFA φ [°] and normal stress σ_w [Pa], and moisture level [%]. WFA φ [°] steadily increased at decreasing normal stress σ_w [Pa] and increasing moisture level [%].

9.3 EVALUATION OF WALL FRICTION ANGLE FOR DIFFERENT SCREW MATERIALS AND FORMULATIONS

In a second step, experiments with samples made of different screw materials were conducted to check if the results from the method described in chapter 9.2 can be linked to the twin screw wet granulation process. The description of the wall/screw material set 2 can be found in Table 17. The correlation of average WFA φ [°] and normal stress σ_w [Pa] for both active formulations 1 and 2 with a DL = 5 % (see Table 22 and Table 23), different moisture levels [%], and all investigated screw materials of set 2 with polished surfaces is depicted in Figure 60.

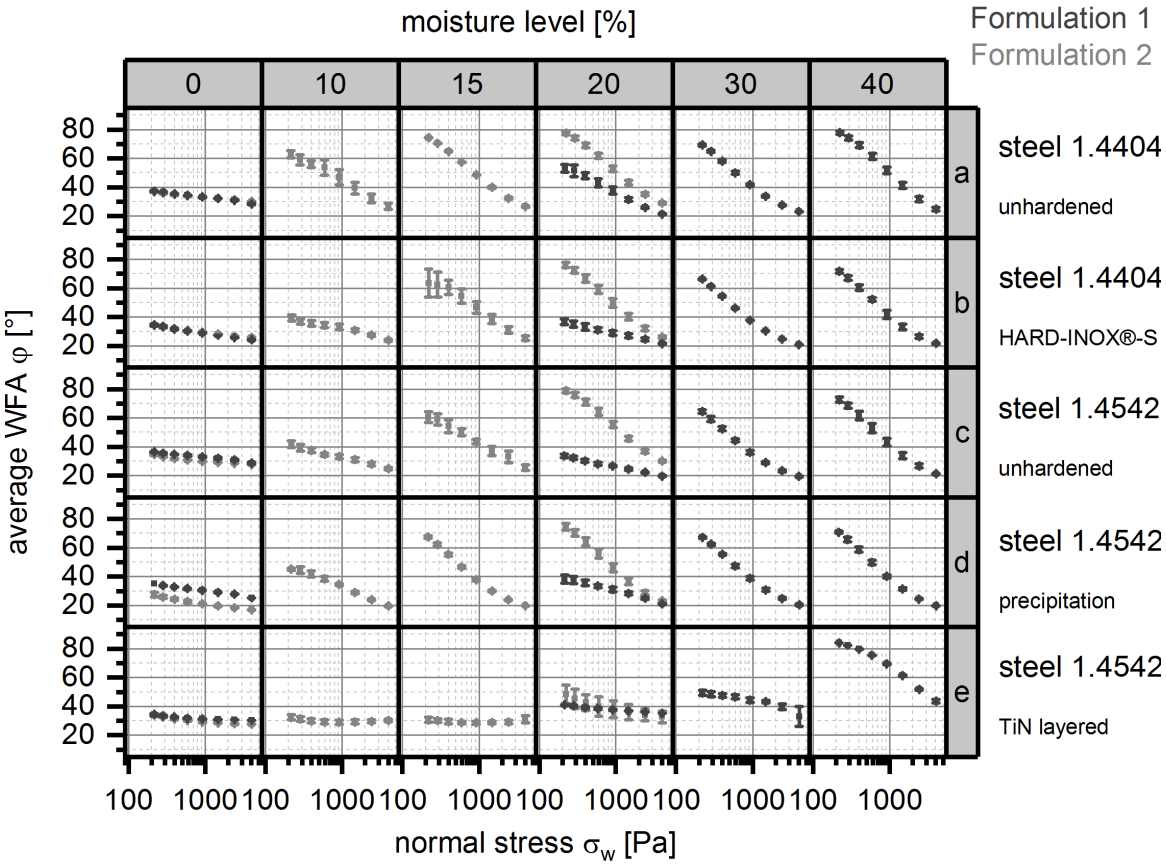

Figure 60 Relationship between average wall friction angle WFA φ [°] and normal stress σ_w [Pa] for different moisture levels [%] (columns) and different screw materials with polished surface (rows) for verum formulation 1 and verum formulation 2; error bars: +/- 1 SD (n = 4)

Except for formulation 2 in the interaction with TiN layered type 1.4542 steel surface, the interactions between all other screw materials and both formulations resulted in decreasing

average WFA φ [°] with increasing normal stress σ_w [Pa] and decreasing moisture level [%]. These correlations were also described for wall material set 1 (see 9.2).

Nevertheless, differences of average WFA φ [°] could be detected as illustrated in Figure 61. WFAs φ [°] did differ between different formulations, screw materials, and surface treatments of these screw materials (polished vs. unpolished); as well as on moisture level [%] and normal stress σ_w [Pa]. Two different screw materials – steel type 1.4404 unhardened and steel type 1.4542 precipitation hardened – were exemplarily chosen for further evaluation of the TSG process.

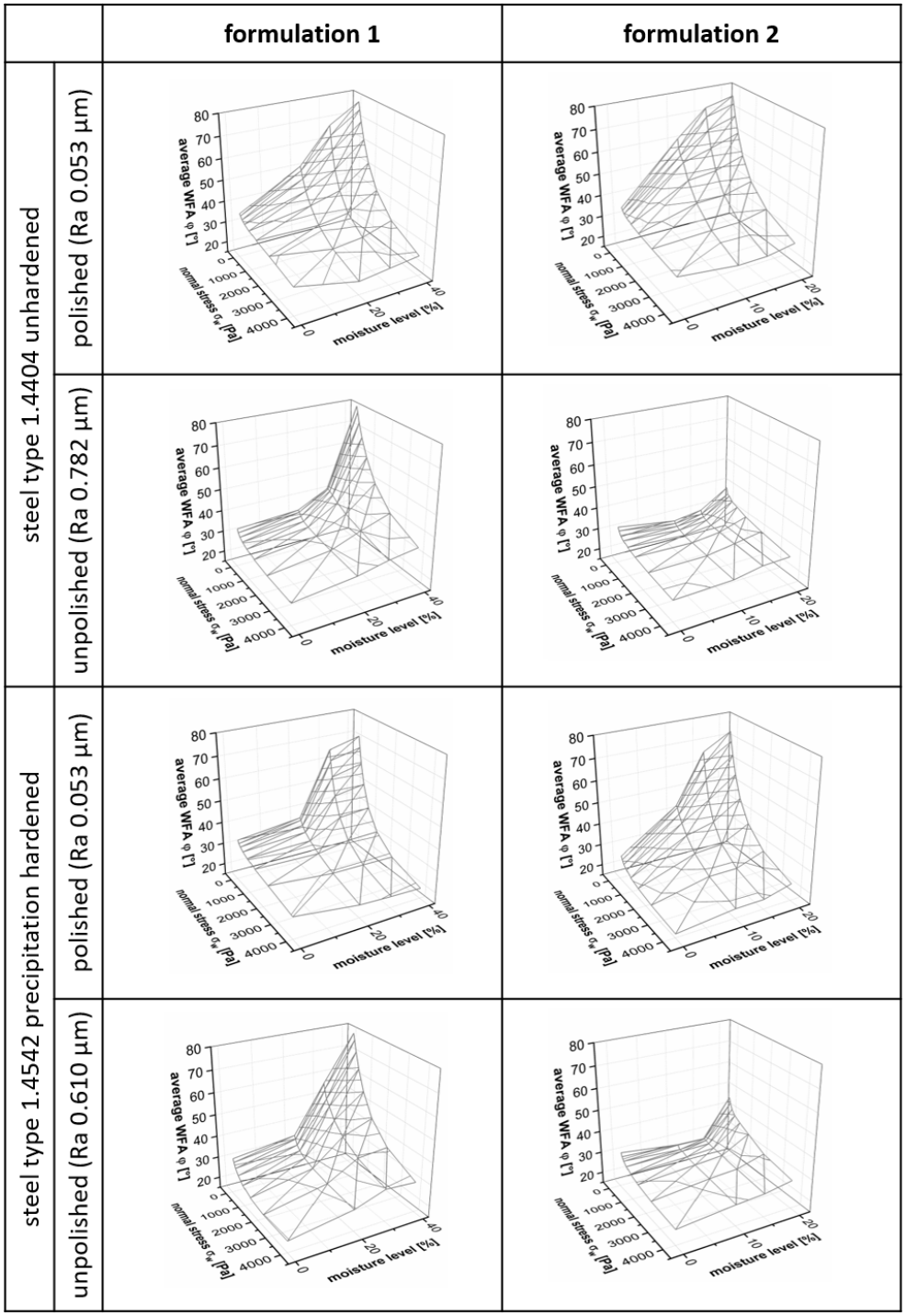

Figure 61 Average wall friction angle WFA φ [°] in relation to different normal stresses σ_w [Pa] and moisture levels [%] for two different screw materials (1.4404 unhardened – 1.4542 precipitation hardened), two different surface treatments (polished – unpolished) and the two verum formulations (formulation 1 and formulation 2)

Considering the surface roughness Ra of polished and unpolished materials it was found, that for almost all materials the values of Ra of polished surfaces are 10 times smaller compared to the unpolished. Different effects of the surface roughness on the WFAs of the evaluated two formulations were found. While formulation 1 did not show big differences between the two surface treatments, formulation 2 showed the "typical" correlations as described earlier between WFA and normal stress regarding moisture level (see 9.2) for polished surfaces of screw material, but not for unpolished surfaces. Interestingly the WFAs describing the interaction between formulation 2 and unpolished screw surfaces were comparatively low ($\varphi < 50$ °), showing a complete different 3D plot (see Figure 60) when compared to their "polished" partner-experiment.

Comparing two specific screw materials with polished surfaces – type 1.4404 unhardened steel and type 1.4542 precipitation hardened steel – average WFA was lower for the type 1.4542 precipitation hardened steel screw than for the type 1.4404 unhardened steel screw. This observation was found for both formulations.

9.4 CASE STUDY INCLUDING BIXX1

9.4.1 Abrasion effects during TSG process

As described by Menth et al. (2018) [72] grey spots occurred on the surface of tablets made of TSG granules using the BIxx1 formulation as described in chapter 11.1.4.2. These spots resulted from grey discoloration of the powder accumulating as a film at the barrel wall during the TSG process and were suspected to result from abrasion effects. The resulting ratio of tablets showing visual defects was 46.5 % related to all tested tablets, at the maximum. Figure 62 shows exemplary how the tablets with visual defects looked like.

Figure 62 Tablets with visual defects caused by abrasion effects during twin screw wet granulation process

Several actions were taken to reach a ratio of visually rated to be affected tablets below the specification limit of 6.5 % of tablets. Table 18 gives an overview of these actions. Decision-making of these actions was based on prior knowledge.

Process parameters were adapted to result in higher shear forces by increasing the powder feed rate PFR [kg/h] and screw speed [rpm]; this consequently resulted also in a higher filling level FL [%]. Furthermore, granulation moisture level ML [%] was increased. Granulator screws were exchanged as given in Table 18. An additional water cooling system was installed to the granulator barrel to reduce the increase of the barrel temperature to a maximum of appr. 28 °C also during those process runs exceeding 15 min.

Table 18 Actions taken to improve TSG process with regard to process parameter settings and equipment settings with the aim to minimize visual defect rate of resulting tablets

		INITIAL: visual defect rate of tablets **above** specification limit	IMPROVED: visual defect rate of tablets **below** specification limit
process parameter setting TSG process	powder feed rate PFR [kg/h]	0.9	2.6
	liquid feed rate LFR [kg/h]	0.3	1.1
	screw speed granulator [rpm]	150	329
	granulation moisture level ML [%]	25	30
	filling level FL inside barrel [%]	6.5	8.6
equipment settings TSG process	granulator screws	steel type: 1.4404 unhardened modular screw elements	steel type: 1.4542 precipitation hardened monolithic screw
	cooling of barrel	no cooling	water cooling

The described optimizations to affect the smooth transport of wetted material do reflect the before mentioned reduction of WFAs and surprisingly did show a positive effect in the production process.

In summary – the sum of the actions was successful, resulting in a visual defect rate of the tested tablets within specification limit of lower than 6.5 %.

9.4.2 Supportive measurements understanding TSG process

9.4.2.1 Evaluation of granulator torque

Conductive power consumption measurements [A] of the twin screw granulator motor enabled granulator torque output [Nm] for several different process parameter settings. As presented in Figure 63 the major impact on granulator torque is given by granulator screw speed.

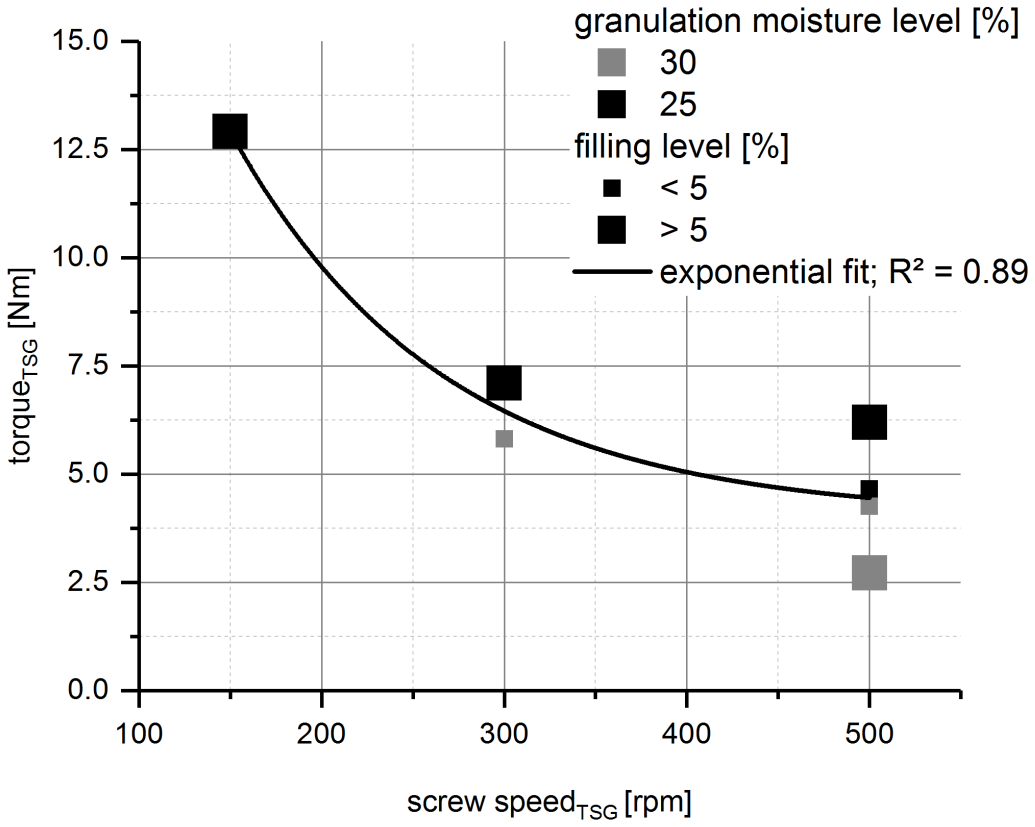

Figure 63 Influence of granulator screw speed [rpm] on granulator torque [Nm] at two different granulation moisture levels [%] (colours) and at different barrel fill levels FL [%] (bullet point size)

At a low screw speed of 150 rpm the granulator torque reached its highest value (12.9 Nm). For a middle screw speed of 300 rpm a granulator torque range between 5.8 Nm and 7.1 Nm was reached. At the highest investigated screw speed of 500 rpm the granulator torque decreased further to a range between 2.7 Nm and 6.2 Nm. This interesting observation led to

the expectation that wall friction measurements with a ring shear tester showing similar trends (decreasing abrasion at increasing normal stress) could serve as an additional supportive method addressing the explanation of abrasion effects inside TSG (s. 9.4.2.2). The finding of decreasing torque at increasing screw speed was also investigated by several other research papers [14, 51, 52, 114]. The influences of barrel filling level FL [%] (affected by the changes in throughput) and granulation moisture level ML [%] on granulator torque were only minor within this study.

9.4.2.2 Evaluation of WFA

As already described in 9.4.2.1, in addition to the evaluation of granulator torque [Nm] wall friction measurements with the BIxx1 formulation were conducted. The purpose of that measurements was to evaluate whether they may help to explain why the actions described in Table 18 led to the improvement in terms of abrasion effects during TSG process. Figure 64 shows the results of wall friction measurements performed with a wet granule mass of the case study formulation at a ML = 25 %.

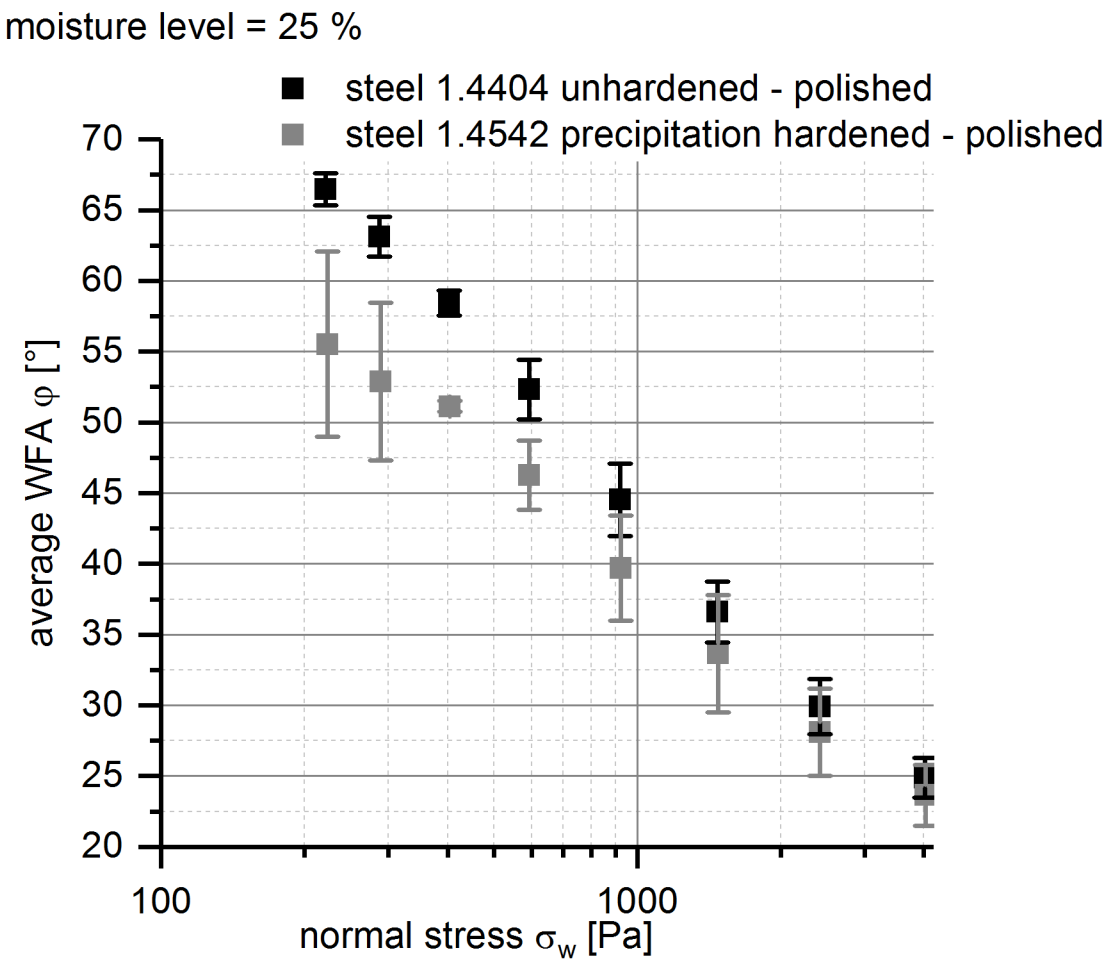

Figure 64 Average wall friction angle WFA φ [°] vs. normal stress σw [Pa], describing the interaction of a formulation with a new API with two different screw materials (1.4404 unhardened polished and 1.4542 precipitation hardened polished) at a predefined moisture level ML = 25 %; error bars: +/- 1 SD (n=4)

Average WFAs are plotted against normal stress for the two different screw materials used for the TSG process. As expected, the average WFA decreased for both screw materials with increasing normal stress. Comparing the screw materials, average WFAs for the precipitation hardened type 1.4542 steel screw were lower than for the unhardened type 1.4404 steel screw for all applied normal stresses.

In a second step, the impact of different granulation moisture levels ML on average WFA was investigated. The interaction between the BIxx1 formulation and the precipitation hardened type 1.4542 steel screw was measured at the two moisture levels ML1 = 25 % and ML2 = 30 %.

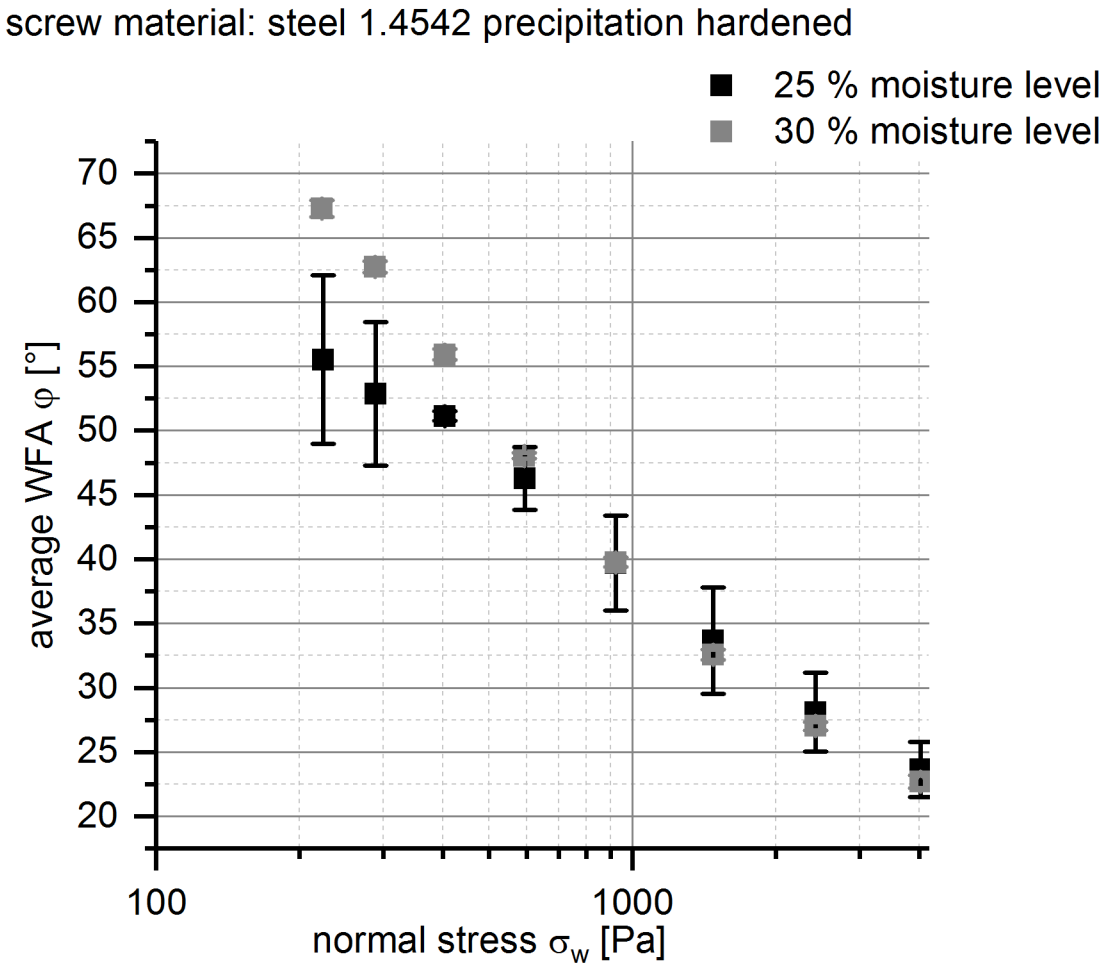

Figure 65 Average wall friction angle WFA φ [°] vs. normal stress σ_w [Pa], describing the interaction of a formulation of a new API with a selected screw material (1.4542 precipitation hardened polished) at two different moisture levels (ML1 = 25 % and ML2 = 30 %); error bars: +/- 1 SD (n=4)

As depicted in Figure 65 for normal stresses σ_w 4 < 898 Pa WFAs are lower at ML1 = 25 % than at ML2 = 30 %. At normal stresses σ_w 4 > 898 Pa this relationship switches so that WFAs are a lower at ML2 = 30 % than at ML1 = 25 % but without showing any significant effects as standard deviations are overlapping for this second case.

9.5 SUMMARY & QBD LEARNING

The wall friction measurements with wall material set 1 (see Table 16), which offers a high variety of different wall materials in terms of surface roughness and treatment, showed the typical correlations between WFA and normal stress as also described in literature [38] confirming the usability of wall friction measurements in this regard. Typically, WFA increases at decreasing normal stress, see Figure 58 for wall materials steel and smooth glass. Furthermore, granulation moisture levels ML were identified to be of high impact on resulting WFA as well, with WFA typically increasing with increasing ML, see also Figure 58. But, within this investigation, some exceptions to these two described correlations were observed. For example, the WFAs measured on the wall material plastic PEEK and the glass material with roughened surface were shown to be quite independent of normal stress (see Figure 58). Another exception occurred. Formulation 1 resulted in a maximum WFA on the glass material with smooth surface at a ML = 20 %, as depicted in Figure 59. For increasing normal stress at MLs > 20 % the WFA was either decreasing or remaining on an equal level when compared to a ML = 20 %. The authors expect the "sponge" effect of cellulose (28) being part of formulation 1 (31.5 % (m/m)) to be responsible for the described effect, as uptaken water might be released under pressure and shear conditions. This leads to a decrease of wall friction angle dependent on moisture level ML at increased shear stress.

In the presented work, the WFA method was evaluated regarding its ability to differentiate between different wall materials, surface treatments of wall materials, and formulations.

As wall materials from set 1 were successfully differentiated by the method, experiments were conducted to test screw material set 2 (see Table 17). In contrast to wall material set 1, screw material set 2 was much more similar in terms of surface roughness, and treatment. Nevertheless, the impact of normal stress, ML, screw materials including their surface treatment, and formulations on WFA could be measured and differentiated with screw material set 2 as well (see Figure 60). The TiN layered screw material showed potential advantages in terms of lower WFAs independent of normal stress in most instances. The evaluation of the two screw materials unhardened 1.4404 steel vs. precipitation hardened 1.4542 steel showed the advantage of precipitation hardened 1.4542 steel screw in terms of friction (see 9.3).

Finally, the case study presented in chapter 9.4 enabled to figure out the connections between all evaluated modules:

- abrasion effects occurring inside TSG resulting in a high visual defect rate of tablets
- adaption of process parameter and equipment settings to minimize these abrasion effects
- granulator torque
- wall friction angle

A clarification of these connections is depicted in Figure 66 and Table 19. Calculation of specific mechanical energy for the granulator (SME) [kWh/t] offered the possibility to evaluate the influence of granulator screw speed, adaption of powder feed rate and granulator torque (based on relationship found in Figure 63) on the improvement of tablets' visual defect rate.

Comparing SME value for initial and improved process parameter settings a decrease of SME to 34.8 % for the improved process parameter setting (SME = 78 kWh/t) compared to the initial process parameter setting (SME = 225 kWh/t) could be calculated. The same trend could be figured out within the wall friction measurement. Within the applied range of normal stresses (200 Pa – 4000 Pa) a decrease of the wall friction angle to 34.8 % of WFA (23 °) at highest normal stress of 4000 Pa compared to the WFA (66 °) obtained at lowest applied normal stress (200 Pa) could be found (see Figure 66 and Table 19), too.

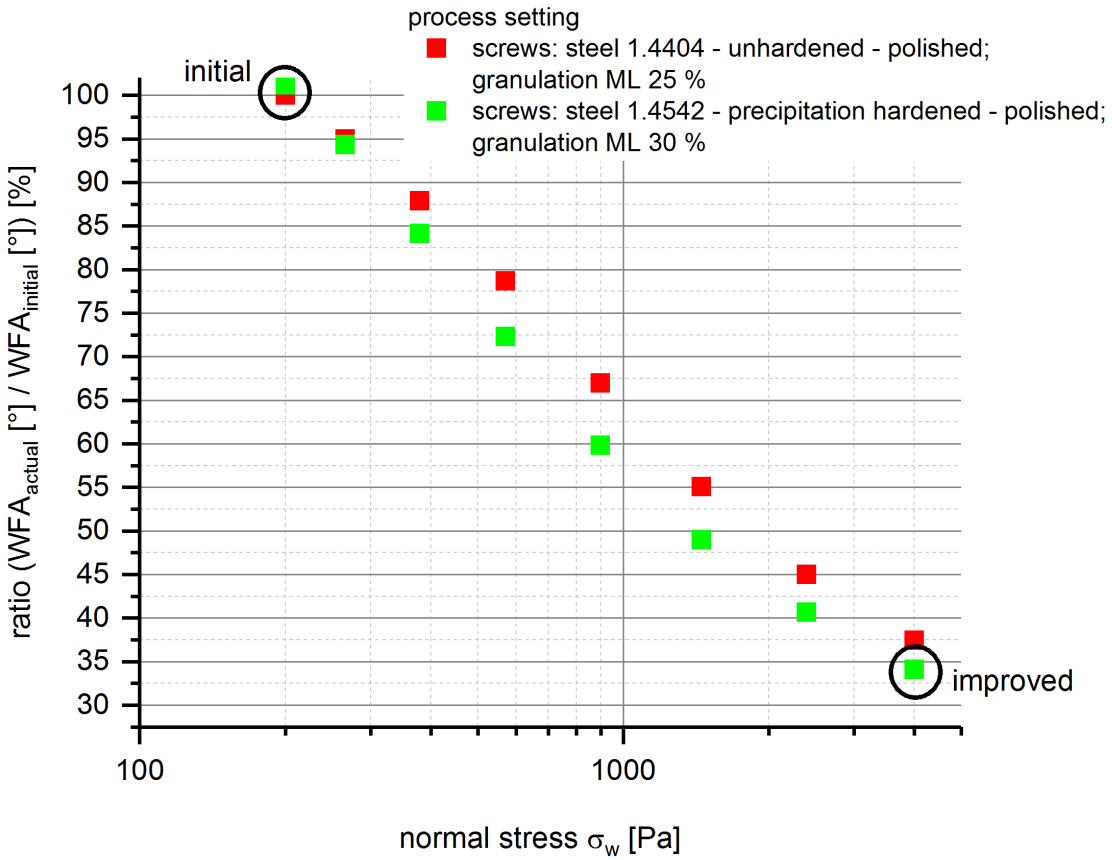

Figure 66 Decrease of measured wall friction angles WFA [°] with a ring shear tester using improved process settings

Table 19 Connection between specific mechanical energy (SME) [kWh/t] during granulation, visual defect rate of the tablets [%] due to abrasion infects inside TSG and measured wall friction angles WFA [°] with a ring shear tester for initial and improved process settings

initial		**improved**
225	**TSG** specific mechanical energy SME [kWh/t]	78
66	**ring shear tester** wall friction angle WFA [°]	23
46.5	visual defect rate$_{tablets}$ [%]	< 6.5

Furthermore, with the help of WFA measurements additional information with regard to exchange of screw material and adaption of granulation moisture level ML could be evaluated. The advantage of the type 1.4542 steel screws with precipitation hardened surface compared to the type 1.4404 unhardened steel screws in terms of friction and improvement of tablets' visual defect rate could be shown. WFAs were lower for measurements using the improved screw material compared to measurements conducted with the initial screw material within the whole applied normal stress range (see Figure 64). The evaluation of the impact of granulation moisture level (ML) on WFAs showed that increasing ML led to either a decrease or increase of WFA and was dependent on applied normal stress (see Figure 65). Therefore, the impact of ML on improvement of tablets' visual defect rate seemed to be minor compared to the adaption of the other process parameter settings and the exchange of the screw pair.

All in all, the case study showed that WFA measurements could serve as a base for explanation and justification of the several actions conducted to improve tablets' visual defect rate (see Table 18) as the connection to the TSG process could be shown evaluating granulator torque and calculating SME. Adapting process parameter settings by increasing screw speed, throughput and fill level of the granulator as well as adapting equipment settings by exchanging screw material were found to have high impact on improving abrasion effects inside TSG. Therefore, WFA measurements were shown to be a helpful tool for the assessment of abrasion induced effects inside TSG – either for troubleshooting purposes or already at the start of any experiments.

10. MATERIALS

10.1 LIST OF APIS AND EXCIPIENTS

All used APIs and excipients are listed with all relevant information in the table below.

Table 20 Overview on APIs and excipients with tradename, supplier and used batch numbers

Name	Tradename	Supplier	Batch #
BIxx1	-	Boehringer Ingelheim Pharma GmbH & Co.KG	3161120 3161620 3170860 3171170
Calciumhydrogen-phosphate	Dicalciumhydrogenphosphat, anhydrous	Chemische Fabrik Budenheim KG	306335
Copovidone	Kollidon VA 64	BASF SE	409777 602025
Crospovidone	Kollidon CL-SF	BASF SE	403283 405105 605676 605676-1 805791-1
Hypromellose	Methocel E5 Prem	The Dow Chemical Company	403576
Lactose	Granulac 200	Meggle Wasserburg GmbH & Co.KG	406543
Mannitol	Pearlitol 50 C	Roquette GmbH	504436 504436-1 804606 807271
Microcrystalline Cellulose	Avicel PH101	FMC Biopolymer	306984-1 500748

Magnesiumstearate	Ligamed	Peter Greven GmbH & Co.KG	308990 407287 504062
Paracetamol/ Acetaminophen	Paracetamol Ph.Eur. Micronized	Mallinckrodt Pharmaceuticals	703860
	Paracetamol Ph.Eur. Powder		703033
Starch pre-gelatinized	Starch 1500	Colorcon Inc.	303151-1
Starch undried	Maize starch (extra-white)	Roquette GmbH	304752 406154
Silicon dioxide highly-dispersed	CAB-O-SIL M5P	Cabot Rheinfelden GmbH & Co.KG	505663

10.2 FORMULATIONS

10.2.1 Raw materials and binary mixtures

For the evaluation of continuous volumetric dosing (see chapter 3) several raw materials and binary mixtures consisting of these raw materials were used. The composition of the used materials is listed in Table 21.

Table 21 Overview on raw materials and binary mixtures used for evaluation of continuous volumetric dosing (chapter 4)

raw material / binary mixture	mass percentage [% (m/m)] component 1	mass percentage [% (m/m)] component 2
MCC	100	-
MAN	100	-
LAC	100	-
STundried	100	-
ST1500	100	-
CA	100	-
LAC:MCC = 2:1	67	33
MAN:MCC = 2:1	67	33
MAN:STundried = 1:1	50	50
CA:MCC = 2:1	67	33
LAC:MCC = 1:2	33	67
MAN:MCC = 1:2	33	67
MAN:STundried = 9:1	90	10

10.2.2 Formulation 1

Formulation 1 (F1) was based on the two fillers Mannitol (MAN) and microcrystalline cellulose (MCC) in a ratio of 2:1 (m/m). For this formulation, a placebo and a verum preblend were prepared. For the verum formulation Acetaminophen micronized (APAP) at a drugload DL = 5 % was added as a model active pharmaceutical ingredient (API). The entire amount of the binder Hypromellose (HPMC) (in cases where the binder was added to the preblend) and half of the amount of the disintegrant Crospovidone (CROS) were added to the preblend consisting of APAP (only for the verum formulation), MAN, and MCC, to result in the intragranular phase. To prepare the final blend the remaining amount of CROS, and magnesiumstearate (MGST) were added to the sieved granules as the extragranular phase. Table 22 shows the composition of placebo and verum formulation.

Table 22 Composition of the formulation 1 with mass percentage [% (m/m)] for Placebo and Verum formulation and function for each excipient and the API

excipient/ API	Placebo: mass percentage [% (m/m)]	Verum: mass percentage [% (m/m)]	function
APAP	-	5.0	**API** - intragranular
MAN	63.0	59.7	**filler** - intragranular
MCC	31.5	29.8	**filler** - intragranular
HPMC	1.5	1.5	**binder** – intragranular
CROS	1.5	1.5	**disintegrant** - intragranular
CROS	1.5	1.5	**disintegrant** - extragranular
MGST	1.0	1.0	**lubricant** – extragranular

10.2.3 Formulation 2

Formulation 2 (F2) was based on the two fillers mannitol (MAN) and starch undried (STA) in a ratio of 9:1 (m/m). The entire amount of the binder copovidone (COPV) and half of the amount of the disintegrant crospovidone (CROS) were added to the preblend consisting of APAP (only for the verum formulation), MAN, and STA, to result in the intragranular phase. To prepare the final blend the remaining amount of CROS, and magnesiumstearate (MGST) were added to the sieved granules as the extragranular phase. For the verum formulation of formulation 2 APAP at a drugload DL = 5 % was added as a model active pharmaceutical ingredient (API) as well as for formulation 1 (s. 10.2.2). Additionally, for the performance of long-term run experiments (see 8) a preblend with another drugload DL = 25 % was prepared. The detailed composition of the formulation 2 (Verum [DL = 5 % and DL = 25 %] and Placebo) is described in Table 23.

Table 23 Composition of the formulation 2 with mass percentage [% (m/m)] for Placebo and Verum formulation and function for each excipient and the API

excipient/ API	Placebo: mass percentage [% (m/m)]	Verum DL = 5 %: mass percentage [% (m/m)]	Verum DL = 25 %: mass percentage [% (m/m)]	function
APAP	-	5.0	25	**API** - intragranular
MAN	82.8	78.3	60.3	**filler** - intragranular
STA	9.2	8.7	6.7	**filler** - intragranular
COPV	4.0	4.0	4.0	**binder** – intragranular
CROS	1.5	1.5	1.5	**disintegrant** – intragranular
CROS	1.5	1.5	1.5	**disintegrant** – extragranular
MGST	1.0	1.0	1.0	**lubricant** – extragranular

10.2.4 BIxx1 formulation

The case study formulation including the new chemical entity (NCE) BIxx1 (blinded API, Boehringer Ingelheim Pharma GmbH & Co.KG) at a DL = 20 % consisted mainly of the two fillers MAN and MCC. COPV was added as a binder. Silicon dioxide (AEROSIL) improved the flowability and half of the amount of CROS was added to the intragranular phase as disintegrant. A detailed composition of the formulation intended for clinical trial supplies is given in Table 24.

Table 24 Composition of the case study formulation including BIxx1 with mass percentage [% (m/m)] and function for each excipient and the API

excipient/ API	mass percentage [% (m/m)]	function
BIxx1	20.0	**API** - intragranular
MAN	47.0	**filler** - intragranular
MCC	23.5	**filler** - intragranular
COPV	2.5	**binder** – intragranular
AEROSIL	1.0	**glidant -** intragranular
CROS	2.5	**disintegrant** - intragranular
CROS	2.5	**disintegrant** - extragranular
MGST	1.0	**lubricant** – extragranular

11. MANUFACTURING AND ANALYTICAL METHODS

11.1 MANUFACTURING

11.1.1 Equipment – overview

An overview on the used manufacturing equipment is given in Table 25.

Table 25 Overview – manufacturing equipment

Process step	Equipment	Manufacturer
Screening	Comil 197 S	Quadro Engineering Corp., Canada
	Comil 196/2	
	Comil 197 U	
	Comil U5	
Blending	freefall blender equipped with: - 400 L container - 190 L containter - 40 L container - 30 L container	Servolift GmbH, Germany
	Turbula blender	Willy A. Bachofen AG Maschinenfabrik, Switzerland
Continuous dosing	ZD12-FB volumetric feeder	Three-Tec GmbH, Switzerland
	ZD22-FB gravimetric feeder	
	MT12 gravimetric feeder	Coperion K-Tron GmbH, Switzerland
	KT20 gravimetric feeder	
Continuous twin screw wet granulation	ZE 16 TSG	Three-Tec GmbH, Switzerland
	ZE 24 TSG	
	Pharma 11 HME TSG	Thermo Fisher Scientific, USA
	Pharma 16 TSG	
Preparation of granulation liquid	Eurostar 200 Control	IKA-Works Inc., USA
	Eurostar 100 Control	

Addition of granulation liquid	peristaltic tube pump	Watson Marlow GmbH, Germany
		Thermo Fisher Scientific, USA
(continuous) Fluid bed drying	Midi dryer (XS-line)	Glatt GmbH, Germany
	Modcos S based on GPCG2	
	Modcos M based on GPCG10	
Tableting	Flexitab	Röltgen GmbH & Co.KG, Germany

11.1.2 Preparation of powder preblends

11.1.2.1 Binary mixtures

Batch sizes of 4 kg were prepared for the binary mixtures used for continuous volumetric dosing evaluation (see chapter 3). Blending of these mixtures took place in a 30 L container freefall blender (Servolift GmbH, Germany) at a rotation speed of 10 rpm for 10 min.

11.1.2.2 Formulation 1

Formulation 1 (F1) placebo:
For the Placebo formulation 1 a total batch size of 73.125 kg was prepared. All intragranular excipients were sieved through a 1.016 mm grater holed screen with a Comil 197 S (Quadro Engineering, Canada) at a rotator speed of 1510 rpm. In a second step, the intragranular excipients were blended in a 400 L container freefall blender (Servolift GmbH, Germany) at a rotation speed of 10 rpm for 15 min.

Formulation 1 (F1) verum:
For the Verum formulation 1 several batches were prepared. All intragranular excipients except MAN (MCC, HPMC [in cases where HPMC was added to the preblend], CROS) were mixed with APAP in a container freefall blender (Servolift, GmbH, Germany) at a rotation speed of 10 rpm for 5 min. After the blending step, the premix was sieved together with the MAN through a 1.016 mm grater holed screen with a Comil sieving machine. Finally, the complete

intragranular excipients including the API were blended at a rotation speed of 10 rpm for 10 min in the same container freefall blender.

An overview on the exact equipment setting and process parameters for each batch is given in Table 26.

Table 26 Overview on equipment setting and process parameters for preparation of powder preblend of formulation 1 per batch

Batch no.	**batch size [kg]**	**sieve machine incl. rotation speed [rpm]**	**container size [kg]**	**link to chapter**
1 (placebo)	73.125	Comil 197 S 1510 rpm	400	9
2 (verum)	97.5	Comil 196/2 630 rpm	400	5 9
3 (verum)	97.5	Comil 197 S 1510 rpm	400	5
4 (verum)	73.125	Comil 196/2 630 rpm	400	6

11.1.2.3 Formulation 2

Formulation 2 (F2) placebo:

Placebo formulation 2 was prepared on the lines of placebo formulation 1 (s. 11.1.2.2). The batch sizes of the two batches were 73.125 kg, too. All intragranular excipients were sieved through a 1.016 mm grater holed screen with a sieving machine. Afterwards, the intragranular excipients were blended in a container freefall blender (Servolift GmbH, Germany) at a rotation speed of 10 rpm for 15 min.

Formulation 2 (F2) verum:

Several batches of verum formulation 2 were prepared. All intragranular excipients except MAN (STA, COPV, CROS) were mixed with APAP in a container freefall blender (Servolift,

GmbH, Germany) at a rotation speed of 10 rpm for 5 min. After the blending step, the premix was sieved together with the MAN through a 1.016 mm grater holed screen with a sieving machine. Finally, the complete intragranular excipients including the API were blended at a rotation speed of 10 rpm for 10 min in the same container freefall blender.
An overview on the exact equipment settings and process parameters for each batch is given in Table 27.

Table 27 Overview on equipment setting and process parameters for preparation of powder preblend of formulation 1 per batch

Batch no.	**batch size [kg]**	**sieve machine incl. rotation speed [rpm]**	**container size [kg]**	**link to chapter**
1 (placebo)	73.125	Comil 197 S 1510 rpm	400	9
2 (placebo)	73.125	Comil 196/2 630 rpm	400	8
3 (verum)	97.5	Comil 196/2 630 rpm	400	5
4 (verum)	73.125	Comil 196/2 630 rpm	400	6 7
5 (verum)	73.125	Comil 196/2 630 rpm	400	7
6 (verum)	97.5	Comil 197 S 1510 rpm	400	9
7 (verum)	64.35	Comil 197 U 1510 rpm	190	8

8 (verum)	64.35	Comil 197 U 1510 rpm	190	8
9 (verum)	64.35	Comil 197 U 1510 rpm	190	8
10 (verum)	73.125	Comil 196/2 630 rpm	400	8

11.1.2.4 BIxx1 formulation

For the case study formulation including BIxx1 (see chapter 9.4) two batches of 8.0 kg and 8.2 kg of powder preblend were prepared. In a first step, MAN was sieved through a 1.016 mm grater holed screen using a Comil U5 (Quadro Engineering, Canada) at a rotator speed of 1670 rpm. Subsequently, all excipients were blended in a 40 L container freefall blender (Servolift GmbH, Germany) at a rotation speed of 10 rpm and a blending time of 32 min. The resulting excipient premix was sieved through a 1.016 mm grater holed screen using a Comil U5 (Quadro Engineering, Canada) at a rotator speed of 1670 rpm. In the next step BIxx1 was added to the sieved excipients premix. Finally, the excipients premix plus BIxx1 were blended in a 40 L container freefall blender (Servolift GmbH, Germany) at a rotation speed of 10 rpm for another 32 min resulting in the final powder preblend.

11.1.3 Preparation of granulation liquid – chapters 5.3 and 6

For the experiments, where a granulation liquid was added to the twin screw granulation process (for F1, chapters 5.3 and 6), preparation of the granulation liquid took place in advance. Therefore, the binder was solved in the water with the help of a stirrer (IKA Works, Inc., USA). Afterwards, the granulation liquid solution was degassed for at least one hour. For the evaluation of different binder addition modes (see chapter 5.3) a separate granulation liquid was prepared per applied granulation moisture level to keep the amount of binder added to the powder preblend constant to the mass percentage given in the table in chapter 10.2. In contrast to the procedure in chapter 5.3, a base granulation liquid was prepared for the lowest applied granulation moisture level for the evaluation of continuous fluid bed drying of formulation 1

(see chapter 6). To result also in higher granulation moisture levels, a second peristatltic pump was installed. The one first pump was adding the base level of granulation liquid into the first liquid port of the granulator to result in the defined mass percentage of binder at a certain powder feed rate and to result in the defined lowest base granulation moisture level, too. The other second pump was adding pure water additionally in a second liquid port of the granulator to result in a higher granulation moisture level than the defined lowest base granulation moisture level.

11.1.4 Continuous process steps

11.1.4.1 Continuous dosing – chapter 4

For the investigations of volumetric dosing behaviour (see chapter 3) a ZD 12 FB-C-1M-200 flat-bottom feeder (Three-Tec GmbH, Switzerland) with a diameter of screws D = 12 mm was used. For all experiments (neat excipients and blends) the hopper (approx. 6.7 L) of the volumetric dosing system was filled to the same level, resulting in identical starting points for the experiments. The increasing mass of the dosed powder was measured every 20 seconds for three different screw speeds (50 UpM, 125 UpM, 200 UpM) using a standard balance until the hopper was empty.

11.1.4.2 Twin screw wet granulation – chapter 9

Twin screw wet granulation experiments investigating the abrasion effects during TSG process (see chapter 9) were performed using the BIxx1 formulation (see 10.2.4). As a twin screw granulator a ZE16 granulator (Three-Tec GmbH, Switzerland) with a diameter of screws D = 16 mm was used. The L/D-ratio of the granulator was 32 with a feeding zone of 10 D and a granulation zone of 22 D. For continuous feeding of powder preblend into the granulator, a ZD12 flat bottom volumetric feeder (Three-Tec GmbH, Switzerland) was applied. A peristaltic tube pump (Watson Marlow GmbH, Germany) was used for adding water as granulation liquid into the granulator.

The power consumption [A] was recorded during processing and enabled to calculate granulator torque for several process parameter settings. The specific mechanical energy was calculated according to Bochmann et al. (2018) [6]. Visual defect rate of tablets was determined after tableting for a defined sample size (n = 200) which was appr. 6 % of the total batch size

in that case. The tablet sample was visually inspected from both sides and all tablets with slight spots as well as specks were sorted out. An example of how tablets with spots and specks looked like is given in Figure 62.

11.1.4.3 Continuous granulation and drying

Each of the three combined continuous granulation and drying lines – based on the Modcos systems (Glatt GmbH, Germany) - consisted of the process units continuous dosing, twin screw wet granulation, a liquid pump for the addition of water during twin screw wet granulation process, and fluid bed drying. Differences between the three lines was the equipment size with regard to performance in terms of possible throughput rate per hour (XS = smallest / lab scale, S = middle / pilot scale, M = largest / production scale).
With regard to the twin screw wet granulation process the powder inlet and liquid inlet port positions for each scale were chosen with the aim to result in similar L/D-ratios (XS: 26; S: 29; M: 27). Furthermore, the screws of all twin screw granulators were built from conveying elements only. In addition, the barrel temperature was tightly controlled by a water cooling system to a target temperature of 20 °C for all scales, if not stated otherwise.
A pneumatic conveying system (Glatt GmbH, Germany) was used at S-line and M-line scale to transport the dried granules from the continuous dryer to the collecting container.

11.1.4.3.1 XS-line equipment – chapter 7

For the XS-line these process units were the following: as continuous feeder a -MT12 gravimetric feeder (Coperion K-Tron GmbH, Switzerland) was used, the twin screw granulator was a Pharma 11 HME granulator (ThermoFisher Scientific, USA) and the fluid bed dryer Midi-Glatt dryer (Glatt GmbH, Germany) operated lot-wise. A peristaltic tube pump (ThermoFisher Scientific, USA) was used for the addition of water during the twin screw wet granulation process.

11.1.4.3.2 S-line equipment – chapter 7

The S-line was built out of a KT20 gravimetric feeder (Coperion K-Tron GmbH, Switzerland), a Pharma 16 twin screw granulator (ThermoFisher Scientific, USA) and a Modcos S, GPCG2-based, continuous fluid bed dryer (Glatt GmbH, Germany). A peristaltic tube pump (Watson

Marlow GmbH, Germany) was used for the addition of water during the twin screw wet granulation process.

11.1.4.3.3 M-line equipment– chapters 5, 6, 7 & 8

M-line scale was equipped with a ZD 22 FB-C-1M-DN300 gravimetric feeder (Three-Tec GmbH, Switzerland), a ZE 24 twin screw granulator (Three-Tec GmbH, Switzerland) and a Modcos M, GPCG10-based, continuous fluid bed dryer (Glatt GmbH, Germany).
A peristaltic tube pump (Watson Marlow GmbH, Germany) was used for the addition of water or granulation liquid during the twin screw wet granulation process.

11.1.4.3.4 Experimental procedure for the evaluation of process parameters – chapters 5, 6, 7

Before starting the granulation and drying process, the dryer was preheated until an outlet air temperature of approx. min 50 °C was reached. For S-line and M-line scale, the collection of dried granules samples per process parameter setting was started after two complete rotations of the carousel inlet of the dryer to only collect material from an estimated steady state of the drying system. Approx. 1 - 3 kg of dried granules were collected per process setting for the two larger scales S and M. For the XS-line several small batches per process setting were produced consecutively until a total amount of approx. 100 g dried granules was reached.

11.1.5 Preparation of final blend

For the preparation of the final blend the dried granules were sieved through a 1.016 mm grater holed screen using a Comil U5 (Quadro Engineering, Canada) at a rotator speed of 1667 rpm in a first step. Afterwards the extragranular amount of CROS was blended with the sieved granules for 10 minutes at a speed of 35 rpm using a turbula mixer (Willy A. Bachofen AG Maschinenfabrik, Switzerland). In a last step the MGST was added and blended for 3 min at 35 rpm in the same turbula mixer.

11.1.6 Tableting

Compression was performed on a pneumatic hydraulic single punch press (Flexitab, Röltgen GmbH & Co. KG, Germany). 8 mm round, bevelled and biconvex (R12) tablets with a mass of 200 mg were produced at different compression forces applying a dwell time of 15 ms. The

range of compression forces was between 5 kN and 25 kN. For each applied compression force a minimum number of 20 tablets was manufactured for further characterisation.
Compression pressure CP was calculated by normalizing the compression force to the applied area (see Table 28).

Table 28 Compression pressure CP at different compression forces

compression force [kN]	**compression pressure CP [MPa]**
5	**93.7**
7.5	**140.6**
10	**187.4**
12.5	**234.3**
15	**281.2**
20	**374.9**
25	**468.6**

11.2 ANALYTICAL METHODS

11.2.1 Analytical methods – equipment & software overview

An overview on the used equipment for the analytical methods is given in Table 29.

Table 29 Overview – analytical methods equipment

	Analytical method	Equipment	Manufacturer
powder and granules	particle density	AccuPyk II 1340	Micromeritics Instrument Corporation, USA
	bulk and tapped density	Stampf-Volumeter PT-TD1	J. Engelsmann AG, Germany
	granulation moisture level and residual water content	HR83 moisture analyser	Mettler Toledo GmbH, USA
		MA100 moisture analyser	Sartorius AG, Germany
	particle size distribution	sieve analysis: Retsch AS 200 control	Retsch Technology GmbH, Germany
		dynamic image analysis: Camsizer X2	
	flowability	Ring shear tester RST-XS.s	Dr.-Ing. Dietmar Schulze Schüttgutmesstechnik, Germany
	wall friction measurement		
tablets	tablets:crushing strength, mass, dimensions	automated tableting tester TTS 11 software	Krämer Elektronik GmbH, Germany

An overview on the used softwares for data evaluation and visualization is given in Table 30.

Table 30 Overview – software used for data evaluation and visualization

Software	Supplier
Excel	Microsoft Office Professional Plus 2016
OriginPro 2017	OriginLab Corporation, USA
Spotfire Analyst Version 7.11.0	Tibco Software Inc., USA
Statistica Version 12	StatSoft GmbH, Germany

11.2.2 Raw material and granules

11.2.2.1 Particle density

The particle density (= appr. true density) of the powder preblend was measured using a helium gas pycnometer (AccuPyc II 1340, Micromeritics Instrument Corporation, USA). For the calculation of the particle density the average of 10 measument cycles was used. To prove whether it is feasible to use the measured true density value of powder preblend without the extragranular phase for calculation of solid fraction of the tablets, for each formulation (F1 and F2) one final blend was measured additionally. The deviations between final blend and powder preblend were < 1 % for both formulations so that it was decided to use true density value of powder preblend for calculation of tablet solid fraction (see appendix Table 46).

11.2.2.2 Bulk and tapped density

Bulk and tapped density were measured according to Ph.Eur [23]. Therefore, a mass of 100 gr material (raw material or granules) was filled into a cylinder with a volume V = 250 mL (Engelsmann STAV II). Determination of the volume for calculation of the bulk density took place. Afterwards the volume was measured after 10, 500, 1250 and 2500 taps (Stampf-Volumeter PT-TD1). Tapped density was calculated using the volume after 1250 taps. The Hausner ratio is the quotient of tap density and bulk density.

11.2.2.3 Granulation moisture level and residual water content

Moisture level of wet granules and residual water content of dried granules was determined using a HR 83 moisture analyzer (Mettler Toledo GmbH, USA) for the M-line experiments (see 11.1.4.3.3) and a MA 100 moisture analyzer (Sartorius AG, Germany) for the S-line and XS-line experiments (see 11.1.4.3.1 and 11.1.4.3.2). To be able to compare all moisture levels

and residual water contents independent of the used device the drying temperature was set to a value of 105 °C and endpoint of analysis was set at evaporation rates smaller than 1.2 mg/min for both devices. A sample amount of 6 g was used. Analysis took place immediately after granulation and immediately after the drying process. If more than one sample was measured for one experimental setting, the average was taken for further analysis.

11.2.2.4 Particle size distribution

Particle size distribution of raw materials was evaluated by sieve analysis.
Therefore, a Retsch AS 200 control sieve tower was used. This sieve tower included 10 sieves of different mesh size (63 µm, 90 µm, 125 µm, 180 µm, 250 µm, 355 µm, 500 µm, 630 µm, 710 µm, 1000 µm). A sample amount of 100 gr was sieved for 10 min using an amplitude of 2 mm and an interval time of 10 seconds.

Figure 67 Retsch sieve tower (source of picture: [94])

Particle size distribution of dried granules was determined using a Camsizer X2 (Retsch Technology GmbH, Germany).

Three aliquots of each sample were analysed, the average was taken for further evaluation. Measurement was performed using the 4 mm X Jet module at a dispersion pressure of 30 kPa.

Figure 68 Camsizer X2 – Retsch Technology GmbH, Germany (source of picture: Manual Camsizer X2)

For both methods, sieve analysis and Camsizer, particle fine fraction was defined as the particle fraction with a size < 63 µm and coarse particle fraction was defined as the particle fraction with a size > 1000 µm. Furthermore, D50 was defined as the cumulative mean particle size.

11.2.2.5 Flowability

The ring shear tester RST-XS.s (Dr.-Ing Dietmar Schulze Schüttguttmesstechnik, Germany) was used to determine the flowability value FFC for each sample. Measurement was conducted according to Schulze (2014) [103].

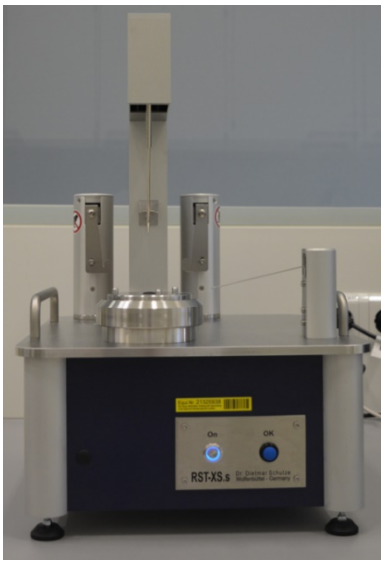

Figure 69 Ring shear tester RST-XS.s – Dr.-Ing Dietmar Schulze Schüttguttmesstechnik, Germany.

A normal stress at preshear of 1000 Pa was applied to the samples. The normal stresses at shear-to-failure were 200 Pa, 500 Pa and 800 Pa. Plotting the recorded shear stresses τ against the applied normal stresses σ, a yield locus is obtained.

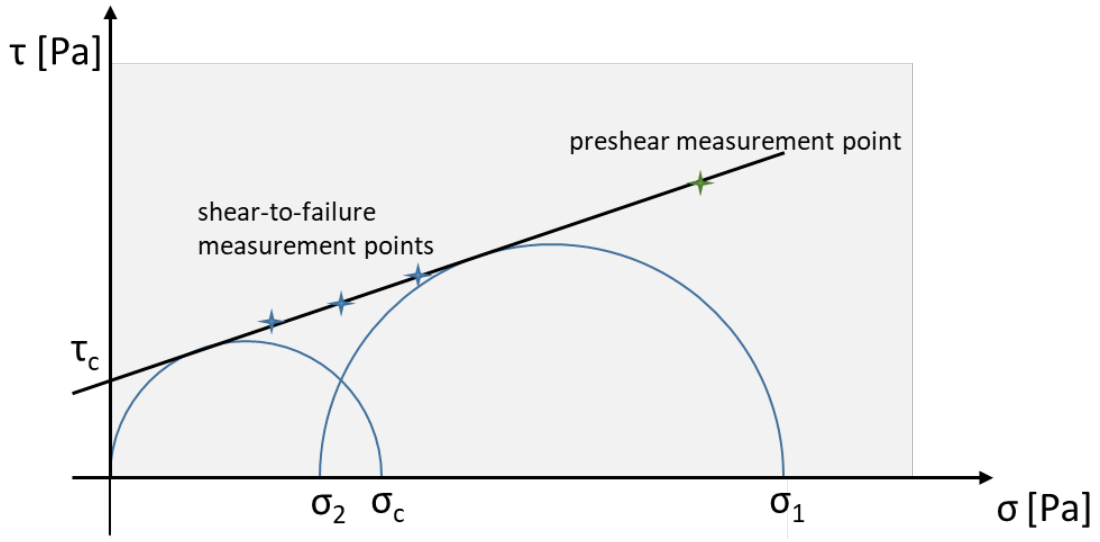

Figure 70 Yield locus – example

The ratio of the consolidation stress σ_1 and the unconfined yield strength σ_c is defined as the FFC value (see Figure 70 and equation (14)).

$$FFC\ [-] = \frac{\sigma_1}{\sigma_c} \tag{14}$$

The classification of different FFC values according to their flowability is given in Table 31.

Table 31 Classification of FFC values according to flowability

FFC	**flowability**
< 1	not flowing
1 – 2	very cohesive
2 – 4	cohesive
4 – 10	easy flowing
> 10	free flowing

11.2.2.6 Wall friction angle determination using a ring shear tester

The specific method of wall friction measurement using a Schulze ring shear tester RST-XS.s (Dr.-Ing. Dietmar Schulze Schüttgutmesstechnik, Germany) within this thesis (chapter 9) is described in the following.

For the wall friction measurements to investigate abrasion effects during TSG process, eight different normal stresses σ_w [Pa] were applied in a range between 200 Pa and 4000 Pa. Measurement points were exponentially distributed and were the following: σ_w 1 = 4000 Pa, σ_w 2 = 2396 Pa, σ_w 3 = 1453 Pa, σ_w 4 = 898 Pa, σ_w 5 = 571 Pa, σ_w 6 = 379 Pa, σ_w 7 = 266 Pa, σ_w 8 = 200 Pa. Within one measurement this cycle of eight different normal stresses was repeated four times. The average WFA φ [°]is the average value of these four repetitions per normal stress σ_w.

Wetting of dry powder material to result in a wet granule mass was done using mortar and pestle. The amount of water to be added to the dry powder preblend to result in a certain granulation moisture level ML [%] was calculated according to equation (16). For the different formulations (see 10.2) different MLs were chosen. Different formulations require different

granulation MLs for successful granulation as ML is a formulation-linked process parameter. For formulation 1 (see 10.2.2) the MLs were ML1 = 0 % (dry powder preblend), ML2 = 20 %, ML3 = 30 %, ML4 = 40 %. For formulation 2 (see 10.2.3) the MLs were ML1 = 0 % (dry powder preblend), ML2 = 10 %, ML3 = 15 %, ML4 = 20 %. For the BIxx1 formulation (see 10.2.4) the investigated MLs were ML1 = 25 % and ML2 = 30 %.

$$mass_{water}[g] = \frac{\frac{ML\,[\%]}{100} * mass_{powder}[g]}{1-\frac{ML\,[\%]}{100}} \quad (16)$$

11.2.3 Tablets

11.2.3.1 Crushing strength, mass and dimensions

Crushing strength, mass, and dimensions (thickness and diameter) of 20 tablets per sample were measured using an automated tablet tester (Krämer Elektronik GmbH, Germany). Measurement of tablets took place 24 hours after the tableting experiment at the earliest (except single samples where not possible for organizational reasons) to allow sufficient relaxation.

11.2.3.2 Tensile strength

Tensile strength TS of tablets was calculated on the base of measured crushing strength F [N] and dimensions thickness t [mm], height of tablet band W [mm] and diameter D [mm] (see Figure 71) according to equation (17) for tensile strength of biconvex round tablets as described by Pitt et al. [85, 86].

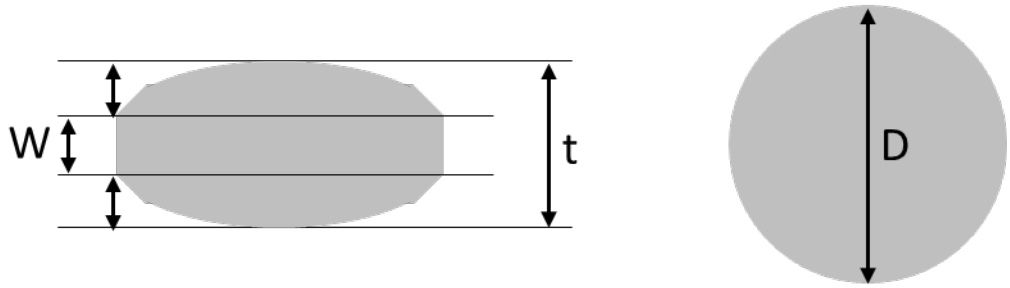

Figure 71 Description of a round, biconvex, bevelled edge tablet

$$TS\ \left[\frac{N}{mm^2}\right] = \frac{10*F}{\pi*D^2} * \left(2.84\frac{t}{D} - 0.126\frac{t}{W} + 3.15\frac{W}{D} + 0.01\right)^{-1} \quad (17)$$

11.2.3.3 Solid fraction SF

Equation (18) shows how solid fraction SF was calculated based on the measured mass m of the tablet, the tablet volume V and the particle density ρ of the powder preblend.

$$\mathrm{SF}\,[-] = \frac{\rho_{\mathrm{apparent}}}{\rho_{\mathrm{true}}} = \frac{\frac{m_{\mathrm{tablet}}}{V_{\mathrm{tablet}}}}{\rho_{\mathrm{true}}} \tag{18}$$

12. SUMMARY

For manufacturing of solid oral dosage forms, several continuous techniques are known. Regarding wet granulation, the continuous twin screw wet granulation is the most common continuous granulation mode. Most research concerning that topic so far, has focused on the twin screw wet granulation technique without applying a continuous drying mode to dry the wet granules. Instead, the wet granules were dried batch-/lot-wise after the continuous granulation step. In contrast to this research, this thesis investigated a complete integrated continuous granulation and drying line including the process units continuous dosing, continuous twin screw wet granulation and continuous fluid bed drying, considering also the quality of resulting tablets.

In the first part of the thesis (chapters 4, 5 and 6), a process understanding for the integrated continuous line was built investigating all three process units.
Powder characterisation of starting materials of a broad range of different excipients and binary mixtures using volumetric dosing mode proved the importance of the hopper fill level for an accurate dosing rate. Furthermore, it could be shown, that both material attributes bulk density and flowability of the excipient or binary mixture are of high importance and therefore critical for the resulting dosing rate and accuracy of dosing rate over time.
Regarding the continuous twin screw wet granulation, two different formulations were investigated and compared in terms of their granulation behaviour. Both formulations were therefore granulated and dried using the integrated continuous granulation and drying line. One formulation included cellulose, the other formulation explicitly did not. For both investigated formulations granulation moisture level was identified to be a critical process parameter and to have a high impact on the particle size distribution of the produced granules. Interestingly the other two investigated granulation-related process parameters powder feed rate and barrel fill level appeared to be of minor importance for resulting granules material attributes and tablet quality attributes. Characteristics of the two formulations and their granulation behaviour were thoroughly investigated and significant differences could be identified and described. Non beneficial granulation behaviour could be overcome and resulting tablets showed improved tabletability as expected.

As the third unit in the process-chain, the continuous fluid bed dryer was evaluated using the same formulations as being used for the investigation of twin screw wet granulation process. The drying performance was investigated by evaluation of the effect of three main process parameters on granule material attributes and tablet quality attributes. Particle fine fraction and residual water content of the dried granules could be identified to be critical material attributes with regard to tabletability and compressibility. It could also be shown that independent of the used formulation both mentioned material attributes could directly and systematically be controlled by the investigated process parameters.

Within development of a new pharmaceutical product scale-up is an important aspect to be considered in addition to the process understanding presented in the first part of the thesis. Therefore, in the second part of the thesis (chapter 7), a scale up approach for three continuous granulation and drying lines was investigated. For twin screw wet granulation process, enhanced scaling aspects were analysed showing e.g. the influence of Froude number on formation of coarse particle fraction. Within systematic evaluation of the applied scaling approach the drying capacity parameter DCP could be established which can further be utilized to adjust the drying capacity across different scales of continuous fluid bed driers. Statistical evaluation of the DoEs per scale enabled to calculate process design spaces for each scale; targeting on identified critical material attributes of the granules that result in good tabletability and compressibility performance. Overall, it could be shown that scaling of the three different continuous granulation and drying lines was successful using the presented scaling approach.

A special feature of continuous manufacturing compared to traditional batch processing is the consideration of time-dependent effects. Out of that reason, the third part of the thesis (chapter 8) deals with long-term effects evaluated during long-term runs using the integrated continuous granulation and drying line. For the continuous dosing unit a fast, more frequent refilling of the hopper was identified to be key for an accurate dosing rate. With regard to the twin screw wet granulation process, it was found that an efficient temperature control is essential to avoid high shear and friction energies inside the granulator. Parameters were identified indicating the stability and healthiness of the granulation system.

Abrasion and friction effects are special, mechanical risks of the twin screw wet granulation process. In the last part of the thesis (chapter 9) that process risk was considered by applying wall friction measurements with a Schulze ring shear tester. Deducted from the evaluation of wall friction angle of different formulations a case study made it possible to link the measured wall friction angles to the calculated specific mechanical energy during twin screw granulation and to the observed visual defect rate of tablets occurring due to abrasion effects during granulation. Thus, wall friction measurements could serve as useful tool to assess abrasion effects inside the twin screw granulator.

To sum up, this work provides systematic process understanding of and for the integrated continuous granulation and drying. Besides the establishment of correlations of process parameters and material and quality attributes (QbD principle), a scaling approach was evaluated and optimized, long-term effects were described and investigated and possibly occurring abrasion effects inside TSG were assessed via wall friction measurement.
The investigations and methods applied in this thesis consider the most important and directly applicable aspects from raw material to tablet for development of a NCE drug product within the pharmaceutical industry.

13. REFERENCES

1 Bandari, S., Nyavanandi, D., Kallakunta, V.R., Janga, K.Y., Sarabu, S., Butreddy, A., Repka, M.A., 2020. Continuous Twin Screw Granulation– An advanced alternative granulation technology for use in the pharmaceutical industry. International Journal of Pharmaceutics 580, 119215.

2 Beer, P., Wilson, D., Huang, Z., Matas, M.D., 2014. Transfer from high-shear batch to continuous twin screw wet granulation: a case study in understanding the relationship between process parameters and product quality attributes. J Pharm Sci 103, 3075–82.

3 Behres, M., Klasen, C.-J., Schulze, D., 1998. Development of a shear cell for measuring the wall friction of bulk solids with a ring shear tester. Powder Handling and Processing 10, 405–409.

4 Berry, R.J., Bradley, M.S.A., Reed, A.R., Farnish, R.J., Angulo, O.A., 2007. Development of An Annular Wall Friction Tester and Test Procedure, Suitable For Equipment Design and Powder Characterisation. 9th International Conference on Bulk Materials Storage, Handling and Transportation, ICBMH 2007.

5 Blackshields, C.A., Crean, A.M., 2017. Continuous powder feeding for pharmaceutical solid dosage form manufacture: a short review. Pharmaceutical Development and Technology 23, 1–7.

6 Bochmann, E., Gryczke, A., Wagner, K., 2018. Validation of Model-Based Melt Viscosity in Hot-Melt Extrusion Numerical Simulation. Pharmaceutics 10, 132.

7 Bradley, M.S.A., Bingley, M.S., Pittman, A.N., 2000. Abrasive wear of steels in handling of bulk particulates: an appraisal of wall friction measurement as an indicator of wear rate. Wear, Wear 243, 25–30.

8 Bradley, M.S.A., Pittman, A.N., Bingley, M., Farnish, R.J., Pickering, J., 2000. Effects of wall material hardness on choice of wall materials for design of hoppers and silos for the discharge of hard bulk solids. Tribology International 33, 845–853.

9 Cartwright, J.J., Robertson, J., D'Haene, D., Burke, M.D., Hennenkamp, J.R., 2013. Twin screw wet granulation: Loss in weight feeding of a poorly flowing active pharmaceutical ingredient. Powder Technology 238, 116–121.

10 Chebli, C., Cartilier, L., 1998. Cross-linked cellulose as a tablet excipient: A binding/disintegrating agent. International Journal of Pharmaceutics 171, 101–110.

11 Dahlgren, G., Tajarobi, P., Simone, E., Ricart, B., Melnick, J., Puri, V., Stanton, C., Bajwa, G., 2019. Continuous Twin Screw Wet Granulation and Drying—Control Strategy for Drug Product Manufacturing. Journal of Pharmaceutical Sciences 108, 3502–3514.

12 De Leersnyder, F., Vanhoorne, V., Bekaert, H., Vercruysse, J., Ghijs, M., Bostijn, N., Verstraeten, M., Cappuyns, P., Assche, I.V., Heyden, Y.V., Ziemons, E., Remon, J.P., Nopens, I., Vervaet, C., Beer, T.D., 2018. Breakage and drying behaviour of granules in a continuous fluid bed dryer: Influence of process parameters and wet granule transfer. European Journal of Pharmaceutical Sciences 115, 223–232.

13 Desbois, L., Tchoreloff, P., Mazel, V., 2019. Influence of the Punch Speed on the Die Wall/Powder Kinematic Friction During Tableting. Journal of Pharmaceutical Sciences 108, 3359–3365.

14 Dhenge, R.M., Fyles, R.S., Cartwright, J.J., Doughty, D.G., Hounslow, M.J., Salman, A.D., 2010. Twin screw wet granulation: Granule properties. Chemical Engineering Journal 164, 322–329.

15 Dhenge, R.M., Cartwright, J.J., Doughty, D.G., Hounslow, M.J., Salman, A.D., 2011. Twin screw wet granulation: Effect of powder feed rate. Advanced Powder Technology 22, 162–166.

16 Dhenge, R.M., Cartwright, J.J., Hounslow, M.J., Salman, A.D., 2012. Twin screw granulation: Steps in granule growth. International Journal of Pharmaceutics 438, 20–32.

17 Dhenge, R.M., Cartwright, J.J., Hounslow, M.J., Salman, A.D., 2012. Twin screw wet granulation: Effects of properties of granulation liquid. Powder Technology 229, 126–136.

18 Dhenge, R.M., Washino, K., Cartwright, J.J., Hounslow, M.J., Salman, A.D., 2013. Twin screw granulation using conveying screws: Effects of viscosity of granulation liquids and flow of powders. Powder Technology 238, 77–90.

19 Djuric, D., Kleinebudde, P., 11AD. Impact of screw elements on continuous granulation with a twin-screw extruder. Journal of Pharmaceutical Sciences 97, 4934–4942.

20 Djuric, D., Melkebeke, B.V., Kleinebudde, P., Remon, J.P., Vervaet, C., 2009. Comparison of two twin-screw extruders for continuous granulation. European Journal of Pharmaceutics and Biopharmaceutics 71, 155–160.

21 Djuric, D., Kleinebudde, P., 2010. Continuous granulation with a twin-screw extruder: impact of material throughput. Pharmaceutical Development and Technology 15, 518–25.

22 Hagrasy, A.S.E., Hennenkamp, J.R., Burke, M.D., Cartwright, J.J., Litster, J.D., 2013. Twin screw wet granulation: Influence of formulation parameters on granule properties and growth behavior. Powder Technology 238, 108–115.

23 10.2 Ph. Eur. 2.9.34 Bulk density and tapped density of powders. Strasbourg, France: European Directorate for the Quality of Medicines & Healthcare (EDQM);2020:384-387.

24 Engisch, W.E., Muzzio, F.J., 2012. Method for characterization of loss-in-weight feeder equipment. Powder Technology 228, 395–403.

25 Engisch, W.E., Muzzio, F.J., 2014. Loss-in-Weight Feeding Trials Case Study: Pharmaceutical Formulation. Journal of Pharmaceutical Innovation 10, 56–75.

26 Engisch, W.E., Muzzio, F.J., 2015. Feedrate deviations caused by hopper refill of loss-in-weight feeders. Powder Technology 283, 389–400.

27 Falk, J., Berry, R.J., Broström, M., Larsson, S.H., 2015. Mass flow and variability in screw feeding of biomass powders - Relations to particle and bulk properties. Powder Technology 276, 80–88.

28 Fekete, R., Peciar, M., Hanzel, M., 2007. Influence of Powder Material Moisture on the Angle of Wall Friction. Particle & Particle Systems Characterization 24, 276–283.

29 Fielden, K.E., Newton, J.M., O'Brien, P., Rowe, R.C., 1988. Thermal studies on the interaction of water and microcrystalline cellulose. The Journal of pharmacy and pharmacology 40, 674–678.

30 Fonteyne, M., Vercruysse, J., Díaz, D.C., Gildemyn, D., Vervaet, C., Remon, J.P., Beer, T.D., 2013. Real-time assessment of critical quality attributes of a continuous granulation process. Pharmaceutical Development and Technology 18, 85–97.

31 Fonteyne, M., Gildemyn, D., Peeters, E., Mortier, S.T.F.C., Vercruysse, J., Gernaey, K.V., Vervaet, C., Remon, J.P., Nopens, I., Beer, T.D., 2014. Moisture and drug solid-state monitoring during a continuous drying process using empirical and mass balance models. European Journal of Pharmaceutics and Biopharmaceutics 87, 616–628.

32 Fonteyne, M., Correia, A., Plecker, S.D., Vercruysse, J., Ilić, I., Zhou, Q., Vervaet, C., Remon, J.P., Onofre, F., Bulone, V., Beer, T.D., 1AD. Impact of microcrystalline cellulose material attributes: A case study on continuous twin screw granulation. International Journal of Pharmaceutics 478, 705–717.

33 Ghijs, M., Schäfer, E., Kumar, A., Cappuyns, P., Assche, I.V., Leersnyder, F.D., Vanhoorne, V., Beer, T.D., Nopens, I., 2019. Modeling of Semicontinuous Fluid Bed Drying of Pharmaceutical Granules With Respect to Granule Size. Journal of Pharmaceutical Sciences 108, 2094–2101.

34 Gorringe, L.J., Kee, G.S., Saleh, M.F., Fa, N.H., Elkes, R.G., 2017. Use of the channel fill level in defining a design space for twin screw wet granulation. International Journal of Pharmaceutics 519, 165–177.

35 Haaker, G., 1999. Wall friction measurements on bulk solids - results of comparative measurements on 9 bulk-solid/wall combinations from 13 laboratories using the Jenike Sheartester. Powder Handling and Processing 11, 19–25.

36 Halford, W., Lawler, C., Grima, A.P., Arnold, P.C., 2013. Some influences on wall friction measurements - a preliminary investigation. Presented at the 11th International Congress on Bulk Material Storage, Handling and Transportation, p. 12.

37 Han, T., 2011. Comparison of Wall Friction Measurements by Jenike Shear Tester and Ring Shear Tester. KONA Powder and Particle Journal, KONA Powder and Particle Journal 29, 118–124.

38 Hancock, B.C., 2019. The Wall Friction Properties of Pharmaceutical Powders, Blends, and Granulations. J. Pharm. Sci., Journal of Pharmaceutical Sciences 108, 457–463.

39 Hopkins, M., 2006. Loss in Weight Feeder Systems. Measurement and Control 39, 237–240.

40 Hsiao, W.-K., Hörmann, T.R., Toson, P., Paudel, A., Ghiotti, P., Stauffer, F., Bauer, F., Lakio, S., Behrend, O., Maurer, R., Holman, J., Khinast, J., 2020. Feeding of particle-based materials in continuous solid dosage manufacturing: a material science perspective. Drug Discovery Today 25, 800–806.

41 Hwang, K.-M., Cho, C.-H., Yoo, S.-D., Cha, K.-I., Park, E.-S., 2019. Continuous twin screw granulation: Impact of the starting material properties and various process parameters. Powder Technology 356, 847–857.

42 ICH guideline Q8 (R2) on pharmaceutical development EMA/CHMP/ICH/167068/2004

43 ICH guideline Q9 on quality risk management EMA/CHMP/ICH/24235/2006

44 ICH guideline Q10 on pharmaceutical quality system EMA/CHMP/ICH/214732/2007

45 Iqbal, T., Fitzpatrick, J.J., 2006. Effect of storage conditions on the wall friction characteristics of three food powders. Journal of Food Engineering 72, 273–280.

46 Jager, P.D., Bramante, T., Luner, P.E., 2015. Assessment of Pharmaceutical Powder Flowability using Shear Cell - Based Methods and Application of Jenikes Methodology. Journal of Pharmaceutical Sciences 104, 3804.

47 Karttunen, A.-P., Poms, J., Sacher, S., Sparén, A., Samblás, C.R., Fransson, M., Juan, L.M.D., Remmelgas, J., Wikström, H., Hsiao, W.-K., Folestad, S., Korhonen, O., Abrahmsén-Alami, S., Tajarobi, P., 2020. Robustness of a continuous direct compression line against disturbances in feeding. International Journal of Pharmaceutics 574, 118882.

48 Keleb, E.I., Vermeire, A., Vervaet, C., Remon, J.P., 2002. Continuous twin screw extrusion for the wet granulation of lactose. International Journal of Pharmaceutics 239, 69–80.

49 Keleb, E.I., Vermeire, A., Vervaet, C., Remon, J.P., 2004. Twin screw granulation as a simple and efficient tool for continuous wet granulation. International Journal of Pharmaceutics 273, 183–194.

50 Kim, S.H., Hwang, K.M., Cho, C.H., Nguyen, T.T., Seok, S.H., Hwang, K.M., Kim, J.Y., Park, C.W., Rhee, Y.S., Park, E.S., 2017. Application of continuous twin screw granulation for the metformin hydrochloride extended release formulation. International Journal of Pharmaceutics 529, 410–422.

51 Kumar, A., Vercruysse, J., Bellandi, G., Gernaey, K.V., Vervaet, C., Remon, J.P., Beer, T.D., Nopens, I., 2014. Experimental investigation of granule size and shape dynamics in twin-screw granulation. International Journal of Pharmaceutics 475, 485–495.

52 Kumar, A., Vercruysse, J., Toiviainen, M., Panouillot, P.E., Juuti, M., Vanhoorne, V., Vervaet, C., Remon, J.P., Gernaey, K.V., Beer, T.D., Nopens, I., 2014. Mixing and transport during pharmaceutical twin-screw wet granulation: Experimental analysis via

chemical imaging. European Journal of Pharmaceutics and Biopharmaceutics 87, 279–289.

53 Kumar, A., Dhondt, J., Vercruysse, J., Leersnyder, F.D., Vanhoorne, V., Vervaet, C., Remon, J.P., Gernaey, K.V., Beer, T.D., Nopens, I., 2016. Development of a process map: A step towards a regime map for steady-state high shear wet twin screw granulation. Powder Technology 300, 73–82.

54 Kumar, A., Alakarjula, M., Vanhoorne, V., Toiviainen, M., Leersnyder, F.D., Vercruysse, J., Juuti, M., Ketolainen, J., Vervaet, C., Remon, J.P., Gernaey, K.V., Beer, T.D., Nopens, I., 2016. Linking granulation performance with residence time and granulation liquid distributions in twin-screw granulation: An experimental investigation. European Journal of Pharmaceutical Sciences 90, 25–37.

55 Kumar, A., Vercruysse, J., Mortier, S.T.F.C., Vervaet, C., Remon, J.P., Gernaey, K.V., Beer, T.D., Nopens, I., 2016. Model-based analysis of a twin-screw wet granulation system for continuous solid dosage manufacturing. Computers and Chemical Engineering 89, 62–70.

56 Lee, K.T., Ingram, A., Rowson, N.A., 2013. Comparison of granule properties produced using Twin Screw Extruder and High Shear Mixer: A step towards understanding the mechanism of twin screw wet granulation. Powder Technology 238, 91–98.

57 Lee, S.L., O'Connor, T.F., Yang, X., Cruz, C.N., Chatterjee, S., Madurawe, R.D., Moore, C.M.V., Yu, L.X., Woodcock, J., 2015. Modernizing Pharmaceutical Manufacturing: from Batch to Continuous Production. Journal of Pharmaceutical Innovation 10, 191–199.

58 Leuenberger, H., 2001. New trends in the production of pharmaceutical granules: batch versus continuous processing. European Journal of Pharmaceutics and Biopharmaceutics 52, 289–296.

59 Li, H., Thompson, M.R., O'Donnell, K.P., 2014. Understanding wet granulation in the kneading block of twin screw extruders. Chemical Engineering Science 113, 11–21.

60 Li, T., Scicolone, J.V., Sanchez, E., Muzzio, F.J., 2019. Identifying a Loss-in-Weight Feeder Design Space Based on Performance and Material Properties. Journal of Pharmaceutical Innovation 15, 482–495.

61 Liu, H., Galbraith, S.C., Ricart, B., Stanton, C., Smith-Goettler, B., Verdi, L., O'Connor, T., Lee, S., Yoon, S., 2017. Optimization of critical quality attributes in continuous twin-screw wet granulation via design space validated with pilot scale experimental data. International Journal of Pharmaceutics 525, 249–263.

62 Lute, S.V., Dhenge, R.M., Hounslow, M.J., Salman, A.D., 2016. Twin screw granulation: Understanding the mechanism of granule formation along the barrel length. Chemical Engineering Research and Design 110, 43–53.

63 Lute, S.V., Dhenge, R.M., Salman, A.D., 2018. Twin Screw Granulation: An Investigation of the Effect of Barrel Fill Level. Pharmaceutics 10, 67.

64 Lute, S.V., Dhenge, R.M., Salman, A.D., 2018. Twin Screw Granulation: Effects of Properties of Primary Powders. Pharmaceutics 10, 68.

65 Markl, D., Warman, M., Dumarey, M., Bergman, E.-L., Folestad, S., Shi, Z., Manley, L.F., Goodwin, D.J., Zeitler, J.A., 2020. Review of real-time release testing of pharmaceutical tablets: State-of-the art, challenges and future perspective. International journal of pharmaceutics 582, 119353.

66 Mazel, V., Diarra, H., Tchoreloff, P., 2019. Effect of friction between powder and tooling on the die-wall pressure evolution during tableting: Experimental and numerical results for flat and concave punches. International Journal of Pharmaceutics 554, 116–124.

67 Meier, R., Thommes, M., Rasenack, N., Moll, K.P., Krumme, M., Kleinebudde, P., 2016. Granule size distributions after twin-screw granulation - Do not forget the feeding systems. European Journal of Pharmaceutics and Biopharmaceutics 106, 59–69

68 Meier, R., Moll, K.-P., Krumme, M., Kleinebudde, P., 6AD. Impact of fill-level in twin-screw granulation on critical quality attributes of granules and tablets. European Journal of Pharmaceutics and Biopharmaceutics 115, 102–112.

69 Mendez Torrecillas, C., Halbert, G.W., Lamprou, D.A., 2017. A novel methodology to study polymodal particle size distributions produced during continuous wet granulation. International Journal of Pharmaceutics 519, 230–239.

70 Meng, W., Kotamarthy, L., Panikar, S., Sen, M., Pradhan, S., Marc, M., Litster, J.D., Muzzio, F.J., Ramachandran, R., 11AD. Statistical analysis and comparison of a continuous high shear granulator with a twin screw granulator: Effect of process parameters on critical granule attributes and granulation mechanisms. International Journal of Pharmaceutics 513, 357–375.

71 Meng, W., Rao, K.S., Snee, R.D., Ramachandran, R., Muzzio, F.J., 2019. A comprehensive analysis and optimization of continuous twin-screw granulation processes via sequential experimentation strategy. International Journal of Pharmaceutics 556, 349–362.

72 Menth, J., Maus M., Wagner K.G., 2018. Establishing Twin screw wet granulation (TSG) as a continuous process step Abstract and poster presentation, APV World Meeting 2018, Granada

73 Menth, J., Maus, M., Wagner, K.G., 2020. Continuous twin screw granulation and fluid bed drying: A mechanistic scaling approach focusing optimal tablet properties. International journal of pharmaceutics 586, 119509.

74 Miyazaki, Y., Lenhart, V., Kleinebudde, P., 2020. Switch of tablet manufacturing from high shear granulation to twin-screw granulation using quality by design approach. International journal of pharmaceutics 579, 119139.

75 Mort, P.R., 2005. Scale-up of binder agglomeration processes. Powder Technology 150, 86–103.

76 Mortier, S.T.F.C., Gernaey, K.V., Beer, T.D., Nopens, I., 2014. Analysing drying unit performance in a continuous pharmaceutical manufacturing line by means of mass - Energy balances. European Journal of Pharmaceutics and Biopharmaceutics 86, 532–543

77 Myerson, A.S., Krumme, M., Nasr, M., Thomas, H., Braatz, R.D., 2015. Control systems engineering in continuous pharmaceutical manufacturing. May 20-21, 2014 Continuous Manufacturing Symposium. Journal of Pharmaceutical Sciences 104, 832–9.

78 Nakamura, S., Otsuka, N., Yoshino, Y., Sakamoto, T., Yuasa, H., 2016. Predicting the occurrence of sticking during tablet production by shear testing of a pharmaceutical powder. Chemical and Pharmaceutical Bulletin 64, 512–516.

79 Osorio, J.G., Sayin, R., Kalbag, A.V., Litster, J.D., Martinez-Marcos, L., Lamprou, D.A., Halbert, G.W., 2017. Scaling of continuous twin screw wet granulation. AIChE Journal 63, 921–932

80 Pauli, V., Elbaz, F., Kleinebudde, P., Krumme, M., 2018. Methodology for a Variable Rate Control Strategy Development in Continuous Manufacturing Applied to Twin-screw Wet-Granulation and Continuous Fluid-bed Drying. Journal of Pharmaceutical Innovation 13, 247–260.

81 Pauli, V., Elbaz, F., Kleinebudde, P., Krumme, M., 2019. Orthogonal Redundant Monitoring of a New Continuous Fluid-Bed Dryer for Pharmaceutical Processing by Means of Mass and Energy Balance Calculations and Spectroscopic Techniques. Journal of Pharmaceutical Sciences 108, 2041–2055.

82 Pauli, V., Kleinebudde, P., Krumme, M., 2020. Predictive Model-Based Process Start-Up in Pharmaceutical Continuous Granulation and Drying. Pharm, Pharmaceutics 12, 67.

83 Peters, J., Teske, A., Taute, W., Döscher, C., Höft, M., Knöchel, R., Breitkreutz, J., 2018. Real-time process monitoring in a semi-continuous fluid-bed dryer – microwave

resonance technology versus near-infrared spectroscopy. International Journal of Pharmaceutics 537, 193–201.

84 Pillai, J.R., Bradley, M.S.A., Berry, R.J., 2007. Comparison between the angles of wall friction measured on an on-line wall friction tester and the Jenike wall friction tester. Powder Technology 174, 64–70.

85 Pitt, K.G., Newton, J.M., Stanley, P., 1988. Tensile fracture of doubly-convex cylindrical discs under diametral loading. Journal of Materials Science 23, 2723–2728.

86 Pitt, K.G., Heasley, M.G., 2013. Determination of the tensile strength of elongated tablets. Powder Technology 238, 169–175.

87 Plumb, K., 2005. Continuous processing in the pharmaceutical industry: Changing the mind set. Chemical Engineering Research and Design 83, 730–738.

88 Portier, C., Pandelaere, K., Delaet, U., Vigh, T., Pretoro, G.D., Beer, T.D., Vervaet, C., Vanhoorne, V., 2020. Continuous twin screw granulation: A complex interplay between formulation properties, process settings and screw design. International Journal of Pharmaceutics 576, 119004.

89 Portier, C., Vigh, T., Pretoro, G.D., Beer, T.D., Vervaet, C., Vanhoorne, V., 2020. Continuous twin screw granulation: Impact of binder addition method and surfactants on granulation of a high-dosed, poorly soluble API. International Journal of Pharmaceutics 577, 119068.

90 Portier, C., Pandelaere, K., Delaet, U., Vigh, T., Kumar, A., Pretoro, G.D., Beer, T.D., Vervaet, C., Vanhoorne, V., 2020. Continuous twin screw granulation: Influence of process and formulation variables on granule quality attributes of model formulations. International journal of pharmaceutics 576, 118981.

91 Prescott, J.K., Ploof, D.A., Carson, J.W., 1999. Developing a Better Understanding of Wall friction. powder handling & processing 11, 27–36.

92 Rantanen, J., Khinast, J., 2015. The Future of Pharmaceutical Manufacturing Sciences. Journal of Pharmaceutical Sciences 104, 3612–3638.

93 Rehrl, J., Sacher, S., Horn, M., Khinast, J., 2020. End-Point Prediction of Granule Moisture in a ConsiGmaTM-25 Segmented Fluid Bed Dryer. Pharmaceutics 12, 452.

94 Retsch-Homepage; https://www.retsch.de/de/applikationen/wissensdatenbank/siebanalyse/ [last access: 21.04.21, 14:02]

95 Roggo, Y., Pauli, V., Jelsch, M., Pellegatti, L., Elbaz, F., Ensslin, S., Kleinebudde, P., Krumme, M., 2020. Continuous manufacturing process monitoring of pharmaceutical solid dosage form: A case study. Journal of pharmaceutical and biomedical analysis 179, 112971.

96 Roggo, Y., Jelsch, M., Heger, P., Ensslin, S., Krumme, M., 2020. Deep learning for continuous manufacturing of pharmaceutical solid dosage form. European Journal of Pharmaceutics and Biopharmaceutics 153, 95–105.

97 Saleh, M.F., Dhenge, R.M., Cartwright, J.J., Hounslow, M.J., Salman, A.D., 2015. Twin screw wet granulation: Binder delivery. International Journal of Pharmaceutics 487, 124–134.

98 Saleh, M.F., Dhenge, R.M., Cartwright, J.J., Hounslow, M.J., Salman, A.D., 2015. Twin screw wet granulation: Effect of process and formulation variables on powder caking during production. International Journal of Pharmaceutics 496, 571–582.

99 Sayin, R., Hagrasy, A.S.E., Litster, J.D., 2015. Distributive mixing elements: Towards improved granule attributes from a twin screw granulation process. Chemical Engineering Science 125, 165–175.

100 Schmidt, A., Waard, H.D., Moll, K.P., Krumme, M., Kleinebudde, P., 2016. Quantitative assessment of mass flow boundaries in continuous twin-screw granulation. Chimia 70, 604–609.

101Schmidtke, R., Schröder, D., Menth, J., Staab, A., Braun, M., Wagner, K.G., 2017. Prediction of solid fraction from powder mixtures based on single component compression analysis. International Journal of Pharmaceutics 523, 366–375.

102Schulze, D., 2011. Flow Properties of Powders and Bulk Solids. Technical paper. https://www.dietmar-schulze.de/grdle1.pdf (accessed 22 January 2021)

103Schulze, D., 2014. Pulver und Schüttgüter - Fließeigenschaften und Handhabung Heidelberg, Springer Verlag

104Seem, T.C., Rowson, N.A., Ingram, A., Huang, Z., Yu, S., Matas, M. de, Gabbott, I., Reynolds, G.K., 2015. Twin screw granulation — A literature review. Powder Technology 276, 89–102.

105Stauffer, F., Ryckaert, A., Hauwermeiren, D.V., Funke, A., Djuric, D., Nopens, I., Beer, T.D., 2019. Heat Transfer Evaluation During Twin-Screw Wet Granulation in View of Detailed Process Understanding. AAPS PharmSciTech 20.

106Stauffer, F., Ryckaert, A., Vanhoorne, V., Hauwermeiren, D.V., Funke, A., Djuric, D., Vervaet, C., Nopens, I., Beer, T.D., 2020. In-line temperature measurement to improve the understanding of the wetting phase in twin-screw wet granulation and its use in process development. International journal of pharmaceutics 584, 119451.

107Tan, L., Carella, A.J., Ren, Y., Lo, J.B., 2011. Process optimization for continuous extrusion wet granulation. Pharmaceutical Development and Technology 16, 302–315.

108Thompson, M.R., Sun, J., 2010. Wet granulation in a twin-screw extruder: Implications of screw design. Journal of Pharmaceutical Sciences 99, 2090–2103.

109Three-Tec Homepage; http://three-tec.ch/dosierwerkzeuge%20und%20leistungen%20fb.htm; last access: 27.11.20, 10:06 am

110Three-Tec Homepage; http://three-tec.ch/dosierwerkzeuge%20und%20leistungen%20fb.htm ; last access: 22.12.2020, 16:27 pm

111Three-Tec Homepage; http://three-tec.ch/schneckensegmente.htm ; last access: 22.12.2020, 08:22 am

112Tye, C.K., Sun, C., Amidon, G.E., 2005. Evaluation of the effects of tableting speed on the relationships between compaction pressure, tablet tensile strength, and tablet solid fraction. Journal of Pharmaceutical Sciences 94, 465–472.

113Vandevivere, L., Denduyver, P., Portier, C., Häusler, O., Beer, T.D., Vervaet, C., Vanhoorne, V., 2020. Influence of binder attributes on binder effectiveness in a continuous twin screw wet granulation process via wet and dry binder addition. International Journal of Pharmaceutics 585, 119466.

114Vanhoorne, V., Vanbillemont, B., Vercruysse, J., Leersnyder, F.D., Gomes, P., Beer, T.D., Remon, J.P., Vervaet, C., 2016. Development of a controlled release formulation by continuous twin screw granulation: Influence of process and formulation parameters. International Journal of Pharmaceutics 505, 61–68.

115Vanhoorne, V., Vervaet, C., 2020. Recent progress in continuous manufacturing of oral solid dosage forms. International journal of pharmaceutics 579, 119194.

116Van Melkebeke, B., Vervaet, C., Remon, J.P., 2008. Validation of a continuous granulation process using a twin-screw extruder. International Journal of Pharmaceutics 356, 224–230.

117Van Snick, B., Holman, J., Cunningham, C., Kumar, A., Vercruysse, J., Beer, T.D., Remon, J.P., Vervaet, C., 2017. Continuous direct compression as manufacturing platform for sustained release tablets. International Journal of Pharmaceutics 519, 390–407.

118Van Snick, B., Grymonpré, W., Dhondt, J., Pandelaere, K., Pretoro, G.D., Remon, J.P., Beer, T.D., Vervaet, C., Vanhoorne, V., 2018. Impact of blend properties on die filling during tableting. International Journal of Pharmaceutics 549, 476–488.

119Van Snick, B., Kumar, A., Verstraeten, M., Pandelaere, K., Dhondt, J., Pretoro, G.D., Beer, T.D., Vervaet, C., Vanhoorne, V., 2019. Impact of material properties and process variables on the residence time distribution in twin screw feeding equipment. International Journal of Pharmaceutics 556, 200–216.

120Vercruysse, J., Díaz, D.C., Peeters, E., Fonteyne, M., Delaet, U., Assche, I.V., Beer, T.D., Remon, J.P., Vervaet, C., 2012. Continuous twin screw granulation: Influence of process variables on granule and tablet quality. European Journal of Pharmaceutics and Biopharmaceutics 82, 205–211.

121Vercruysse, J., Delaet, U., Assche, I.V., Cappuyns, P., Arata, F., Caporicci, G., Beer, T.D., Remon, J.P., Vervaet, C., 2013. Stability and repeatability of a continuous twin screw granulation and drying system. European Journal of Pharmaceutics and Biopharmaceutics 85, 1031–8.

122Vercruysse, J., Peeters, E., Fonteyne, M., Cappuyns, P., Delaet, U., Assche, I.V., Beer, T.D., Remon, J.P., Vervaet, C., 2015. Use of a continuous twin screw granulation and drying system during formulation development and process optimization. European Journal of Pharmaceutics and Biopharmaceutics 89, 239–47.

123Verstraeten, M., Hauwermeiren, D.V., Lee, K., Turnbull, N., Wilsdon, D., Ende, M. am, Doshi, P., Vervaet, C., Brouckaert, D., Mortier, S.T.F.C., Nopens, I., Beer, T.D., 2017. In-depth experimental analysis of pharmaceutical twin-screw wet granulation in view of detailed process understanding. International Journal of Pharmaceutics 529, 678–693.

124Wang, Y., Li, T., Muzzio, F.J., Glasser, B.J., 2017. Predicting feeder performance based on material flow properties. Powder Technology 308, 135–148.

125Yadav, I.K., Holman, J., Meehan, E., Tahir, F., Khoo, J., Taylor, J., Benedetti, A., Aderinto, O., Bajwa, G., 2019. Influence of material properties and equipment configuration on loss-in-weight feeder performance for drug product continuous manufacture. Powder Technology 348, 126–137.

126Yu, L.X., 2008. Pharmaceutical Quality by Design: Product and Process Development, Understanding, and Control. Pharmaceutical Research 25, 781–791.

127Yu, L.X., Amidon, G., Khan, M.A., Hoag, S.W., Polli, J., Raju, G.K., Woodcock, J., 2014. Understanding Pharmaceutical Quality by Design. The AAPS journal 16, 771–783.

128Yu, L.X., Kopcha, M., 2017. The future of pharmaceutical quality and the path to get there. International Journal of Pharmaceutics 528, 354–359.

129Yu, S., Reynolds, G.K., Huang, Z., Matas, M.D., Salman, A.D., 2014. Granulation of increasingly hydrophobic formulations using a twin screw granulator. International Journal of Pharmaceutics 475, 82–96.

14. APPENDIX

14.1 CHAPTER 5.2

Table 32 Overview on detailed experimental setup – chapter 5.2

		GRANULATION				DRYING		
formulation	**exp. no.**	**PFR [kg/h]**	**LFR [g/min]**	**ML [%]**	**screw speed [rpm]**	**DRS [rph]**	**IAFR [m³/h]**	**IAT [°C]**
F1	1	15	44.1	15	225	20	300	75
F1	2	15	44.1	15	300	20	300	75
F1	3	15	74.7	23	225	20	300	85
F1	4	15	74.7	23	300	20	300	85
F1	5	20	78.2	19	343	20	330	85
F1	6	25	73.5	15	375	20	360	85
F1	7	25	73.5	15	500	20	360	85
F1	8	25	124.5	23	375	20	360	95
F1	9	25	124.5	23	500	20	360	95
F2	1	10	18.5	10	150	20	270	60
F2	2	10	18.5	10	200	20	270	60
F2	3	10	41.7	20	150	20	300	75
F2	4	10	41.7	20	200	20	300	75
F2	5	20	58.8	15	343	20	320	65
F2	6	30	55.6	10	450	20	370	75
F2	7	30	55.6	10	600	20	370	75
F2	8	30	125.0	20	450	20	420	95
F2	9	-	-	-	-	-	-	-

Table 33 Granules MAs – formulation 1 – chapter 5.2

exp.no	**LoD [%]**	**FFC [-]**	**D10 [µm]**	**D50 [µm]**	**D90 [µm]**	**<63µm [%]**	**>1000µm [%]**
1	0.72	5.3	30.9	144.6	1421.9	27.6	20.6
2	0.96	4.1	26.7	98.8	1771.1	36.1	22.5
3	0.78	5.6	37.3	140.0	1702.3	24.2	18.5
4	1.99	5.9	35.5	226.0	2036.2	25.6	29.3
5	0.93	4.7	26.8	87.5	1873.7	39.4	22.0

6	0.80	4.0	22.0	57.7	1242.3	53.8	12.1
7	0.98	4.4	26.9	121.0	2031.1	35.1	27.8
8	1.40	4.7	35.7	138.3	1962.4	26.1	25.3
9	2.59	4.6	29.8	140.6	2001.6	32.8	28.1

Table 34 Tablet MAs – formulation 1 –chapter 5.2

exp.no	CP [MPa]	mass [mg]	mass s.rel [%]	height [mm]	height s.rel [%]	crushing strength [N]	crushing strength s.rel [%]
1	94	199.4	1.60	3.97	1.26	46	4.35
1	187	197.4	0.61	3.67	0.54	96	4.17
1	281	197.8	0.71	3.60	0.56	125	3.20
1	375	197.3	0.51	3.57	0.56	138	2.90
1	469	199.3	0.50	3.58	0.56	148	2.03
2	94	194.2	1.91	3.89	1.80	44	4.55
2	187	190.1	1.00	3.58	0.84	92	3.26
2	281	197.1	0.71	3.60	0.56	126	3.17
2	375	197.9	0.86	3.58	0.84	138	3.62
2	469	196.3	0.92	3.54	0.85	148	2.03
3	94	198.1	0.81	3.92	0.77	50	4.00
3	187	196.4	0.51	3.64	0.55	103	2.91
3	281	197.6	0.86	3.60	0.83	132	2.27
3	375	199.1	0.60	3.59	0.56	146	3.42
3	469	200.9	0.60	3.60	0.56	151	2.65
4	94	194.5	0.82	3.88	0.77	49	4.08
4	187	197	0.56	3.64	0.55	102	2.94
4	281	200.1	0.50	3.62	0.55	134	3.73
4	375	199.9	0.80	3.60	0.56	144	3.47
4	469	198.8	1.16	3.57	1.12	153	2.61
5	94	195.7	1.64	3.90	1.28	50	4.00
5	187	193.3	1.14	3.60	0.83	108	2.78
5	281	195.8	0.82	3.57	0.56	138	2.90
5	375	200.4	0.70	3.61	0.55	157	2.55
5	469	200.9	0.90	3.60	0.56	167	2.40
6	94	196.7	1.07	3.95	1.01	45	4.44

6	187	198.4	0.71	3.68	0.82	102	2.94
6	281	199.3	0.90	3.62	0.55	134	2.99
6	375	200.8	1.05	3.62	0.83	153	2.61
6	469	202.5	0.99	3.63	0.55	161	2.48
7	94	204.6	1.17	4.06	0.99	48	4.17
7	187	198.3	1.77	3.67	1.36	104	3.85
7	281	196.6	1.07	3.59	0.84	134	2.99
7	375	198	0.86	3.58	0.84	150	2.00
7	469	198.8	1.06	3.58	0.84	159	3.14
8	94	196.5	0.81	3.90	0.51	51	1.96
8	187	201.1	0.54	3.70	0.54	113	3.01
8	281	202	0.64	3.64	0.55	141	2.84
8	375	201	0.55	3.61	0.55	150	2.67
8	469	202.1	0.49	3.61	0.55	159	2.52
9	94	194.6	0.92	3.89	0.77	49	4.08
9	187	199.2	0.75	3.68	0.82	108	2.78
9	281	197.6	0.81	3.60	0.56	137	2.19
9	375	198.1	0.81	3.58	0.84	151	3.65
9	469	198.2	0.71	3.57	0.56	161	2.48

Table 35 Granules MAs – formulation 2 – chapter 5.2

exp.no	LoD [%]	FFC [-]	D10 [µm]	D50 [µm]	D90 [µm]	<63µm [%]	>1000µm [%]
1	0.88	15.3	133.8	462.5	1364.8	3.9	19.6
2	0.88	25.8	119.3	384.4	1209.7	4.9	13.4
3	1.55	11.2	299.9	742.5	1621.2	1.2	32.5
4	0.85	18.1	286.3	654.6	1447.8	1.1	26.5
5	0.95	10.4	62.8	194.8	582.2	10.1	2.8
6	0.63	5.0	28.0	491.1	1926.4	22.3	36.3
7	0.81	2.7	23.4	295.9	2296.4	32.9	38.2
8	2.35	10.3	288.1	742.4	1782.8	2.4	32.3

Table 36 Tablet MAs – formulation 2 –chapter 5.2

exp.no	CP [MPa]	mass [mg]	mass s.rel [%]	height [mm]	height s.rel [%]	crushing strength [N]	crushing strength s.rel [%]
1	94	201.9	0.45	4.04	0.25	52	3.85
1	187	201.9	0.45	3.80	0.53	119	4.20
1	281	201.9	0.74	3.70	0.54	146	6.75
1	375	200.6	0.60	3.66	0.55	160	8.13
1	469	201.0	0.40	3.65	0.27	165	4.85
2	94	196.2	0.61	3.98	0.75	50	4.00
2	187	202.8	0.54	3.82	0.52	117	3.42
2	281	199.7	0.40	3.67	0.27	157	7.01
2	375	200.7	0.65	3.65	0.55	172	5.23
2	469	203.2	0.20	3.67	0.27	181	3.31
3	94	199.4	0.70	4.04	0.50	53	3.77
3	187	204.7	0.54	3.84	0.26	127	3.16
3	281	199.8	0.75	3.66	0.82	164	2.44
3	375	207.5	3.67	3.72	0.54	179	4.78
3	469	208.3	3.70	3.70	0.81	181	3.87
4	94	195.0	6.21	4.08	0.49	49	4.08
4	187	203.2	0.64	3.82	0.52	118	5.08
4	281	200.8	0.72	3.69	0.81	154	4.73
4	375	200.7	0.67	3.66	0.55	169	3.95
4	469	204.6	0.36	3.70	0.27	165	7.46
5	94	199.1	0.45	4.05	0.25	42	4.76
5	187	198.9	0.35	3.77	0.27	102	4.90
5	281	199.3	0.35	3.67	0.27	140	2.14
5	375	201.0	0.40	3.66	0.27	157	4.46
5	469	200.7	0.38	3.64	0.27	159	7.99
6	94	196.2	1.33	4.02	1.00	28	3.57
6	141	202.1	1.88	3.96	1.77	50	8.00
6	187	199.9	2.50	3.80	2.11	75	6.67
6	234	198.8	0.84	3.71	0.81	93	4.55
6	281	191.9	1.88	3.60	1.39	102	4.90
7	94	199.1	2.41	4.08	1.96	24	8.33
7	141	197.4	2.43	3.86	1.81	45	4.44

7	187	201.4	1.49	3.83	1.04	66	6.06
7	234	206.0	1.12	3.83	0.78	87	4.60
7	281	203.6	1.47	3.76	1.33	95	6.32
8	94	202.2	1.24	4.10	0.98	45	4.44
8	187	207.0	0.66	3.87	0.52	109	3.09
8	281	203.2	0.74	3.72	0.81	143	5.59
8	375	203.6	0.49	3.68	0.54	156	4.48
8	469	203.7	0.59	3.68	0.54	161	4.35

14.2 CHAPTER 5.3

Table 37 Overview on detailed experimental setup – chapter 5.3

		GRANULATION				DRYING		
binder addition	**exp. no.**	**PFR [kg/h]**	**LFR [g/min]**	**ML [%]**	**screw speed [rpm]**	**DRS [rph]**	**IAFR [m³/h]**	**IAT [°C]**
binder added to granulation liquid	1	15	48,7	15	175	20	300	85
	2	15	63,5	19	175	20	300	90
	3	15	79,7	23	175	20	300	95
binder added to powder preblend	1	15	44,1	15	175	20	300	85
	2	15	58,6	19	175	20	270	90
	3	15	74,7	23	175	20	270	95

Table 38 Granules MAs – evaluation of binder addition formulation 1 – chapter 5.3

binder addition	**ML [%]**	**LoD [%]**	**FFC [-]**	**D10 [µm]**	**D50 [µm]**	**D90 [µm]**	**<63µm [%]**	**>1000µm [%]**
binder added to powder preblend	15	1.12	4.6	23.0	61.9	1071.6	50.8	11.0
	19	0.76	4.9	23.1	63.1	701.7	49.9	5.1
	23	1.04	5.0	24.7	69.4	713.9	46.0	5.1
binder added to granulation liquid	15	0.67	6.0	29.9	132.1	740.0	30.0	3.0
	19	0.68	7.9	38.7	390.9	1178.9	19.0	17.4
	23	0.64	6.0	50.0	356.1	1156.0	14.2	15.5

Table 39 Tablet MAs – evaluation of binder addition formulation 1 – chapter 5.3

binder addition	ML [%]	CP [MPa]	mass [mg]	mass s.rel [%]	height [mm]	height s.rel [%]	crushing strength [N]	crushing strength s.rel [%]
binder added to powder preblend	15	94	206.5	0.77	4.10	0.73	48	4.17
	15	187	200.8	0.70	3.71	0.81	104	3.85
	15	281	201.5	0.69	3.65	0.55	135	2.96
	15	375	197.4	0.91	3.57	0.84	145	2.76
	15	469	198.9	1.46	3.57	1.40	156	3.85
	19	94	204.2	1.67	4.05	1.73	47	4.26
	19	187	197.2	1.37	3.66	1.09	99	4.04
	19	281	194.4	0.67	3.54	0.85	126	2.38
	19	375	197	0.66	3.57	0.56	140	2.86
	19	469	200.6	0.70	3.60	0.56	153	1.96
	23	94	197.1	1.37	3.93	1.02	46	4.35
	23	187	199.9	0.85	3.69	0.81	100	3.00
	23	281	200.8	0.70	3.64	0.55	130	3.08
	23	375	200.3	0.55	3.61	0.55	143	2.80
	23	469	200.3	0.65	3.60	0.56	153	2.61
binder added to granulation liquid	15	94	197.4	1.17	3.94	1.02	54	3.70
	15	187	204.3	0.69	3.77	0.53	116	3.45
	15	281	202.5	0.59	3.67	0.54	146	3.42
	15	375	205	0.78	3.67	0.54	160	3.13
	15	469	204.8	0.93	3.65	0.55	165	3.03
	19	94	202.2	0.54	4.02	0.50	59	3.39
	19	187	202.7	0.54	3.75	0.53	124	4.03
	19	281	203.8	0.59	3.67	0.54	153	3.92
	19	375	206.5	0.73	3.69	0.81	171	3.51
	19	469	203.3	0.59	3.64	0.55	174	2.87
	23	94	200.5	0.55	3.98	0.50	60	3.33
	23	187	201.8	0.35	3.71	0.27	123	4.07
	23	281	202.8	0.44	3.66	0.27	153	2.61
	23	375	202.1	0.45	3.63	0.28	163	3.07
	23	469	202.4	0.59	3.63	0.28	171	3.51

14.3 CHAPTER 6

Table 40 Overview on detailed experimental planning – chapter 6

		GRANULATION				DRYING		
formulation	**exp. no.**	**PFR [kg/h]**	**LFR [g/min]**	**ML [%]**	**screw speed [rpm]**	**DRS [rph]**	**IAFR [m³/h]**	**IAT [°C]**
F1	1	20	118.1	25	250	30	380	80
F1	2	20	118.1	25	250	10	380	80
F1	3	20	65.0	15	250	30	340	80
F1	4	20	65.0	15	250	10	340	80
F1	5	20	89.8	20	250	20	360	87
F1	6	20	118.1	25	250	30	380	94
F1	7	20	118.1	25	250	10	380	94
F1	8	20	65.0	15	250	30	340	94
F1	9	20	65.0	15	250	10	340	94
F2	1	20	83.3	20	250	30	360	70
F2	2	20	83.3	20	250	10	360	70
F2	3	20	37.0	10	250	30	320	70
F2	4	20	37.0	10	250	10	320	70
F2	5	20	58.8	15	250	20	340	80
F2	6	20	83.3	20	250	30	360	90
F2	7	20	83.3	20	250	10	360	90
F2	8	20	37.0	10	250	30	320	90
F2	9	20	37.0	10	250	10	320	90

Table 41 Granules MAs – formulation 1 – chapter 6

exp.no	LoD [%]	FFC [-]	D10 [µm]	D50 [µm]	D90 [µm]	<63µm [%]	>1000µm [%]
1	2.83	7.9	49.5	498.7	1539.5	14.2	27.9
2	3.11	5.3	41.6	439.3	2199.0	18.9	29.5
3	1.97	3.7	26.2	151.4	1790.3	34.0	22.6
4	1.18	4.6	31.2	483.9	2567.5	24.0	33.8
5	0.96	5.7	34.9	711.9	2077.7	21.2	41.2
6	1.64	5.8	47.8	518.2	1648.6	14.5	28.8
7	1.37	4.7	36.1	296.7	2467.0	24.8	30.2
8	2.71	6.5	45.3	718.5	2547.5	14.9	40.1
9	0.65	5.1	27.8	383.0	2347.0	27.5	31.9

Table 42 Tablet MAs – formulation 1 –chapter 6

exp.no	CP [MPa]	mass [mg]	mass s.rel [%]	height [mm]	height s.rel [%]	crushing strength [N]	crushing strength s.rel [%]
1	94	199.2	0.60	3.91	0.51	59	3.39
1	187	201.4	0.60	3.67	0.54	121	3.39
1	281	199.9	0.45	3.58	0.28	153	2.61
1	375	199.4	0.45	3.55	0.28	168	2.98
1	469	199.2	0.55	3.54	0.56	172	2.91
2	94	195.6	0.56	3.86	0.52	58	3.45
2	187	201.2	0.50	3.66	0.55	121	4.13
2	281	202.4	0.79	3.60	0.56	147	4.08
2	375	201.8	0.50	3.58	0.28	163	3.07
2	469	202.2	0.64	3.58	0.28	168	2.38
3	94	199.3	1.35	3.94	1.02	55	3.64
3	187	199.4	0.85	3.67	0.82	116	4.31
3	281	199.7	1.10	3.59	0.84	148	2.70
3	375	200.6	1.15	3.58	0.84	162	3.09
3	469	199.8	0.80	3.55	0.56	171	2.34
4	94	199.7	0.65	3.97	0.50	54	3.70
4	187	200.7	0.70	3.69	0.81	119	3.36
4	281	205.9	0.97	3.68	0.82	158	3.16

4	375	202.8	0.74	3.60	0.56	167	4.19
4	469	203.4	1.03	3.59	0.84	177	4.52
5	94	198.3	1.92	3.94	1.52	55	3.64
5	187	200.0	0.80	3.68	0.54	120	3.33
5	281	200.4	1.05	3.59	0.84	150	3.33
5	375	201.5	0.69	3.58	0.28	170	2.35
5	469	200.5	0.95	3.55	0.85	179	2.79
6	94	201.7	0.59	3.96	0.51	60	3.33
6	187	202.0	0.54	3.74	0.53	123	3.25
6	281	202.1	0.30	3.66	0.27	155	1.94
6	375	202.0	0.45	3.63	0.28	174	1.72
6	469	202.3	0.44	3.63	0.28	177	2.82
7	94	199.6	0.85	3.98	0.75	60	3.33
7	187	202.3	0.54	3.75	0.53	122	2.46
7	281	205.0	0.59	3.71	0.54	156	3.21
7	375	200.3	1.50	3.60	1.11	169	2.96
7	469	201.6	0.84	3.60	0.83	179	2.79
8	94	201.2	0.80	4.03	0.74	59	3.39
8	187	200.3	0.50	3.73	0.54	121	4.13
8	281	200.6	0.60	3.65	0.27	152	3.30
8	375	200.7	0.75	3.63	0.55	168	2.38
8	469	199.6	0.45	3.60	0.56	173	2.31
9	94	205.2	0.78	4.13	0.48	53	3.77
9	187	202.9	1.03	3.79	1.06	113	2.65
9	281	202.8	0.89	3.69	0.81	145	2.76
9	375	204.8	1.66	3.69	1.36	167	3.59
9	469	195.8	0.87	3.55	0.85	166	2.41

Table 43 Granules MAs – formulation 2 – chapter 6

exp.no	**LoD [%]**	**FFC [-]**	**D10 [µm]**	**D50 [µm]**	**D90 [µm]**	**<63µm [%]**	**>1000µm [%]**
1	3.70	8.1	241.1	610.2	1301.4	1.5	21.4
2	3.54	6.6	182.4	609.3	1308.1	2.9	22.4
3	0.71	6.7	25.2	154.5	1160.6	29.5	15.3
4	0.85	5.2	19.3	104.4	713.1	37.2	3.9

5	0.55	7.6	36.5	218.6	1120.9	19.1	12.2
6	3.19	5.2	234.5	707.0	1639.1	2.5	30.8
7	2.18	19.0	243.0	639.8	1404.7	2.0	24.4
8	0.49	5.3	28.5	117.2	610.1	29.4	2.4
9	0.52	5.5	20.3	96.4	697.4	38.8	5.0

Table 44 Tablet MAs – formulation 2 –chapter 6

exp.no	CP [MPa]	mass [mg]	mass s.rel [%]	height [mm]	height s.rel [%]	crushing strength [N]	crushing strength s.rel [%]
1	94	204.0	0.69	4.04	0.74	60	3.33
1	187	204.2	0.49	3.85	0.52	106	2.83
1	281	202.0	0.54	3.76	0.53	109	2.75
1	375	199.8	0.70	3.72	0.54	112	3.57
1	469	201.7	0.69	3.75	0.80	109	4.59
2	94	203.1	1.62	3.99	1.50	63	4.76
2	187	202.4	0.99	3.83	1.04	87	4.60
2	281	203.5	1.18	3.83	1.31	94	5.32
2	375	199.6	0.80	3.76	1.06	83	6.02
2	469	201.1	0.50	3.79	0.53	84	5.95
3	94	202.1	1.98	4.13	1.45	28	3.57
3	141	199.4	0.85	3.90	0.77	52	3.85
3	187	196.6	0.81	3.75	0.80	78	2.56
3	234	198.9	0.96	3.72	0.81	98	3.06
3	281	198.5	0.71	3.68	0.54	110	4.53
4	94	195.6	0.66	4.03	0.74	26	3.85
4	141	200.7	1.64	3.92	1.28	53	3.77
4	187	203.6	1.77	3.86	1.30	81	2.47
4	234	203.2	1.57	3.78	1.32	99	3.03
4	281	202.7	1.92	3.73	1.61	114	7.04
5	94	200.1	0.80	4.10	0.73	37	2.70
5	141	201.3	0.50	3.92	0.51	70	2.86
5	187	201.1	0.55	3.82	0.52	100	2.00
5	234	201.0	0.55	3.74	0.53	122	3.28
5	281	200.7	0.55	3.69	0.54	136	2.94

6	94	197.8	0.61	3.97	0.50	69	2.90
6	187	201.8	0.40	3.82	0.26	142	2.82
6	281	198.4	0.40	3.70	0.54	159	1.89
6	375	200.5	0.50	3.72	0.54	111	3.60
6	469	201.0	0.55	3.72	0.54	110	4.55
7	94	201.7	0.59	4.05	0.49	57	3.51
7	187	198.7	0.65	3.73	0.54	110	4.55
7	281	200.7	0.46	3.68	0.54	143	3.67
7	375	199.3	0.65	3.64	0.55	151	2.65
7	469	198.4	0.60	3.61	0.55	150	2.67
8	94	200.1	0.65	4.13	0.73	28	3.57
8	141	199.9	0.70	3.93	0.76	53	1.89
8	187	200.3	1.20	3.81	1.05	82	2.44
8	234	201.1	0.91	3.76	1.06	100	2.00
8	281	201.3	0.94	3.72	0.81	110	2.20
9	94	200.1	0.60	4.13	0.48	24	4.17
9	141	201.6	1.19	3.95	1.01	51	5.88
9	187	198.5	0.60	3.80	0.53	75	2.67
9	234	201.5	0.89	3.77	0.80	95	2.11
9	281	200.3	1.05	3.70	0.81	106	2.83

14.4 CHAPTER 7

Table 45 Drying performance per scale – chapter 7.4

scale	ML [%]	residual water content [%]
XS-Line	10	0.79
XS-Line	10	1.09
XS-Line	10	0.76
XS-Line	10	0.46
XS-Line	10	0.61
XS-Line	15	0.68
XS-Line	15	0.79
XS-Line	15	0.6
XS-Line	15	0.62
XS-Line	15	0.57
XS-Line	15	0.76
XS-Line	15	0.63
XS-Line	20	3.27
XS-Line	20	1.82
XS-Line	20	1.93
XS-Line	20	1.5
XS-Line	20	0.54
S-Line	10	0.74
S-Line	10	0.73
S-Line	10	0.59
S-Line	10	0.57
S-Line	15	0.71
S-Line	20	1.93
S-Line	20	1.69
S-Line	20	4.45
S-Line	20	0.46
M-Line	10	0.71
M-Line	10	0.85
M-Line	10	0.49
M-Line	10	0.52
M-Line	15	0.55

M-Line	20	3.70
M-Line	20	3.54
M-Line	20	3.19
M-Line	20	2.18

statistical models – regression equations:

XS-Line (19)

fine fraction:

$$y = 178.1834 - 8.9001 * ML + 0.3454 * ML^2 + 0.5145 * DRS - 0.0246 * DRS^2 - 2.7428 * IAT + 0.0236 * IAT^2 - 0.0288 * ML * DRS - 0.0484 * ML * IAT + 0.0146 * DRS * IAT; R^2 = 0.96$$

XS-line (20)

residual water content:

$$y = 20.77403 - 0.13186 * ML + 0.01066 * ML^2 - 0.12907 * DRS + 0.00287 * DRS^2 - 0.51827 * IAT + 0.00387 * IAT^2 + 0.0047 * ML * DRS - 0.0025 * ML * IAT - 0.00052 * DRS * IAT; R^2 = 0.81$$

S-Line (21)

fine fraction:

$$y = 106.5419 - 7.6755 * ML + 1.1488 * DRS - 0.3317 * IAT + 0.0024 * ML * DRS + 0.0522 * ML * IAT - 0.0184 * DRS * IAT; R^2 = 0.99$$

S-Line (22)

residual water content:

$$y = 4.982431 - 0.381875 * ML - 0.104375 * DRS - 0.047375 * IAT + 0.010513 * ML * DRS + 0.003987 * ML * IAT; R^2 = 0.70$$

M-Line (23)

fine fraction:

$$y = 76.6025 - 3.6895 * ML - 0.846 * DRS + 0.068 * IAT + 0.0404 * ML * DRS - 0.0034 * ML * IAT + 0.00018 * DRS * IAT ; R^2 = 0.99$$

M-Line (24)

residual water content:

$$y = -2.83117 + 0.44876 * ML - 0.0377 * DRS + 0.01955 * IAT + 0.00336 * ML * DRS - 0.00331 * ML * IAT; R^2 = 0.89$$

14.5 CHAPTER 11.2.2.1

Table 46 Particle density used for calculation of SF in chapters 5, 6 and 7 (preblend) and comparison to an exemplary final blend

	particle density [g/cm³] ± SD	
	F1 verum – DL 5 %	**F2** verum – DL 5 %
preblend	1.5040 ± 0.0006	1.4717 ± 0.0011
final blend (exemplary)	1.4915 ± 0.0006	1.4597 ± 0.0010
deviation particle density preblend – final blend [%]	0.83	0.82

LIST OF FIGURES

LIST OF TABLES